E-Area Vault Concrete Material Property and Vault Durability/Degradation Projection Recommendations

M.A. Phifer

February 2014

SRNL-STI-2013-00706, Revision 0

DISCLAIMER

Printed in the United States of America

**Prepared for
U.S. Department of Energy**

E-Area Vault Concrete Material Property and Vault Durability/Degradation Projection Recommendations

M.A. Phifer

February 2014

Savannah River National Laboratory ™

OPERATED BY SAVANNAH RIVER NUCLEAR SOLUTIONS

REVIEWS AND APPROVALS

AUTHORS:

_____
M.A. Phifer, Radiological Performance Assessment, SRNL   Date

TECHNICAL REVIEW:

_____
B.T. Butcher, Radiological Performance Assessment, SRNL, Reviewed per E7 2.60   Date

APPROVAL:

_____
D.A. Crowley, Manager   Date
Radiological Performance Assessment, SRNL

_____
R.S. Aylward, Manager   Date
Environmental Restoration Technology, SRNL

_____
F.L. Fox, Deputy Director   Date
Solid Waste Management

EXECUTIVE SUMMARY

Subsequent to the 2008 E-Area Low-Level Waste Facility (ELLWF) Performance Assessment (PA) (WSRC 2008), two additional E-Area vault concrete property testing programs have been conducted (Dixon and Phifer 2010 and SIMCO 2011a) and two additional E-Area vault concrete durability modeling projections have been made (Langton 2009 and SIMCO 2012). All the information/data from these reports has been evaluated and consolidated herein by the Savannah River National Laboratory (SRNL) at the request of Solid Waste Management (SWM) to produce E-Area vault concrete hydraulic and physical property data and vault durability/degradation projection recommendations that are adequately justified for use within associated Special Analyses (SAs) and future PA updates.

Based upon this evaluation the following are recommended in regards to the E-Area vault concrete property values for use in ELLWF SAs and PAs:

- Utilize the property values provided in Table 5-1 for saturated hydraulic conductivity, tortuosity, effective diffusion coefficient, dry bulk density, porosity, and particle density.
- Utilize the characteristic curve data provided in Table 3-8.
- Utilize the uncertainty distributions provided in Table 3-10.

The Low Activity Waste (LAW) and Intermediate Level (IL) Vaults structural degradation predictions produced by Carey 2006 and Peregoy 2006, respectively, which were used as the basis for the 2008 ELLWF PA, remain valid based upon the results of the E-Area vault concrete durability simulations reported by Langton 2009 and those reported by SIMCO 2012. Therefore revised structural degradation predictions are not required so long as the mean thickness of the closure cap overlying the vaults is no greater than that assumed within Carey 2006 and Peregoy 2006. For the LAW Vault structural degradation prediction (Carey 2006), the mean thickness of the overlying closure cap was taken as nine feet. For the IL Vault structural degradation prediction (Peregoy 2006), the mean thickness of the overlying closure cap was taken as eight feet. The mean closure cap thicknesses as described here for both E-Area Vaults will be included as a key input and assumption (I&A) in the next revision to the closure plan for the ELLWF (Phifer et al. 2009). In addition, it has been identified as new input to the PA model to be assessed in the ongoing update to the new PA Information UDQE (Flach 2013). Once the UDQE is approved, the SWM Key I&A database will be updated with this new information.

TABLE OF CONTENTS

LIST OF TABLES

LIST OF FIGURES

LIST OF ACRONYMNS

AASHTO	American Association of State Highway and Transportation Officials
CBP	Cementitious Barriers Partnership
CLSM	Controlled Low Strength Material
CRESP	Consortium for Risk Evaluation with Stakeholder Participation
C-S-H	calcium silicate hydrate
DOE	Department of Energy
ECN	Energy Research Centre of the Netherlands
ELLWF	E-Area Low-Level Waste Facility
EM	Environmental Management
GSA	General Separations Area
I&A	input and assumption
IL	Intermediate Level
ILNT	Intermediate Level Non-Tritium
ILT	Intermediate Level Tritium
LAW	Low Activity Waste
na	Not analyzed
NIST	National Institute of Standards and Technology
NRC	Nuclear Regulatory Commission
PC	Performance Category
PA	Performance Assessment
RH	relative humidity
SA	Special Analysis
SRNL	Savannah River National Laboratory
SRNS	Savannah River Nuclear Solutions
SRS	Savannah River Site
SWM	Solid Waste Management
WSRC	Westinghouse Savannah River Company or Washington Savannah River Company

LIST OF ABBREVIATIONS

A	materials constant
D_e	effective diffusion coefficient
D_m	molecular diffusion coefficient of the species in open water
k_r	relative permeability
K_{sat}	saturated hydraulic conductivity
S	saturation
Std Dev	standard deviation
η	porosity
ρ_s	particle density
ρ_b	dry bulk density
τ	tortuosity
t	time
X_c	distance of the carbonation front
ψ	suction head

1.0 Introduction

The E-Area Low-Level Waste Facility (ELLWF) is located within the General Separations Area (GSA) of the Savannah River Site (SRS). The ELLWF contains six different types of disposal units including the Low Activity Waste (LAW) Vault and the Intermediate Level (IL) Vault. The LAW Vault is an above-grade, reinforced concrete vault. It is approximately 643 feet long, 145 feet wide, and 27 feet high at the roof crest. It is divided into three modules along its length, which are approximately 214 feet long and contain four cells each. The 12 cell total is designed to contain more than 12,000 B-25 boxes of waste. After the entire LAW Vault has been filled, it will be operationally closed, by sealing exterior vault openings, including those between modules, with reinforced concrete equivalent to that utilized within the vault floor, walls and roof. The IL Vault is a below-grade, reinforced concrete vault. It consists of two modules, which together encompass a 278.83-foot by 48.5-foot area. The Intermediate Level Tritium (ILT) module contains two cells, whose inside dimensions are 25-foot by 44.5-foot by 26-foot. The Intermediate Level Non-Tritium (ILNT) module contains seven identical cells, whose inside dimensions are 25-foot by 44.5-foot by 28.42-foot deep. The area between the two modules provides manhole access to the subdrain system. Waste contained within metal or concrete containers are placed within the IL Vault and grouted in place. After the entire IL Vault has been filled, it will be operationally closed, by installing a greater than 2-foot thick permanent reinforced concrete roof slab and overlying bonded-in-place fiberboard insulation and waterproof membrane roofing over the entire vault. Final closure of the LAW and IL Vaults will take place at final closure of the entire ELLWF, at the end of the 100-year institutional control period. Final closure will consist of one or more closure caps installed over all the disposal units and a drainage system. (Phifer et al. 2006)

A Performance Assessment (PA) for the ELLWF, including the LAW and IL Vaults, was approved by the Department of Energy (DOE) in 2008 (WSRC 2008). The hydraulic and physical properties of the E-Area vault concrete (i.e. LAW and IL Vaults) utilized within the 2008 ELLWF PA (WSRC 2008) were based upon the results of a 1993 materials characterization program (Yu et al. 1993). Structural analyses (Carey 2006 and Peregoy 2006) of the vaults were conducted in order to estimate structural cracking and time of collapse as input to the 2008 ELLWF PA (WSRC 2008). Subsequent to the 2008 ELLWF PA (WSRC 2008), two additional E-Area vault concrete property testing programs have been conducted (Dixon and Phifer 2010 and SIMCO 2011a) and two additional E-Area vault concrete durability modeling projections have been made (Langton 2009 and SIMCO 2012). All the information/data from these reports has been evaluated and consolidated herein in order to produce E-Area vault concrete hydraulic and physical property data and vault durability/degradation projection recommendations that are adequately justified for use within associated Special Analyses (SA) and future PA updates. Evaluation and consolidation of the information/data is necessary in order to reconcile the data collected at different times and by different methods, to provide consistent durability/degradation projections for both vaults, and to provide documentation that can be referenced.

2.0 E-Area Vault Concrete Formulation

The formulation of the concrete utilized for all concrete in the IL Vault, including shielding tees and plugs, and the bulk of the concrete utilized in the LAW Vault is provided in Table 2-1. Within the LAW Vault this concrete formulation was utilized for the continuous footer, floor slab, interior and exterior walls, and the cast-in-place roof slab. This formulation was not utilized for the American Association of State Highway and Transportation Officials (AASHTO) Type IV bridge beams and precast deck panels of the LAW Vault (Phifer et al. 2006).

Table 2-1. E-Area Vault Concrete Formulation and Properties.

Ingredient	Quantity
Type II cement (ASTM C 150)	120 lbs/cu yd
Grade 120 Blast furnace slag (ASTM C 989)	275 lbs/cu yd
Type F Fly ash (ASTM C 618)	135 lbs/cu yd
No 10. sand (ASTM C 33)	1,270 lbs/cu yd
No. 67 granite aggregate (maximum ¾ in) (ASTM C 33)	1,750 lbs/cu yd
Water (maximum)	240 lbs/cu yd (28.8 gallons)
Maximum water to cementitious material ratio	0.45
Property	**Value**
Specified minimum dry bulk density	147 lbs/cu ft (2.35 g/cm^3)
Minimum compressive strength at 28 days	4000 psi

Notes to Table 2-1:
- Concrete formulation specified in drawing SE5-6-2003319
- Concrete formulation specified in Specification C-SPS-G-00041 Mix Identifier C-4000-8-S-2-AB (WSRC 1994)
- Very high quality workmanship was implemented for placement of this concrete (WSRC 2005)
- Drawing SE5-6-2003319 required a very extensive curing procedure which involved the application of curing compound and a minimum 14 day curing using either insulating blankets or a burlap wet cure.

3.0 E-Area Vault Concrete Hydraulic and Physical Properties

The following sections provide the E-Area vault concrete hydraulic and physical properties utilized within the 2008 ELLWF PA (WSRC 2008), the results from three programs to test for these properties (Yu et al. 1993; Dixon and Phifer 2010; and SIMCO 2011a), recommended property values for use of future PAs, and the recommended property uncertainty representation for use of future PAs.

3.1 <u>E-Area Vault Concrete Hydraulic and Physical Properties utilized in 2008 ELLWF PA</u>

The hydraulic and physical property data utilized within the 2008 ELLWF PA (WSRC 2008) to represent the initial conditions of E-Area vault concrete were provided in Phifer et al. 2006. The data included saturated hydraulic conductivity, effective diffusion coefficient, dry bulk density, porosity, particle density, and characteristic curves (suction head/saturation/relative permeability). The following are the sources of the data utilized:

- The saturated hydraulic conductivity, dry bulk density, and porosity values utilized were obtained from the 1993 materials characterization program conducted by Core Laboratories (Yu et al. 1993) that included testing of E-Area vault concrete (see Section 3.2 below).
- The particle density value was calculated from the porosity and dry bulk density (Phifer et al. 2006).
- The effective diffusion coefficient value was a representative value for high quality concrete based upon a literature review (Phifer et al. 2006).
- The characteristic curves were produced based upon a literature review (Phifer et al. 2006) and selection of the Baroghel-Bouny et al. 1999 data for high performance concrete (Mix BH) as most representative the E-Area vault concrete.

Table 3-1 provides the nominal values of saturated hydraulic conductivity, effective diffusion coefficient, dry bulk density, porosity, and particle density utilized, and Figure 3-1 provides the characteristic curves (suction head/saturation/relative permeability) utilized within the 2008 ELLWF PA (WSRC 2008) to represent the initial conditions of E-Area vault concrete.

Since the 2008 ELLWF PA (WSRC 2008) was completed, two additional E-Area vault concrete testing programs have been conducted in addition to the 1993 program (Yu et al. 1993). During 2009, testing of E-Area vault concrete was conducted for saturated hydraulic conductivity, water retention characteristics, dry bulk density, and porosity by a standard geotechnical laboratory (Dixon and Phifer 2010) as outlined in Section 3.3. During 2010, testing of E-Area vault concrete was conducted for saturated hydraulic conductivity, water retention characteristics, diffusion coefficient and tortuosity, total porosity, and bulk density by a leading concrete laboratory as outlined in Section 3.4 (SIMCO 2011a). The data produced for the E-Area vault concrete during each of the testing programs are reviewed in Sections 3.2 through 3.4. Sections 3.5 and 3.6 provide recommendations for the parameter values and associated uncertainty distributions, respectively, to utilize in a future ELLWF PA revision.

Table 3-1. 2008 ELLWF PA E-Area Vault Concrete Properties.

Saturated Hydraulic Conductivity (cm/s)	Effective Diffusion Coefficient [1] (cm^2/s)	Dry Bulk Density (g/cm^3)	Porosity (-)	Particle Density (g/cm^3)
1.0E-12	5.0E-08	2.11	0.184	2.59

[1] Assuming a molecular diffusion coefficient in open water for a representative species (NaCl) of 1.6E-5cm^2/s (Bruins 2003) associated with the effective diffusion coefficient, the tortuosity would be 0.0031 (Tortuosity (τ) = Effective diffusion coefficient (D_e) ÷ molecular diffusion coefficient of the species in open water (D_m)).
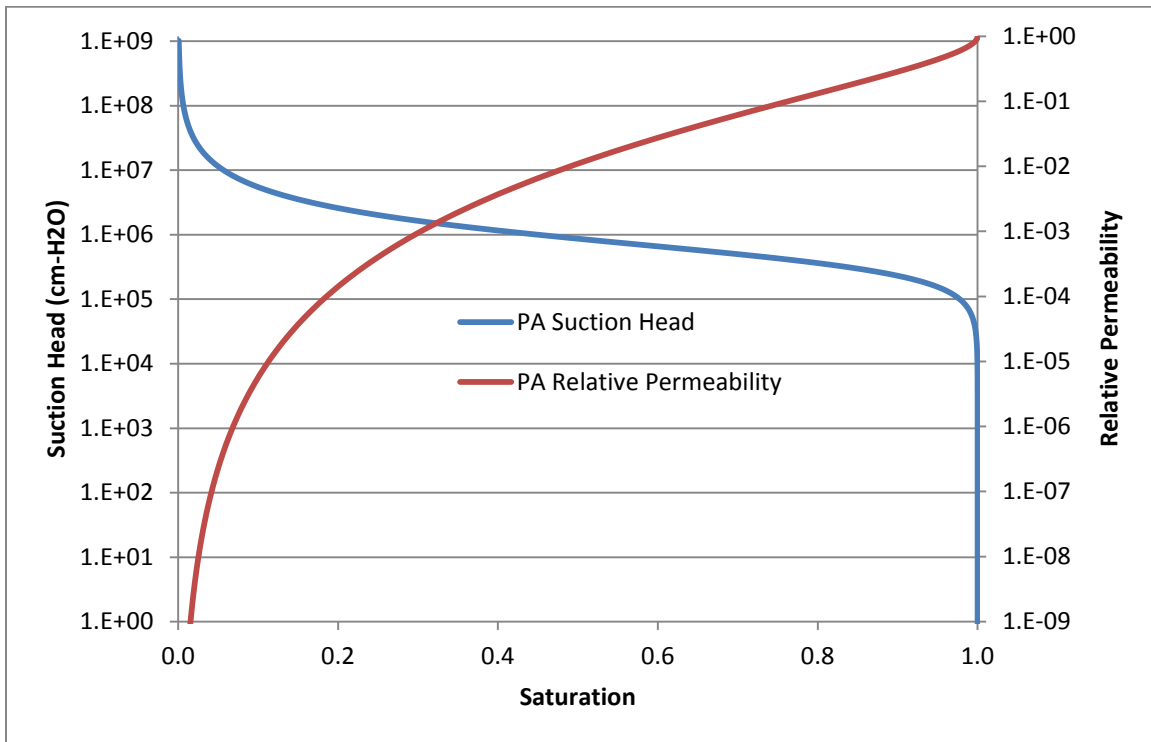
Figure 3-1. 2008 ELLWF PA E-Area Vault Concrete Characteristic Curves.

3.2 1993 E-Area Vault Concrete Testing by Core Laboratories (Yu et al. 1993)

During 1992 and 1993, a materials characterization program was conducted and documented by Yu et al. 1993. The program included testing of the E-Area vault concrete by Core Laboratories to determine its saturated hydraulic conductivity, water retention properties, dry bulk density, and porosity.

A 1-foot by 1-foot by 1-foot block of E-Area vault concrete (it is assumed that this block was associated with the E-Area concrete test wall) was supplied to Core Laboratories. However, there is no documentation of the mix formulation or of the source of the material (laboratory mode sample or a sample from an actual pour) (Dixon and Phifer 2010). Core Laboratories drilled ten 1-½ inch diameter samples from the E-Area vault concrete bulk sample and trimmed them to right cylinders approximately two inches long. These drilled and trimmed samples were utilized for all the testing conducted (Phifer et al. 2006).

Saturated hydraulic conductivity testing of these samples was conducted on samples pressure-saturated for a week with water, and then the samples were mounted in an epoxy coating to prevent bypass flow. It is assumed that the samples were mounted in a horizontal orientation. Tap water was injected into the sample at a constant upstream pressure of 50 psi (gradients approaching 700), and the flow rate out of the sample was measured until the flow rate essentially obtained steady state. The viscosity and density of the tap water was determined so that both intrinsic permeability and saturated hydraulic conductivity to the tap water could be determined (Phifer et al. 2006). To prevent undue influence of large aggregates on saturated hydraulic conductivity results, ASTM D5084 (ASTM 2010) requires that the sample diameter and height each be at least six times greater than the largest particle size within the sample. Based upon this

criterion the samples should have had a minimal diameter and height of 4.5 inches (sample maximum aggregate size is ¾ inches). The smaller Core Laboratories sample size could have biased the saturated hydraulic conductivity measurement as the coarse aggregate would have represented a larger percentage of the overall sample diameter.

Core Laboratories attempted to determine the water retention characteristics of the samples; however, the methodology utilized was inappropriate for such a determination. They de-saturated the samples in humidified air under a pressure of 35 psi. The samples were then completely immersed in tap water and subjected to increasing pressures from 1 to 35 psi. At each pressure increment the samples were allowed to "equilibrate" and a final sample weight was determined. This produced increasing water contents with pressure. Immersion of the samples and the application of increasing pressures simply forced more water into the samples. Such measurements have no relationship to water retention properties. The water retention data reported by the Core Laboratories does not represent the water retention characteristics of the E-Area vault concrete, therefore those data are not reproduced herein (Phifer et al. 2006).

The dry bulk density and total porosity of the cementitious samples were determined in conjunction with other tests and are based upon dimensional and weight measurements (Phifer et al. 2006).

Table 3-2 provides summary saturated hydraulic conductivity, dry bulk density, porosity, and particle density data for the E-Area vault concrete (Phifer et al. 2006).

Table 3-2. Summary Core Laboratories E-Area Vault Concrete Properties (Yu et al. 1993).

Sample	Saturated Hydraulic Conductivity (cm/s)	Dry Bulk Density (g/cm^3)	Calculated Porosity (-)	Calculated Particle Density [1] (g/cm^3)
1E	na	2.12	0.164	2.54
2E	7.21E-13	2.10	0.181	2.57
3E	na	2.07	na	-
4E	1.19E-12	2.15	0.193	2.66
5E	na	2.11	na	-
7E	1.22E-12	2.11	0.198	2.63
Count	3	6	4	4
Average	1.04E-12	2.11	0.184	2.59
Std Dev of Population	2.79E-13	0.026	0.0148	0.054
Std Dev of Mean	1.61E-13	0.010	0.0074	0.027
Variance of the Mean	2.59E-26	0.0001	0.000005	0.0007

Note to Table 3-2:
- Std Dev = standard deviation
- na = not analyzed

[1] Particle density calculated as $\rho_s = \rho_b / (1 - \eta)$ where ρ_b is dry bulk density and η is porosity.

3.3 <u>2009 E-Area Vault Concrete Testing by MACTEC (Dixon and Phifer 2010)</u>

During 2009, hydraulic and physical property testing of E-Area vault concrete was conducted and documented by Dixon and Phifer 2010. Testing included saturated hydraulic conductivity, water retention characteristics, dry bulk density, and porosity.

Core samples collected from the E-Area concrete test wall (Figure 3-2) were supplied to MACTEC Engineering and Consulting, Inc., a standard concrete/geotechnical testing laboratory. The concrete test wall was a test pour of the E-Area vault concrete prior to construction of the LAW and IL Vaults. The concrete test wall utilized the same concrete formulation used for the LAW and IL Vaults and was placed and cured in the same manner (Abramczyk 2009). Therefore, it is assumed that the hydraulic and physical properties of the test wall concrete would be representative of the vault concrete. Previously, site construction forces cut a block of concrete from the wall to test a new cutting method. Two, six-inch nominal diameter and two, three-inch nominal diameter cores were collected from this block using a wet abrasive coring bit and drill motor (Figure 3-3). This coring was conducted in April, 2009. These cores were collected from approximately the center of the block by drilling through the entire thickness of the block. Both of the six-inch diameter cores and one of the three-inch diameter cores were submitted for testing per standard ASTM methods to MACTEC (Dixon and Phifer 2010).

Saturated hydraulic conductivity testing was conducted on the six-inch diameter cores using ASTM D5084, Standard Test Methods for Measurement of Hydraulic Conductivity of Saturated Porous Materials Using a Flexible Wall Permeameter - Method F (constant volume-falling head (by mercury), rising tailwater elevation) (ASTM 2004). A sub-core was cut by MACTEC from the center of each six-inch diameter core for hydraulic conductivity testing. The samples tested were on the order of 5.7 inches in diameter by five inches high (Dixon and Phifer 2010). The flexible wall permeameter technique was developed primarily for soils but has also been used for measuring concrete permeability. The method has a practical limit of 1E-09 cm/sec using standard hydraulic systems and temperature environments (ASTM 2004). Strategies, which could have been taken to increase the measurement sensitivity but were not taken, include the use of finer temperature control, unsteady-state (transient) measurements, use of gravimetric rather than volumetric measurement of outflow, use of a significantly larger sample diameter, use of higher hydraulic gradients, longer testing times, and use of lower viscosity fluid. Other items, such as, elimination of any possible chemical gradients and bacterial growth, and strict verification of leakage, should also be considered when testing such low permeability materials (ASTM 2004). Standard concrete/geotechnical testing laboratories are typically not prepared to employ these further strategies to increase sensitivity. The saturated hydraulic conductivity testing by MACTEC was conducted at gradients less than 22.5 over time periods of less than three days and at the recorded saturated hydraulic conductivities the total outflow would have been significantly less than 1 cm^3 (Dixon and Phifer 2010). Under such testing conditions and at such low permeabilities, this is probably not enough time to achieve equilibrium conditions and accurately measure such low saturated hydraulic conductivities.

Water retention testing was conducted on the three-inch diameter cores using ASTM D2325 by pressure plate apparatus (ASTM 2000). Two wafers were cut by MACTEC from the three-inch diameter core for water retention testing; one from the top and one from the bottom portion of the core. The samples tested were on the order of 2.7 inches in diameter by one-inch high. Volumetric water content was converted to percent saturation by dividing the water content at each applied pressure by the saturated water content (Dixon and Phifer 2010).

Dry bulk density and porosity were determined on the six-inch diameter samples used for saturated hydraulic conductivity testing using a modified version of ASTM C642 (ASTM 2006). (Dixon and Phifer 2010)

Table 3-3 provides summary saturated hydraulic conductivity, dry bulk density, porosity, and particle density data for the ELLWF vault concrete. Table 3-4 provides the water retention data and Figure 3-4 provides the resulting average water retention data (Dixon and Phifer 2010).

Figure 3-2. ELLWF Concrete Test Wall Previously Cut Concrete Block.

Figure 3-3. Core Collection (April 2009).

Table 3-3. Summary MACTEC E-Area Vault Concrete Properties (Dixon and Phifer 2010).

Sample Id	Saturated Hydraulic Conductivity (cm/s)	Dry Bulk Density (g/cm^3)	Porosity (-)	Particle Density (g/cm^3) [1]
TWL-001	6.6E-10	2.19	0.133	2.53
TWL-002	3.3E-10	2.25	0.116	2.55
Average	5.0E-10	2.22	0.125	2.54

[1]   Particle density calculated as $\rho_s = \rho_b / (1 - \eta)$.

Table 3-4. Summary MACTEC E-Area Vault Concrete Water Retention Data (Dixon and Phifer 2010).

Sample Id	Dry Bulk Density (g/cm^3)	Potential (bars)						
		0.00	-0.10	-0.50	-1.0	-5.0	-10.0	-15.0
		Volumetric Moisture Content (cm^3/cm^3)						
TWL-003, Top	2.12	0.147	0.142	0.135	0.134	0.130	0.129	0.129
TWL-003, Bottom	2.20	0.150	0.143	0.141	0.141	0.140	0.140	0.140
Average	2.16	0.149	0.143	0.138	0.138	0.135	0.135	0.135
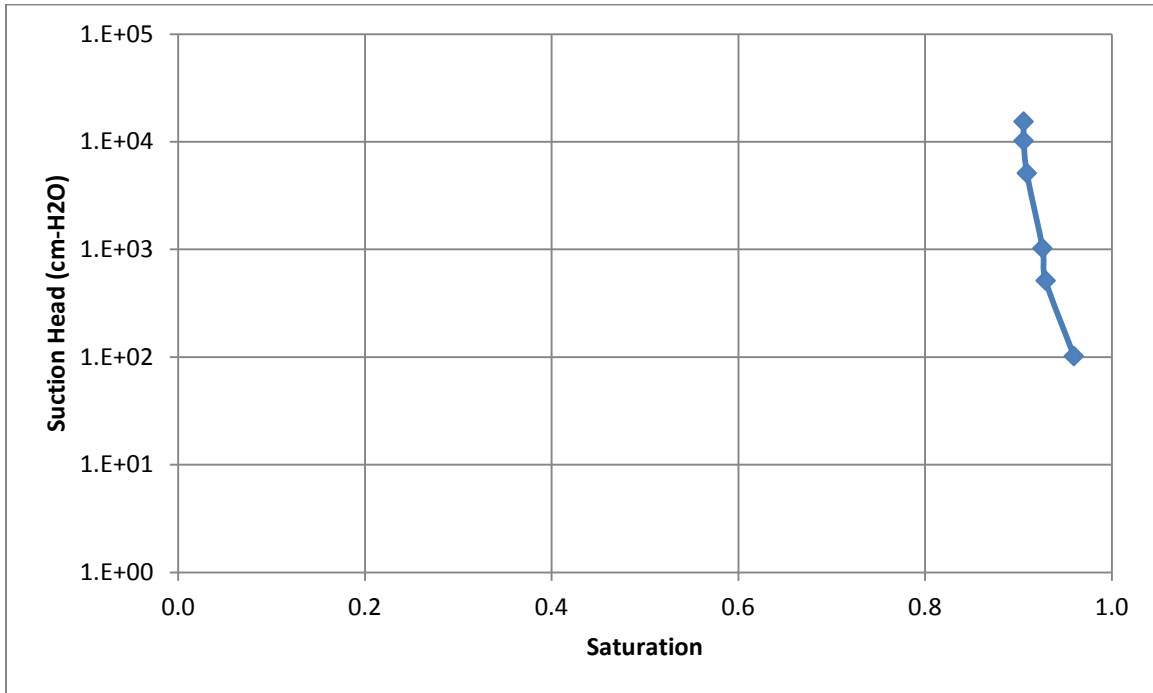
Figure 3-4. MACTEC E-Area Vault Concrete Average Water Retention Data.

3.4 2010 E-Area Vault Concrete Testing by SIMCO Technologies (SIMCO 2011a)

During 2010 hydraulic and physical property testing of E-Area vault concrete was conducted by SIMCO Technologies, Inc. and documented by SIMCO in a report (SIMCO 2011a). Appendix A provides the 2011 SIMCO report. SIMCO is a recognized leader in concrete science with a state-of-the-art in-house concrete laboratory. They are also the developers of the Software for Transport and Degradation in Unsaturated Materials (STADIUM®) code, which is used to evaluate concrete characteristics based upon laboratory tests and to estimate the service life of concrete based upon its characteristics and exposure environment. Additionally SIMCO is a member of the Cementitious Barriers Partnership (CBP) which also includes the DOE Environmental Management (EM), Savannah River National Laboratory (SRNL), Vanderbilt University Department of Civil and Environmental Engineering, Consortium for Risk Evaluation with Stakeholder Participation (CRESP), the National Institute of Standards and Technology (NIST), U.S. Nuclear Regulatory Commission (NRC), and Energy Research Centre of the Netherlands (ECN).

Core samples collected from the ELLWF concrete test wall were supplied to SIMCO Technologies, Inc. Five cores, nominally six-inch diameter by twelve-inch long, were collected by coring the test wall itself (Figure 3-5) in March, 2010. All five cores were submitted to SIMCO for testing. Testing included saturated hydraulic conductivity, water retention characteristics, diffusion coefficient and tortuosity, total porosity, and bulk density.

Saturated hydraulic conductivity was determined by analyzing the results of the drying laboratory test within STADIUM® MTC (SIMCO 2011) as detailed within the text and SIMCO 2011a Appendix D. The drying laboratory test is a modification of ASTM C1585, Standard Test

Method for Measurement of Rate of Absorption of Water by Hydraulic-Cement Concretes (ASTM 2013). The drying laboratory test consisted of periodically weighing initially saturated samples as they dried under constant relative humidity (50%) and temperature (23°C) conditions. Two sizes of samples (4.1 inch diameter by two-inch high and 4.1 inch diameter by 4.1 inch high) were cut by SIMCO from the nominal six-inch diameter cores. The STADIUM$^®$ MTC laboratory module uses the moisture transport model in STADIUM$^®$ to analyze the drying laboratory test results. The moisture transport model accounts for both liquid and vapor transport out of the sample. This is a much more sensitive method than the ASTM D5084 flexible wall permeameter method (ASTM 2004).

Water retention characteristics were determined by fitting desorption isotherm laboratory test data to the STADIUM$^®$ moisture transport model isotherm (SIMCO 2011) and to the Van Genuchten relationship as detailed within the text and SIMCO 2011a Appendix B. The desorption isotherm laboratory test consisted of periodically weighing initially saturated samples until a constant mass (equilibrium) was observed at four different relative humidities (RHs of 33%, 75%, 85% and 92%) and determining the saturation at each relative humidity. The relative humidities were maintained by saturated salt solutions (i.e. $MgCl_2 \cdot 6H_2O$ for 33% RH, NaCl for 75% RH, KCL for 85% RH, and KNO_3 for 92% RH). Samples (four-inch diameter by 0.4 inch high) were cut by SIMCO from the nominal six-inch diameter cores. In addition, the saturation at 50% relative humidity was obtained from the drying test and 100% saturation was assumed to occur at a relative humidity of 100%.

Effective diffusion coefficients and tortuosity were determined by analyzing the results of the migration test, which is a modified version of ASTM C1202, Standard Test Method for Electrical Indication of Concrete's Ability to Resist Chloride Ion Penetration, within STADIUM$^®$ IDC (SIMCO 2011) as detailed within the text and SIMCO 2011a Appendix A. The modified chloride penetration test consists of applying an external potential across the sample to accelerate ion transport and measuring the currents. Samples (four-inch diameter by two-inch high) were cut by SIMCO from the nominal six-inch diameter cores. The measured currents were then analyzed within STADIUM$^®$ IDC to obtain the effective diffusion coefficients and tortuosity.

Total porosity and dry bulk density were determined per ASTM C642, Standard Test Method for Density, Absorption, and Voids in Hardened Concrete (ASTM 2013).

Table 3-5 provides summary saturated hydraulic conductivity, tortuosity, effective diffusion coefficient, dry bulk density, porosity, and particle density for the ELLWF vault concrete. Table 3-6 and Figure 3-6 provide the average water retention data.

Figure 3-5. ELLWF Concrete Test Wall.

Table 3-5. Summary SIMCO E-Area Vault Concrete Properties (SIMCO 2011a).

Saturated Hydraulic Conductivity (cm/s)	Tortuosity (-)	Effective Diffusion Coefficient [1] (cm^2/s)	Dry Bulk Density (g/cm^3)	Porosity (-)	Particle Density (g/cm^3) [2]
8.2E-14	0.0040	6.4E-08 (NaCl)	2.54	0.1578	3.02

[1] $D_e = \tau \times D_m$ (Assuming a D_m for a representative species (NaCl) of 1.6E-5 cm^2/s (Bruins 2003) with the τ of 0.0040, the D_e would be 6.4E-08 cm^2/s.)

[2] Particle density calculated as $\rho_s = \rho_b / (1 - \eta)$.

Table 3-6. Summary SIMCO E-Area Vault Concrete Average Water Retention Data (SIMCO 2011a).

Relative Humidity (%)	33	50	75	85	92	100
Average Saturation (-)	0.55	0.65	0.89	0.86	0.90	1.00
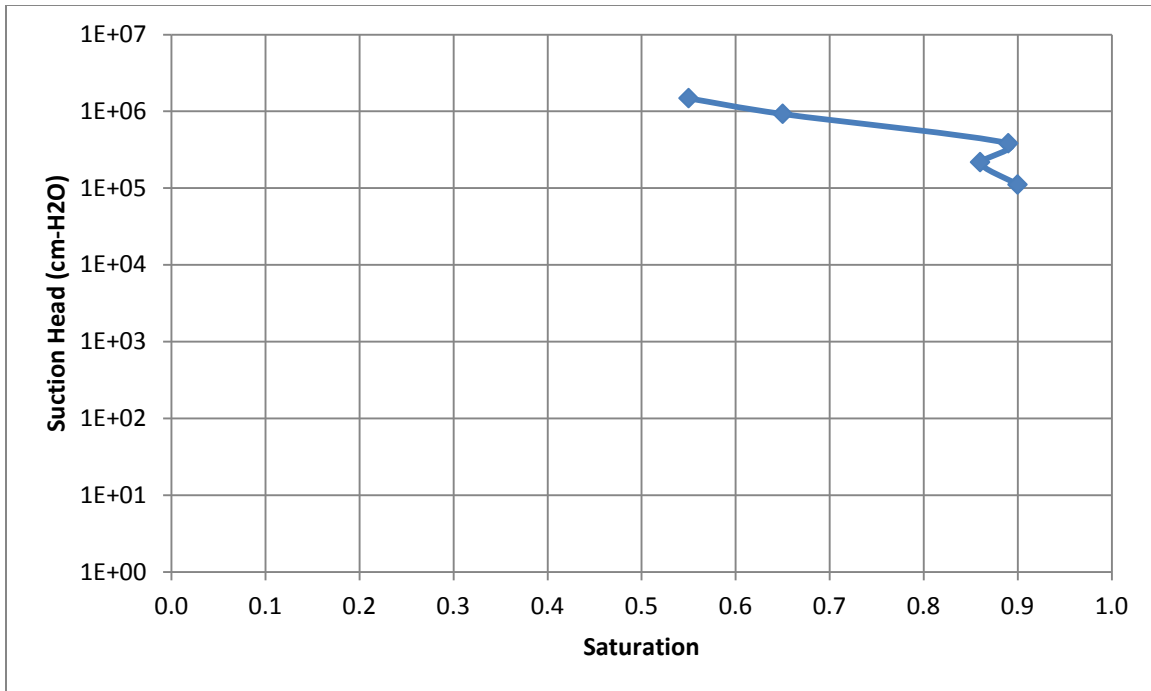
Figure 3-6. SIMCO E-Area Vault Concrete Average Water Retention Data.

3.5 <u>E-Area Vault Concrete Hydraulic and Physical Property Summary and Recommendations</u>

Table 3-7 provides a summary of the nominal hydraulic and physical property values utilized in the 2008 ELLWF PA along with the property values as measured by the three laboratories. Additionally Table 3-7 provides the recommended nominal property values for use in future PA and Special Analysis (SA) modeling. The following provides the rationale for these recommendations:

- It is recommended that a saturated hydraulic conductivity of 1.0E-12 cm/s be utilized as the nominal value. As outlined in Section 3.3, MACTEC saturated hydraulic conductivity testing was conducted at relatively low gradients over a very short time frame resulting in very little measured outflow such that it is likely that equilibrium conditions required by the method were probably not achieved and measurement accuracy was probably an issue. Additionally, the method utilized by MACTEC has a practical limit of 1E-09 cm/sec. For these reasons the MACTEC results should not be utilized. As outlined in Section 3.4, the SIMCO results are considered to be the most accurate of the three because SIMCO is a leader in the field and the test methodology was designed specifically for cementitious materials. While the mix formulation and source of the E-Area vault concrete material tested by Core Laboratories was not documented and the samples were small which resulted in some uncertainty associated with the results (Section 3.2), the saturated hydraulic conductivity results were indicative of high quality concrete and formed the basis for the value used in the 2008 ELLWF PA. In order to maintain some conservatism, it is recommended that the previously used saturated hydraulic conductivity of 1.0E-12 cm/s continue to be used rather than the most recent results from SIMCO (i.e. 8.2E-14 cm/s).
- It is recommended that a tortuosity of 0.0040 and an effective diffusion coefficient of 6.4E-08 cm^2/s (NaCl) be utilized as the nominal values. The 2008 ELLWF PA effective

diffusion coefficient and resulting tortuosity values used represented high quality concrete based upon a literature review (Phifer et al. 2006). Only SIMCO conducted testing of the E-Area concrete for these parameters. The assumed values utilized in the 2008 ELLWF PA are very similar to the tested values produced by SIMCO. Therefore it is recommended that the SIMCO values be utilized as the nominal values.

- It is recommended that 2.54 g/cm^3, 0.158, and 3.02 g/cm^3, be utilized as the nominal values for dry bulk density, porosity, and particle density, respectively. As outlined in Section 3.2, the mix formulation and source of the E-Area vault concrete material tested by Core Laboratories was not documented and therefore significant uncertainties are associated with the results. The SIMCO results are considered the best due to their concrete testing qualifications relative to those of MACTEC.

Figure 3-7 provides a graph of the characteristic curves utilized in the 2008 ELLWF PA along with the water retention test results produced by MACTEC and SIMCO. As outlined in Section 3.2, the methodology utilized by Core Laboratories was inappropriate for the determination of water retention characteristics and therefore their reported results are not reproduced in Figure 3-7. The air entry pressure of a material is the pressure required to force air into the largest pores of the material. Typical concrete air entry pressures range from 1.0E+05 to 5.0E+05 cm-H_2O (Rockhold et al. 1993; Savage and Jassen 1997; Baroghel-Bounty et al. 1999; and Phifer et al. 2006). As seen in Figure 3-7 the air entry pressure associated with the MACTEC water retention test results would be significantly less than 100 cm-H_2O. Based upon the MACTEC results, at a pressure of 102 cm-H_2O, the saturation of the concrete was 96%. This would indicate that air had already entered at a pressure three orders of magnitude below that documented within the literature. It is more likely that the procedures used by MACTEC allowed evaporation from the samples to occur resulting in erroneous results. Based upon this the MACTEC results should not be utilized. As seen in Figure 3-7 the SIMCO water retention results closely follow the PA suction head curve utilized within the 2008 ELLWF PA and confirms that the characteristic curves utilized in the 2008 ELLWF PA are reasonable and should continue to be utilized as the nominal representation. The recommended E-Area vault concrete characteristic curve data are reproduced in Table 3-8.

Table 3-7. E-Area Vault Concrete Property Summary and Recommendations.

Data Set	Saturated Hydraulic Conductivity (cm/s)	Tortuosity (-)	Effective Diffusion Coefficient (cm²/s)	Dry Bulk Density (g/cm³)	Porosity (-)	Particle Density (g/cm³)
2008 ELLWF PA	1.0E-12	0.0031	5.0E-08 (NaCl)	2.11	0.184	2.59
Core Laboratories	1.04E-12	na	na	2.11	0.184	2.59
MACTEC	5.0E-10	na	na	2.22	0.125	2.54
SIMCO	8.2E-14	0.0040	6.4E-08 [1] (NaCl)	2.54	0.1578	3.02
Recommended Value	1.0E-12	0.0040	6.4E-08 [1] (NaCl)	2.54	0.158	3.02

Note to Table 3-7:

- na = not analyzed

[1] $D_e = \tau \times D_m$ (Assuming a D_m for a representative species (NaCl) of 1.6E-5 cm^2/s (Bruins 2003) with a τ of 0.0040, the D_e would be 6.4E-08 cm^2/s.)
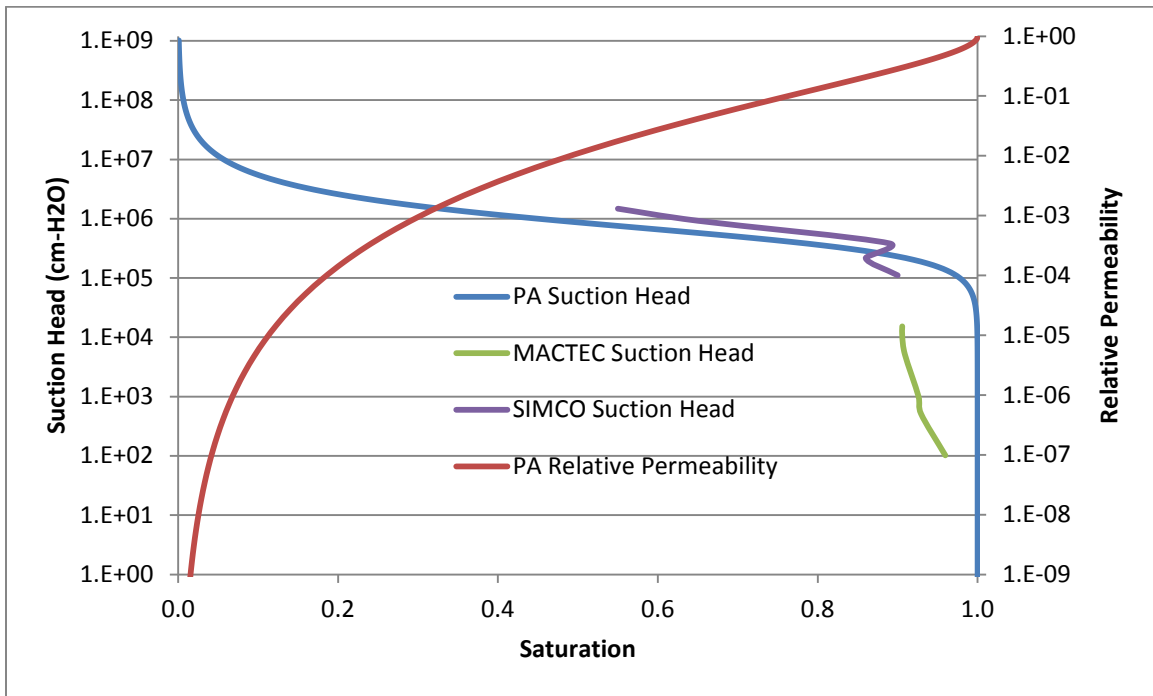
Figure 3-7. E-Area Vault Concrete Characteristic Curves Summary and Recommendations.

Table 3-8. Recommended E-Area Vault Concrete Characteristic Curve Data.

Saturation S [1] (-)	Suction Head ψ (cm)	Relative Permeability kr [1] (-)	Saturation S [1] (-)	Suction Head ψ (cm)	Relative Permeability kr [1] (-)	Saturation S [1] (-)	Suction Head ψ (cm)	Relative Permeability kr [1] (-)
1	0	1	0.9980	2.86E+04	8.64E-01	0.0949	5.80E+06	4.45E-06
1.0000	5.00E-02	1.00E+00	0.9973	3.29E+04	8.46E-01	0.0832	6.67E+06	2.43E-06
1.0000	1.00E-01	1.00E+00	0.9965	3.79E+04	8.25E-01	0.0730	7.67E+06	1.32E-06
1.0000	2.00E-01	1.00E+00	0.9954	4.35E+04	8.02E-01	0.0640	8.82E+06	7.21E-07
1.0000	5.00E-01	1.00E+00	0.9940	5.01E+04	7.76E-01	0.0561	1.01E+07	3.93E-07
1.0000	1.00E+00	1.00E+00	0.9922	5.76E+04	7.46E-01	0.0492	1.17E+07	2.14E-07
1.0000	2.00E+00	1.00E+00	0.9898	6.62E+04	7.14E-01	0.0432	1.34E+07	1.16E-07
1.0000	5.00E+00	1.00E+00	0.9867	7.61E+04	6.78E-01	0.0378	1.54E+07	6.34E-08
1.0000	1.00E+01	1.00E+00	0.9826	8.76E+04	6.38E-01	0.0332	1.77E+07	3.45E-08
1.0000	2.00E+01	1.00E+00	0.9774	1.01E+05	5.95E-01	0.0291	2.04E+07	1.88E-08
1.0000	5.00E+01	1.00E+00	0.9707	1.16E+05	5.48E-01	0.0255	2.35E+07	1.02E-08
1.0000	1.00E+02	9.99E-01	0.9621	1.33E+05	4.98E-01	0.0223	2.70E+07	5.55E-09
1.0000	2.00E+02	9.99E-01	0.9511	1.53E+05	4.46E-01	0.0196	3.10E+07	3.02E-09
1.0000	5.00E+02	9.97E-01	0.9373	1.76E+05	3.91E-01	0.0172	3.57E+07	1.64E-09
1.0000	1.00E+03	9.94E-01	0.9200	2.03E+05	3.36E-01	0.0150	4.10E+07	8.93E-10
1.0000	1.15E+03	9.93E-01	0.8988	2.33E+05	2.82E-01	0.0132	4.72E+07	4.86E-10
1.0000	1.32E+03	9.92E-01	0.8731	2.68E+05	2.30E-01	0.0116	5.43E+07	2.64E-10
1.0000	1.52E+03	9.91E-01	0.8426	3.08E+05	1.82E-01	0.0101	6.24E+07	1.44E-10
1.0000	1.75E+03	9.90E-01	0.8070	3.54E+05	1.39E-01	0.0089	7.18E+07	7.81E-11
1.0000	2.01E+03	9.89E-01	0.7667	4.07E+05	1.03E-01	0.0078	8.25E+07	4.25E-11
1.0000	2.31E+03	9.87E-01	0.7221	4.68E+05	7.32E-02	0.0068	9.49E+07	2.31E-11
1.0000	2.66E+03	9.85E-01	0.6740	5.39E+05	5.04E-02	0.0060	1.09E+08	1.26E-11
1.0000	3.06E+03	9.83E-01	0.6236	6.20E+05	3.35E-02	0.0052	1.25E+08	6.83E-12
1.0000	3.52E+03	9.81E-01	0.5721	7.13E+05	2.15E-02	0.0046	1.44E+08	3.72E-12
1.0000	4.05E+03	9.78E-01	0.5209	8.19E+05	1.34E-02	0.0040	1.66E+08	2.02E-12
0.9999	4.65E+03	9.75E-01	0.4710	9.42E+05	8.19E-03	0.0035	1.91E+08	1.10E-12
0.9999	5.35E+03	9.71E-01	0.4233	1.08E+06	4.87E-03	0.0031	2.19E+08	5.98E-13
0.9999	6.15E+03	9.67E-01	0.3785	1.25E+06	2.85E-03	0.0027	2.52E+08	3.25E-13
0.9999	7.08E+03	9.63E-01	0.3371	1.43E+06	1.64E-03	0.0024	2.90E+08	1.77E-13
0.9998	8.14E+03	9.58E-01	0.2991	1.65E+06	9.33E-04	0.0021	3.34E+08	9.61E-14
0.9998	9.36E+03	9.52E-01	0.2647	1.90E+06	5.25E-04	0.0018	3.84E+08	5.23E-14
0.9997	1.08E+04	9.45E-01	0.2338	2.18E+06	2.93E-04	0.0016	4.41E+08	2.84E-14
0.9996	1.24E+04	9.37E-01	0.2061	2.51E+06	1.63E-04	0.0014	5.08E+08	1.55E-14
0.9995	1.42E+04	9.29E-01	0.1815	2.88E+06	9.00E-05	0.0012	5.84E+08	8.41E-15
0.9993	1.64E+04	9.19E-01	0.1596	3.31E+06	4.96E-05	0.0011	6.71E+08	4.57E-15
0.9991	1.88E+04	9.08E-01	0.1403	3.81E+06	2.72E-05	0.0009	7.72E+08	2.49E-15
0.9988	2.16E+04	8.95E-01	0.1232	4.38E+06	1.49E-05	0.0008	8.88E+08	1.35E-15
0.9985	2.49E+04	8.80E-01	0.1081	5.04E+06	8.15E-06	0.0007	1.02E+09	7.35E-16

[1]　All saturation and relative permeability values are unique; the number of significant figures provided in the table was selected for clarity.

3.6 E-Area Vault Concrete Hydraulic and Physical Property Uncertainty Representation

Based upon a literature review (Phifer et al. 2006) Table 3-9 provides the typical ranges of values for concrete hydraulic and physical properties for comparison to the recommended values for the E-Area vault concrete from Table 3-7. Because the typical range of concrete values provided in Table 3-9 represents a range of concrete formulations that underwent different degrees of curing, the uncertainty associated with the E-Area vault concrete recommended values would be small in comparison to the typical range of concrete values. Because the SIMCO results essentially represent one measurement per property, an uncertainty cannot be assigned based upon the SIMCO results alone. Multiple E-Area vault concrete results from the Core Laboratory testing, however, are available for saturated hydraulic conductivity, dry bulk density, porosity, and particle density (Table 3-2). Therefore the recommended uncertainty distributions provided in Table 3-10 are based upon the uncertainty distributions developed for the Core Laboratory results (see Table 3-2). The standard deviation of the mean has been adjusted from the values provided

in Table 3-2 for dry bulk density, porosity, and particle density based upon the proportionality of the recommended values to that of the average value in Table 3-2. The uncertainty distributions for the recommended saturated hydraulic conductivity are the same as those provided in Table 3-2.

The log saturated effective diffusion coefficient standard deviation of the mean can be reasonably derived from that of the associated log saturated hydraulic conductivity standard deviation of the mean (Phifer et al. 2006). This is considered reasonable because both the saturated hydraulic conductivity and saturated effective diffusion coefficient of cementitious materials are dependent upon the pore structure characteristics (i.e., porosity, pore size distribution, connectivity of pores, and extent of separation and microcracking at aggregate paste interfaces). As shown in Table 3-9 the typical range of concrete saturated hydraulic conductivity is from 1.0E-13 to 1.0E-08 cm/s (i.e., 5 orders of magnitude), whereas that of concrete saturated effective diffusion coefficient is from 1.0E-08 to 5.0E-07 cm^2/s (i.e., 1.7 orders of magnitude). Based upon these ranges and the link between conductivity and diffusivity, the log saturated effective diffusion coefficient standard deviation of the mean for these materials will be assigned that of their respective log saturated hydraulic conductivity standard deviation of the mean modified by the factor 1.7/5. The tortuosity distribution has been derived from that of the effective diffusion coefficient as outlined in a note to Table 3-10.

Table 3-9. Typical Range of Concrete Property Values versus E-Area Vault Concrete Recommended Nominal Values.

Data Set	Saturated Hydraulic Conductivity (cm/s)	Tortuosity (-)	Effective Diffusion Coefficient (cm^2/s)	Dry Bulk Density (g/cm^3)	Porosity (-)	Particle Density (g/cm^3)
Literature Range	1.0E-13 to 1.0E-08 [1]	0.0006 to 0.025 [2]	1.0E-08 to 5.0E-07	1.90 to 2.70	0.09 to 0.20	2.4 to 3.0 [3]
Recommended Value	1.0E-12	0.0040	6.4E-08 (NaCl)	2.54	0.158	3.02

[1] A saturated hydraulic conductivity of 1.0E-10 to 1.0E-12 cm/s is more typical for high quality concrete.

[2] $\tau = D_e \div D_m$ (Assuming a D_m for a representative species (NaCl) of 1.6E-5 cm^2/s (Bruins 2003) the τ would range from 0.025 to 0.0006 based upon a D_e range of 4.0E-07 to 1.0E-08 cm^2/s.)

[3] Particle density calculated as $\rho_s = \rho_b / (1- \eta)$.

Table 3-10. Recommended E-Area Vault Concrete Uncertainty Distributions.

Uncertainty Distribution Parameter	Saturated Hydraulic Conductivity (cm/s)	Log Saturated Hydraulic Conductivity (cm/s)	Tortuosity [1] (-)	Log Tortuosity [1] (-)	Saturated Effective Diffusion Coefficient (cm^2/s)	Log Saturated Effective Diffusion Coefficient (cm^2/s)	Dry Bulk Density (g/cm^3)	Porosity (-)	Particle Density (g/cm^3)
Recommended Nominal Value	1.00E-12	-12.00	0.004	-2.40	6.40E-08	-7.19	2.540	0.158	3.02
Distribution Type	-	normal [2]	-	normal [2]	-	normal [2]	normal	normal	normal
Standard Deviation of Mean	-	0.074	-	0.025	-	0.025	0.0125	0.0064	0.0313
Variance of the Mean	-	0.0055	-	0.000635	-	0.000635	0.000157	0.000041	0.000977
Mean Minimum (3 sigma)	-	-12.22	-	-2.47	-	-7.27	2.502	0.139	2.926
Mean Maximum (3 sigma)	-	-11.78	-	-2.32	-	-7.12	2.578	0.177	3.114

[1] $\tau = D_e \div D_m$ (Assuming a D_m for a representative species (NaCl) of 1.6E-5 cm^2/s (Bruins 2003))

[2] Saturated hydraulic conductivity, tortuosity, and effective diffusion coefficient are log normally distributed therefore the log of saturated hydraulic conductivity, tortuosity, and effective diffusion coefficient is normally distributed

4.0 LAW and IL Vault Durability/Degradation Projections

A 2006 LAW Vault structural analysis (Carey, 2006) and a 2006 IL Vault structural analysis (Peregoy, 2006) based upon rebar corrosion as the predominant concrete degradation mechanism were conducted and utilized as input to the 2008 ELLWF PA (WSRC 2008). Since issuance of the 2008 ELLWF PA (WSRC 2008) two ELLWF vault concrete durability modeling studies have been completed. An evaluation of the implications of these two ELLWF vault concrete durability modeling studies on the degradation assumptions utilized in the 2008 ELLWF PA (WSRC 2008) are presented in the following sections.

4.1 <u>2006 LAW Vault Structural Degradation Prediction (Carey 2006)</u>

Carey 2006 conducted a Monte Carlo structural degradation prediction analysis of the LAW Vault. The analysis consisted of 1) structural analysis considering applicable degradation mechanisms to estimate cracking due to static and seismic loads and predicting the time of collapse (collapse analysis); and 2) a separate structural analysis to estimate the extent of cracking for both static and seismic induced differential settlements (differential settlement analysis). The analysis was based upon the following primary assumptions:

- The mean thickness of the overlying closure cap was taken as nine feet.
- Oxic and anoxic rebar corrosion was considered the primary concrete degradation mechanism in the analysis. Anoxic corrosion in a high pH environment (0.00008 cm/yr) was considered for all rebar. A two-step oxic rebar corrosion (i.e. breakdown of passivating layer followed by oxic corrosion) was considered for the top and bottom rebar.
- Sulfate and magnesium attack, alkali and calcium hydroxide leaching, and carbonation were considered negligible and were neglected in the analysis.
- Cracks due to differential settlement do not affect the primary load path of the building and will not affect the collapse of the structure. Therefore differential settlement can be considered independently of the collapse analysis.

Carey 2006 documented the following significant degradation points in the life of the LAW Vault:

- Upon placement of the closure cap overburden over the LAW Vault, non-through slab static cracking of the roof slab will occur and remain fairly constant over time.
- Upon placement of the closure cap overburden over the LAW Vault, non-through wall static cracking of the exterior side walls will occur and increase slightly over time.
- It is anticipated that the LAW Vault roof slab will collapse due to closure cap and seismic loading and rebar corrosion at a mean time of 2805 years with a standard deviation of 920 years.
- It is anticipated that the LAW Vault exterior side walls will collapse due to closure cap and seismic loading and rebar corrosion at a mean time of 9415 years with a standard deviation of 2290 years.
- It is anticipated that differential settlement due to seismic loading could result in side wall through-wall cracking that opens into the roof slab. The probability of such an event occurring over a 1000 year period has been determined to be 0.8%.
- It is anticipated that differential settlement due to seismic loading could result in side wall through-wall cracking that opens into the footer. The probability of such an event occurring over a 1000 year period has been determined to be 1.2%.

- Within 50 to 100 years after placement of the closure cap overburden over the LAW Vault, it is anticipated that differential settlement between the footers and floor slab will occur due to static (i.e. closure cap) loading differences between the two. This will result in a separation between the footers and floor slab.
- It is anticipated that differential settlement beneath the floor slab due to seismic loading could result in flexural cracking of the floor slab. The probability of such an event occurring over a 1000 year period has been estimated to be 50%.

4.2 <u>LAW Vault Structural Degradation Considerations in 2008 ELLWF PA</u>

The LAW Vault structural degradation prediction by Carey 2006 (see Section 4.1) was incorporated into the LAW Vault vadose-zone groundwater flow and transport modeling as outlined in Section 3.6.4.2 of the 2008 ELLWF PA (WSRC 2008). Based upon the degradation prediction two LAW Vault vadose zone cross-sections were evaluated. The first cross-section included only that cracking that had a probability of unity. Cracking with a probability of unity included non-through slab static cracking of the roof slab and side walls due to placement of the closure cap overburden and separation of the footers and floor slab due to differential settlement resulting from placement of the closure cap overburden. The second cross-section included all cracking, both that with and without a probability of unity. The additional cracking considered for the second cross-section included the seismically induced through slab cracking of the roof slab and side walls. The estimates of crack sizes, locations, and timing for each major structural component of the LAW Vault, provided by Carey 2006, was used to adjust the saturated hydraulic conductivity (K_{sat}) of the concrete from its intact value of 1.0E-12 cm/s (Phifer et al. 2006) for both the first and second cross-sections based upon the National Institute of Standards and Technology approach (Snyder 2003). No crack healing or infilling was assumed. Infilling will reduce the K_{sat} for the crack, which typically will produce slower water movement and slower transport of contaminants. Each cross-section was independently analyzed in separate vadose zone models. Vadose zone results (in terms of contaminant flux to the water table) from each cross-section were subsequently combined in the aquifer transport analyses by applying length-weighting factors based on the length of each cross-section relative to the overall length of one LAW Vault module. Based upon the geometry of anticipated cracking and its zone of influence a length-weighting factor of 0.96885 was assigned to the first cross-section and 0.03115 to the second cross-section. Carey 2006 (see Section 4.1) estimated that the LAW Vault roof would structurally fail at a mean time of 2,805 years with a standard deviation of 920 years, however within the vadose-zone groundwater flow and transport modeling it was assumed that the roof would fail at 1,800 years after placement of the closure cap overburden. At roof failure it was assumed that the LAW Vault roof would collapse into the vault itself and that subsidence of the overlying closure cap would occur due to the estimated subsidence potential of approximately 21 feet (Jones and Phifer 2006). At collapse only one LAW Vault vadose-zone cross-section was necessary.

4.3 <u>2006 IL Vault Structural Degradation Prediction (Peregoy 2006)</u>

Peregoy 2006 conducted a structural degradation prediction analysis of the IL Vault. The analysis consisted of: 1) Monte Carlo structural analysis considering applicable degradation mechanisms to predict the time of roof and side collapse due to static and seismic loads; 2) structural analysis to predict the extent and depth of cracking due to static loads; and 3) structural analysis to evaluate the effects of differential settlement due to large seismic events. The analysis was based upon the following primary assumptions:

- The mean thickness of the overlying closure cap was taken as eight feet.

- Oxic and anoxic rebar corrosion was considered the primary concrete degradation mechanism in the analysis. Anoxic corrosion in a high pH environment (0.00008 cm/yr) was considered for all rebar. A two-step oxic rebar corrosion (i.e. breakdown of passivating layer followed by oxic corrosion) was considered for the top and bottom rebar.

Peregoy 2006 documented the following significant degradation points in the life of the IL Vault:

- Upon placement of the closure cap overburden over the IL Vault, non-through-slab static cracking of the roof slab will occur and increase slightly over time.
- Upon placement of the closure cap overburden over the IL Vault, non-through-wall static cracking of the exterior side and end walls will occur and increase slightly over time.
- It is anticipated that the IL Vault roof slab will collapse due to closure cap and seismic loading and rebar corrosion at a mean time of 6703 years with a standard deviation of 1976 years. While the space between disposed containers is grouted, the containers themselves contain significant internal void space, therefore collapse is assumed due to this void space.
- It is anticipated that the IL Vault roof slab will collapse due to rebar corrosion and a beyond Performance Category 4 (PC-4) earthquake event, if the PC-4 earthquake occurs at 5985 years or after. A PC-4 earthquake is one with a recurrence interval of 10,000 years at the facility location (DOE 2002). The probability of a beyond-PC-4 earthquake is 3% over a 1,000 year period.
- It is anticipated that the IL Vault exterior side and end walls will collapse due to closure cap and seismic loading and rebar corrosion at a mean time of 9427 years with a standard deviation of 2795 years.
- It is anticipated that differential settlement due to PC-4 seismic loading or greater will result in cracking of the ILNT Cell #4 floor slab construction and control joints and extend a limited distance up the associated exterior wall vertical construction and control joints. The probability of a PC-4 earthquake is 9.5% over a 1,000 year period.

4.4 IL Vault Structural Degradation Considerations in 2008 ELLWF PA

The IL Vault structural degradation prediction by Peregoy 2006 (see Section 4.3) was incorporated into the IL Vault vadose-zone groundwater flow and transport modeling as outlined in Section 4.6.3.2 and Table 4-2 of the 2008 ELLWF PA (WSRC 2008). Upon placement of the closure cap overburden over the IL Vault, Peregoy 2006 estimated that non-through-slab static cracking of the roof slab, exterior side, and end walls would occur and increase slightly over time. The estimates of crack sizes and locations at 5,000 years were utilized to adjust the K_{sat} of the roof slab, exterior side, and end wall concrete from its intact value of 1.0E-12 cm/s (Phifer et al. 2006), which was then incorporated in the model, beginning at time zero. The method of calculating the K_{sat} was based upon the NIST approach (Snyder 2003). No crack healing or infilling was assumed. Infilling will reduce the K_{sat} for the crack, which typically will produce slower water movement and slower transport of contaminants. Based upon the estimated impact to the Cell #4 (i.e., center cell) floor and walls due to differential settlement predicted from a PC-4 earthquake (Peregoy 2006), through wall cracking of Cell #4 floor and walls was assumed to occur at 400 years and the Cell #4 floor and walls were assigned gravel hydraulic properties at that time. In order to take this into account a separate simulation was conducted for Cell 4. Peregoy 2006 (see Section 4.3) estimated that the IL Vault roof would structurally fail at a mean time of 6,703 years with a standard deviation of 1,976 years, however within the vadose-zone groundwater flow and transport modeling it was assumed that the roof would fail at 1,900 years after placement of the closure cap overburden. At roof failure it was assumed that the IL Vault

roof would collapse into the vault itself and that subsidence of the overlying closure cap would occur due to an estimated maximum subsidence potential of 19 feet.

4.5 2009 E-Area Vault Concrete Durability Simulations (Langton 2009)

Durability (i.e. service life) simulations of the E-Area vault concrete were conducted by SIMCO Technologies, Inc. utilizing their STADIUM® ionic transport and chemical equilibrium modules (SIMCO 2011) based upon a concrete surrogate, for which necessary data existed (Langton 2009). Table 4-1 provides the formulation and properties for the surrogate concrete, which can be compared to the E-Area Vault concrete formulation and properties provided in Table 2-1. The STADIUM® ionic transport module (SIMCO 2011) simulates the ingress of the contaminants and leaching of the ionic species in the pore solution in saturated/unsaturated, isothermal/non-isothermal cementitious materials (i.e. pore solution concentrations over time). The STADIUM® chemical equilibrium module (SIMCO 2011) simulates the equilibrium between the pore solution concentrations and the solid phases of the hydrated cement paste: portlandite (calcium hydroxide), calcium silicate hydrate (C-S-H), ettringite, mono-sulfates, etc. and the resulting modifications to the microstructure of the cementitious material (i.e. solid phase mineralogy and porosity over time).

The one-dimensional service life simulations were based upon the case illustrated in Figure 4-1 with the vadose zone water and leachate characteristics outlined in Table 4-2 (Langton 2009). A 30 cm thick concrete cross-section was selected for modeling because 1-foot thick concrete with the Table 2-1 concrete formulation is the minimum exterior concrete thickness for the LAW and IL Vaults (WSRC 2008) (i.e. LAW Vault concrete floor is 1-foot thick). Assuming a leachate solution on one side of the concrete and vadose zone pore water on the other side is also a conservative assumption. It is not likely that leachate will be constantly in contact with all LAW and IL Vault interior concrete. The LAW Vault should not fill up with water because it is anticipated that differential settlement between the footers and floor slab will occur (Carey 2006) providing a significant pathway for water release from the LAW Vault. The IL Vault interior will be filled with grout and Controlled Low Strength Material (CLSM), and it is not anticipated that the CLSM, in particular, will be saturated due to its drainage characteristics which are similar to soil. It is also anticipated that the vadose zone surrounding the vaults will be significantly unsaturated due to the overlying closure cap which will limit infiltration.

The simulation indicates that the primary result of E-Area vault concrete contact with leachate on one side and vadose zone pore water on the other is decalcification (portlandite dissolution and C-S-H crystalline calcium aluminate hydrates decalcification) and a resulting increase in porosity (Langton 2009). Concrete degradation due to chloride-induced corrosion, sulfate attack, and carbonation-induced corrosion were discounted due to very low anticipated concentrations of Cl^-, SO_4^{-2}, and carbonate in the leachate or vadose zone water. Table 4-3 provides the decalcification prediction. As can be seen from Table 4-3 the prediction of the decalcification depth is pH dependent as follows:

- Sides exposed to water with a pH of 12.4 had no decalcification and no porosity increase,
- Sides exposed to water with a pH of 11.1 had a maximum decalcification depth of 1.5 cm with an accompanying porosity increase over 2,000 years, and
- Sides exposed to water with a pH of 9.4 or less had a decalcification depth ranging from 2.2 to 2.6 cm with an accompanying porosity increase over 2,000 years.

The typical concrete cover for reinforcing steel (rebar) in both the LAW and IL Vaults is 2.375 inches (Drawings SE5-6-2008801 and SE5-6-2003318). The simulation indicates that the zone of

decalcification and porosity increase does not reach the rebar within the time period assumed for vault collapse within the 2008 ELLWF PA (WSRC 2008), which is 1,800 years for the LAW Vault and 1,900 years for the IL Vault. So increased rebar corrosion due to concrete mineralogical changes does not appear to be a concern prior to the assumed vault collapse. Therefore this E-Area vault concrete durability simulation conforms with and provides additional justification for the LAW and IL Vault structural degradation predictions produced by Carey 2006 and Peregoy 2006, respectively.

Table 4-1. E-Area Vault Surrogate Concrete Formulation and Properties (Langton 2009).

Ingredient	Quantity
Type I cement	295 lbs/yd^3 (175 kg/m^3)
Blast furnace slag	177 lbs/yd^3 (105 kg/m^3)
Type F Fly ash	118 lbs/yd^3 (70 kg/m^3)
Fine aggregates	1,315lbs/yd^3 (780 kg/m^3)
Coarse aggregates	1,669 lbs/yd^3 (990 kg/m^3)
Water to cementitious material ratio	0.45
Property	**Value**
Porosity	12.4%
Tortuosity	0.00493
Saturated Hydraulic Conductivity (Permeability)	4.2E-13 cm/s (4.3E-22 m^2)
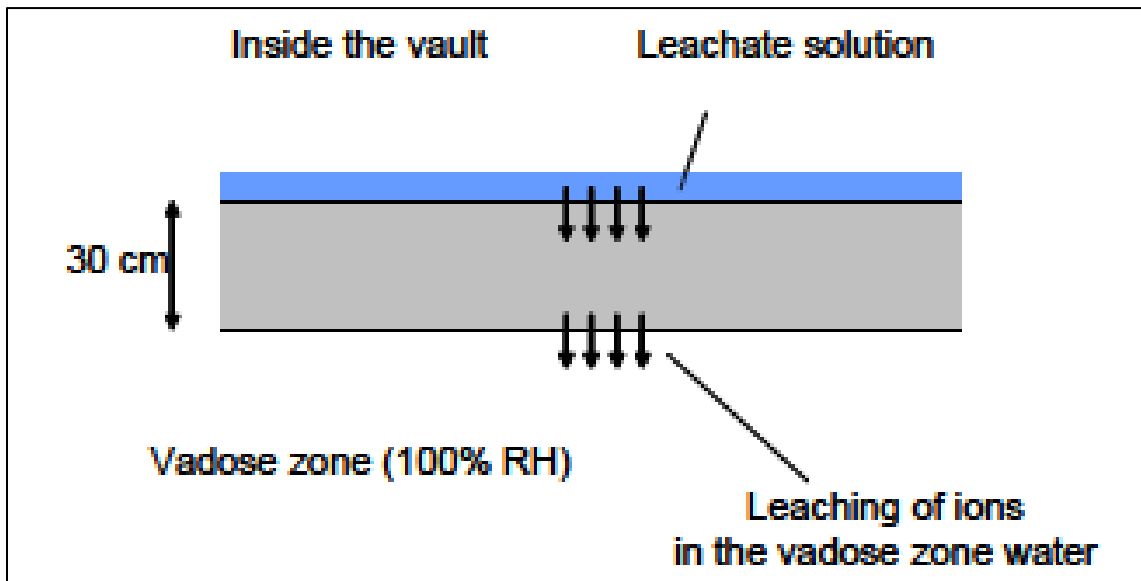
Figure 4-1. One-Dimensional Case Simulated (Langton 2009).

Table 4-2. Assumed Leachate and Vadose Zone Water (Langton 2009).

Ionic Species	Concentration (mmol/L)			
	pH=7.0 Vadose Zone Water	pH=9.4 Leachate	pH=11.1 Leachate	pH=12.4 Leachate
OH$^-$	0	1.23	5.63	42.83
Na$^+$	0	0.13	0.13	0.13
Ca^{+2}	0	1.00	3.2	21.8
Al(OH)$^{-4}$	0	0.90	0.90	0.90

Table 4-3. Concrete Decalcification (Langton 2009).

pH=9.4			pH=11.1			pH=12.4		
Years	x=0 (cm)	x=L (cm)	Years	x=0 (cm)	x=L (cm)	Years	x=0 (cm)	x=L (cm)
50	0.312	0.425	50	0.204	0.425	50	0.0	0.425
100	0.542	0.542	100	0.204	0.542	100	0.0	0.542
250	0.790	0.921	250	0.425	0.921	250	0.0	0.921
500	1.201	1.349	500	0.663	1.201	500	0.0	1.058
750	1.503	1.503	750	0.790	1.503	750	0.0	1.503
1000	1.829	1.829	1000	0.921	1.829	1000	0.0	1.663
1500	2.183	2.182	1500	1.201	2.182	1500	0.0	1.829
2000	2.565	2.370	2000	1.503	2.370	2000	0.0	2.182

Notes to Table 4-3:
- The C-S-H phase decalcification depth corresponds to the position where the C-S-H has lost 80% of its portlandite-like fraction.
- X=0 is the decalcification depth from the leachate side (Figure 4-1)
- X=L is the decalcification depth from the vadose zone pore water side (Figure 4-1)

4.6 <u>2012 SIMCO E-Area Concrete Long-Term Durability Simulation (SIMCO 2012)</u>

As outlined in Section 3.4, hydraulic and physical property testing of E-Area vault concrete (see Table 2-1 for the formulation) was conducted by SIMCO Technologies, Inc. (SIMCO 2011a). Table 3-5 provides a summary of these test results. New service life simulations with the input of this actual E-Area concrete data were conducted by SIMCO Technologies, Inc. (SIMCO 2012) utilizing their STADIUM® ionic transport and chemical equilibrium modules (SIMCO 2011). Section 4.5 provides a brief description of the STADIUM® ionic transport and chemical equilibrium modules. Appendix B provides the 2012 SIMCO report.

The one-dimensional scenarios outlined in Figures 4-2 through 4-4 were modeled by SIMCO. Scenario 1 (Figure 4-2) is the same scenario reported by Langton 2009, but it uses the measured E-Area vault concrete data rather than that from a concrete surrogate. Scenarios 2 and 3 took into account carbonation that could occur from vault opening (i.e. 1994) to the assumed sealing of the vaults (i.e. 2025) and the assumed construction of a closure cap over the vaults (i.e. 2125), respectively (WSRC 2008). Based upon the SIMCO E-Area vault concrete hydraulic and physical property testing documented in SIMCO 2011a, a carbonation front extended into the ELLWF concrete test wall approximately 16 mm and occurred over an 18 year exposure period (ELLWF concrete test wall was constructed around 1992 and the core was delivered to SIMCO in 2010). The depth of carbonation is roughly proportional to the square root of time for concrete

kept continuously dry at normal relative humidities (Duncan and Reigel 2011) as shown in the following equation:

$$X_C = A(t)^{1/2}$$

Where, X_c = distance of the carbonation front, t = time and A = materials constant

Based upon a carbonation depth of 16 mm over 18 years the materials constant, A, would be 3.7 mm/yr$^{1/2}$. From vault opening (i.e. 1994) to the assumed sealing of the vaults (i.e. 2025), a carbonation depth of 2 cm (0.8 inches) is estimated from the above equation (Figure 4-3, Scenario 2). From vault opening (i.e. 1994) to the assumed construction of a closure cap over the vaults (i.e. 2125), a carbonation depth of 4 cm (0.8 inches) is estimated (Figure 4-4, Scenario 3). Carbonation in the interior of the vault is assumed to stop once the vault is sealed, and carbonation on the exterior of the vault is assumed to stop once the vault is covered.

As with the simulation reported by Langton 2009, these simulations indicate that the primary result of E-Area vault concrete contact with leachate on one side and vadose zone pore water on the other is decalcification, even in cases where initial carbonation is considered. Concrete degradation due to chloride-induced corrosion, sulfate attack, and carbonation-induced corrosion were again discounted. Table 4-4 provides the maximum depth of decalcification predicted over 2,000 years, including the results of the simulation reported by Langton 2009 (see Table 4-3). A comparison of Scenario 1 with the previous scenario reported by Langton 2009 indicates that relative to decalcification the actual E-Area vault concrete preforms better than the previously modeled surrogate concrete. Additionally, consideration of initial carbonization actually reduces the maximum predicted decalcification thickness, due to pore clogging by calcite near the concrete boundaries. Therefore these simulations also indicate that the zone of decalcification does not reach the rebar within the time period assumed for vault collapse within the 2008 ELLWF PA (WSRC 2008), which is 1,800 years for the LAW Vault and 1,900 years for the IL Vault. So increased rebar corrosion due to concrete mineralogical changes does not appear to be a concern prior to the assumed vault collapse. Therefore these E-Area vault concrete durability simulations conform with and provide additional justification for the LAW and IL Vault structural degradation predictions produced by Carey 2006 and Peregoy 2006, respectively.
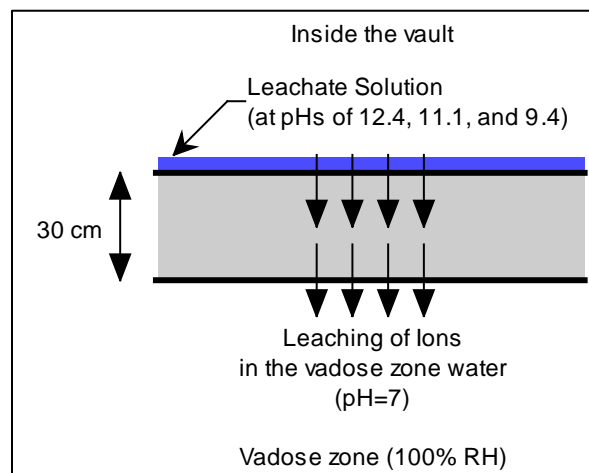
Figure 4-2. Scenario 1: 30 cm Thick Concrete with No Carbonation.
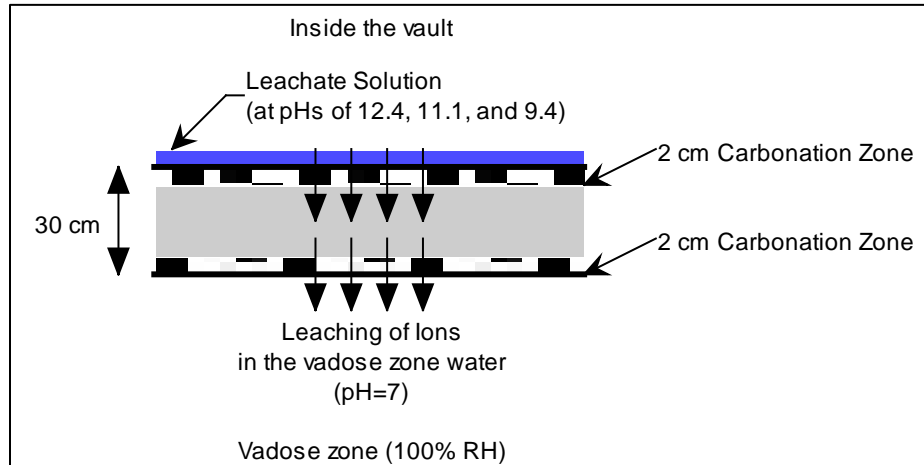
Figure 4-3. Scenario 2: 30 cm Thick Concrete with Carbonation (1994 to 2025).
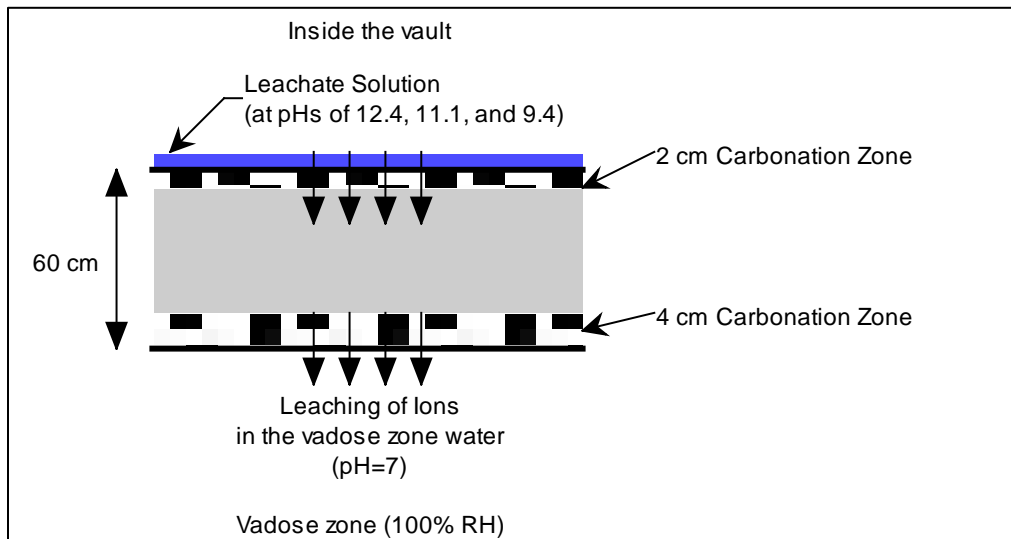
Figure 4-4. Scenario 3: 60 cm Thick Concrete with Carbonation (1994 to 2025).

Table 4-4. Maximum Depth of Decalcification Predicted over 2,000 Years.

pH	Previous Scenario (Langton 2009) (cm)	Scenario 1 (cm)	Scenario 2 (cm)	Scenario 3 (cm)
7	2.4	~2	~1.5	~1.6
9.4	2.6	~2	~1.5	~1.6
11.1	1.5	~0.3	~1	~1
12.4	0	0	~1	~1

4.7 <u>LAW and IL Vault Durability/Degradation Projection Summary and Recommendations</u>

Both the E-Area vault concrete durability simulations reported by Langton 2009 (Section 4.5) and those reported herein (Section 4.6) confirm and provide additional justification for the LAW and IL Vault structural degradation predictions produced by Carey 2006 and Peregoy 2006, respectively. The Carey 2006 and Peregoy 2006 predictions form the basis for the vault degradation assumptions utilized within the 2008 ELLWF PA (WSRC 2008). Therefore revised structural degradation predictions are not required so long as the mean thickness of the closure cap overlying the vaults is no greater than that assumed within Carey 2006 and Peregoy 2006. For the LAW Vault structural degradation prediction (Carey 2006) the mean thickness of the overlying closure cap was taken as nine feet. For the IL Vault structural degradation prediction Peregoy 2006), the mean thickness of the overlying closure cap was taken as eight feet.

5.0 Conclusions and Recommendations

The performance of the LAW and IL Vaults within the 2008 ELLWF PA (WSRC 2008) was primarily based upon the following:

- The E-Area vault concrete hydraulic and physical properties as determined from the 1993 materials characterization program (Yu et al. 1993).
- Structural analyses (Carey 2006 and Peregoy 2006) of the vaults that provided estimates of structural cracking and time of collapse.

Subsequent to the 2008 ELLWF PA, two additional E-Area vault concrete property testing programs have been conducted (Dixon and Phifer 2010 and SIMCO 2011a) and two additional E-Area vault concrete durability modeling projections have been made (Langton 2009 and SIMCO 2012). All the information/data from these reports has been evaluated and consolidated herein in order to produce E-Area vault concrete hydraulic and physical property data and vault durability/degradation projection recommendations that are adequately justified for use within pertinent SA and future PA updates.

Based upon this evaluation the following are recommended in regards to the E-Area vault concrete property values for use in ELLWF SAs and PAs:

- Utilize the property values provided in Table 5-1 below for saturated hydraulic conductivity, tortuosity, effective diffusion coefficient, dry bulk density, porosity, and particle density.
- Utilize the characteristic curve data provided in Table 3-8.
- Utilize the uncertainty distributions provided in Table 3-10.

The LAW and IL Vault structural degradation predictions produced by Carey 2006 and Peregoy 2006, respectively, remain valid based upon the results of the E-Area vault concrete durability simulations reported by Langton 2009 (Section 4.5) and those reported herein (Section 4.6). Therefore revised structural degradation predictions are not required so long as the mean thickness of the closure cap overlying the vaults is no greater than that assumed within Carey 2006 and Peregoy 2006. For the LAW Vault structural degradation prediction (Carey 2006) the mean thickness of the overlying closure cap was taken as nine feet. For the IL Vault structural degradation prediction (Peregoy 2006), the mean thickness of the overlying closure cap was taken as eight feet. The mean closure cap thicknesses as described here for both E-Area Vaults will be included as a key input and assumption (I&A) in the next revision to the closure plan for the ELLWF (Phifer et al. 2009).   In addition, it has been identified as new input to the PA model to

be assessed in the ongoing update to the new PA Information UDQE (Flach 2013). Once the UDQE is approved, the SWM Key I&A database will be updated with this new information.

Table 5-1. E-Area Vault Concrete Recommended Property Values.

Saturated Hydraulic Conductivity (cm/s)	Tortuosity (-)	Effective Diffusion Coefficient (cm²/s)	Dry Bulk Density (g/cm³)	Porosity (-)	Particle Density (g/cm³)
1.0E-12	0.0040	6.4E-08 [1] (NaCl)	2.54	0.158	3.02

[1] $D_e = \tau \times D_m$ (Assuming a D_m for a representative species (NaCl) of 1.6E-5 cm²/s (Bruins 2003) with a τ of 0.0040, the D_e would be 6.4E-08 cm²/s.)

6.0 References

Abramczyk, G. A. 2009. Personal correspondence on 2/12/09. (Glenn Abramczyk was the Assistant Project Manager in charge of the design and construction of the LAW and IL Vaults).

ASTM 2000. Standard Test Method for Capillary-Moisture Relationships for Coarse- and Medium-Textured Soils by Porous-Plate Apparatus, ASTM D 2325-68 (Reapproved 2000), ASTM International, West Conshohocken, PA. 2000.

ASTM 2004. Standard Test Methods for Measurement of Hydraulic Conductivity of Saturated Porous Materials Using a Flexible Wall Permeameter, ASTM D 5084-03, ASTM International, West Conshohocken, PA. January 2004.

ASTM 2006. Standard Test Method for Density, Absorption, and Voids in Hardened Concrete, ASTM C642-06, ASTM International, West Conshohocken, PA. August 2006.

ASTM 2010. Standard Test Methods for Measurement of Hydraulic Conductivity of Saturated Porous Materials Using a Flexible Wall Permeameter, ASTM D 5084-10, ASTM International, West Conshohocken, PA. August 2010.

ASTM 2012. Standard Test Method for Electrical Indication of Concrete's Ability to Resist Chloride Ion Penetration, ASTM C1202-12, ASTM International, West Conshohocken, PA. March 2012.

ASTM 2013. Standard Test Method for Measurement of Rate of Absorption of Water by Hydraulic-Cement Concretes ASTM C1585-13, ASTM International, West Conshohocken, PA. February 2013.

ASTM 2013. Standard Test Method for Density, Absorption, and Voids in Hardened Concrete, ASTM C642, ASTM International, West Conshohocken, PA. February 2013.

Baroghel-Bouny, V., Mainguy, M., Lassabatere, T., and Coussy, O. 1999. "Characterization and identification of equilibrium and transfer moisture properties for ordinary and high performance cementitious materials," Cement and Concrete Research, Vol. 29, pp. 1225-1238. 1999.

Bruins, H. R., 2003, Coefficients of Diffusion in Liquids, in E. W. Washburn, ed., International Critical Tables of Numerical Data, Physics, Chemistry and Technology, Knovel, Norwich, New York, page 3414.

Butcher, B. T. 2013. E-Area Low-Level Waste Facility Performance Assessment Maintenance Program – FY2013 Implementation Plan, SRNL-STI-2013-00511 Draft, Savannah River National Laboratory, Aiken, South Carolina. August 2013.

Carey, S. 2006. Low Activity Waste (LAW) Vault Structural Degradation Prediction, T-CLC-E-00018, Rev. 1. Washington Savannah River Company, Aiken, South Carolina. June 15, 2006.

Dixon, K. L. and Phifer, M. A. 2010. Hydraulic and Physical Property Data for E-Area Test Wall Concrete from MACTEC Testing Laboratory, SRNL-6200-2009-00035, Savannah River National Laboratory, Aiken, South Carolina. August 18, 2010.

Duncan, A.J. and Reigel, M.M. 2011. Evaluation of the Durability of the Structural Concrete of Reactor Buildings at SRS, SRNL-STI-2010-00729, Rev. 0, Savannah River National Laboratory, Aiken, South Carolina. February 2011.

Flach, G. P. 2013. Unreviewed Disposal Question Evaluation: Impact of New Information since 2008 PA on Current Low-Level Solid Waste Operations, SRNL-STI-2013-00011, Rev. 0. Savannah River National Laboratory, Aiken, SC. February 2013.

Jones, W. E. and Phifer, M. A. 2007. E-Area Low-Activity Waste Vault Subsidence Potential and Closure Cap Performance (U), WSRC-TR-2005-00405, Washington Savannah River Company, Aiken, SC. August 2007.

Langton, C. A. 2009. Final Report: 2009 E-Area LAWV/ILV Concrete and CIG Grout Durability Simulations for Exposure to Leachates with pHs between 7 and 12.4, SRNL-STI-2009-00665, Rev. 0, Savannah River National Laboratory, Aiken, SC. November 2009.

Peregoy, W. 2006. Structural Evaluation of Intermediate Level Waste Storage Vaults for Long-Term Behavior, T-CLC-E-00024, Rev. 0. Washington Savannah River Company, Aiken, South Carolina. June 27, 2006

Phifer, M. A., Crapse, K. P., Millings, M. R., and Serrato, M. G. 2009. Closure Plan for the E-Area Low-Level Waste Facility, SRNL-RP-2009-00075, Rev. 0. Savannah River National Laboratory, Aiken, SC. March 16, 2009.

Phifer, M. A., Millings, M. R., and Flach, G. P. 2006. Hydraulic Property Data Package for the E-Area And Z-Area Vadose Zone Soils, Cementitious Materials, and Waste Zones, WSRC-STI-2006-00198. Washington Savannah River Company, Aiken, South Carolina. September 2006.

Rockhold, M. L., Fayer, M. J., and Heller, P. R. 1993. Physical and Hydraulic Properties of Sediments and Engineered Materials Associated with Grouted Double-Shell Tank Waste Disposal at Hanford, PNL-8813, Pacific Northwest Laboratory, Richland, Washington. September 1993. Appendix J within Performance Assessment of Grouted Double-Shell Tank Waste Disposal at Hanford, WHC-SD-WM-EE-004, Rev. 0, Volume 2, Westinghouse Hanford Company, Richland, Washington. October 1993.

Savage, B. M. and Janssen, D. J. 1997. "Soil Physics Principles Validated for Use in Predicting Unsaturated Moisture Movement in Portland Cement Concrete," ACI Materials Journal, V. 94, No. 1, January-February 1997, pp. 63-70.

SIMCO 2011. STADIUM$^®$ IDC – A SIMCO Solution (http://www.stadium-software.com/), SIMCO Technologies, Inc. 2011.

SIMCO 2011a. Final Report, Subcontract no. RA00097S, SIMCO Technologies Inc., Quebec, Canada. March 18, 2011. (See Appendix A)

SIMCO 2012. E-Area Concrete Long-Term Durability Simulations Final Report, Subcontract no. RA00097, SIMCO Technologies Inc., Quebec, Canada. January 25, 2012. (See Appendix B)

Snyder, K. A. 2003. Condition Assessment of Concrete Nuclear Structures Considered for Entombment, National Institute of Standards and Technology (NIST), NISTIR 7026. July 14, 2003.

SRNS 2010. E-Area Low-Level Waste Facility Performance Assessment and Savannah River Site Composite Analysis Maintenance Program – FY2010 Implementation Plan, SRNS-RP-2010-00179, Rev. 0, Savannah River Nuclear Solutions, Savannah River Site, Aiken, SC. March 2010.

SRNS 2011. E-Area Low-Level Waste Facility Performance Assessment and Savannah River Site Composite Analysis Maintenance Program – FY2011 Implementation Plan, SRNS-STI-2011-00130, Rev. 0, Savannah River Nuclear Solutions, Savannah River Site, Aiken, SC. March 2011.

WSRC 1994. Furnishing and Delivery of Concrete (U), C-SPS-G-00041, Revision 2, Westinghouse Savannah River Company, Aiken, South Carolina. September 29, 1994.

WSRC 2005. Response to Action Items from Public Meetings between NRC and DOE to Discuss RAI for the Savannah River Site, CBU-PIT-2005-00203, Rev. 1, Westinghouse Savannah River Company, Aiken, South Carolina. September 2005.

WSRC 2008. E-Area Low-Level Waste Facility DOE 435.1 Performance Assessment, WSRC-STI-2007-00306, Rev. 0, Washington Savannah River Company, Aiken, SC. July 2008.

Yu, A. D., Langton, C. A., and Serrato, M. G. 1993. Physical Properties Measurement Program (U), WSRC-RP-93-894, Westinghouse Savannah River Company, Aiken, South Carolina. June 30, 1993.

Drawing SE5-6-2003318, Burial Ground Expansion ILT & ILNT Vaults General Notes and Legend Concrete, Rev. 2

Drawing SE5-6-2003319, Burial Ground Expansion ILT & ILNT Vaults Technical Guidelines for Conc. Construction Sheet 1 (U) Concrete, Rev. 4

Drawing SE5-6-2008801, Burial Ground Expansion LAW Vault General Notes and Legend Concrete, Rev. 4

Page Intentionally Blank

Appendix A. 2010 E-Area Vault Concrete Testing by SIMCO Technologies (SIMCO 2011a)

Page Intentionally Blank

Savannah River Nuclear Solutions

Subcontract no. RA00097S

Final Report

March 18th 2011

Prepared by:

SIMCO Technologies Inc.
203-1400 Boul. du Parc-Technologique
Quebec QC   G1P 4R7
Canada
(418) 656-1003 tel | (418) 656-6083 fax

Abstract

The objective of this project was to evaluate the transport properties of field concrete from the E-Area Low-Level Waste Facility (ELLWF) Intermediate Level Vault (ILV) / Low Activity Waste Vault (LAWV) Concrete Test Wall. Various laboratory experiments were carried out to evaluate porosity, permeability, isotherms, ionic diffusion coefficient, pore solution chemistry, chloride penetration as well as carbonation depth. These transport properties can be used as input parameters in the reactive transport model STADIUM® to predict the service life of structures exposed to aggressive environments.

1. Field concrete mixture proportions

The field concrete tested in this project was prepared with a ternary binder made of Type II cement, blast furnace slag and type F fly ash, and the water to binder ratio is 0.45. Table 1 shows the mixture proportions of the concrete. It should be mentioned that no information about the chemical compositions of the binder was available for the analysis.

Table 1 – E-Area LLWF LAW Vault and IL Vault Concrete Formulation

Ingredient	Quantity	
	lbs/cu yd	**kg/m^3**
Type II cement (ASTM C 150)	120	71
Grade 120 Blast furnace slag (ASTM C 989)	275	163
Type F Fly ash (ASTM C 618)	135	80
No 10. sand (ASTM C 33)	1,270	754
No. 67 aggregate (maximum ¾ in) (ASTM C 33)	1,750	1038
Water (maximum)	240	142
Maximum water to cementitious material ratio	0.45	0.45
Specified minimum dry density	147 lbs/cu ft	2356
Minimum compressive strength at 28 days	4000 psi	28 MPa

2. Field concrete cores and test specimens

A total of five (5) concrete cores, size Ø145 mm×300 mm (Ø5.7 in. × 12 in.), were received by SIMCO Technologies inc. on April 1st, 2010 (Figure 1). These cores were sampled from the ELLWF ILV/LAWV Concrete Test Wall and were approximately 20 years-old at the time they were extracted. Upon reception, cylindrical test specimens were made from the cores as shown in Figures 2 and 3. To prepare specimens for migration and isotherm tests, 4-in. cores had to be extracted from the 6-in. cores (Figure 2). The test specimens have different dimensions, as summarized in Table 2.

The specimens, with the exception of those used for the porosity and carbonation depth tests, were then immersed in limewater (i.e. saturated $Ca(OH)_2$) for at least 30 days before being tested because most of the scheduled laboratory tests require saturated specimens. The use of limewater for curing or re-saturation simulates the strong basic (high pH) condition inside the concrete pore solution so as to avoid leaching of calcium and hydroxide from the specimens, which would alter test results. The use of limewater to cure and store concrete sample is common practice and specified in many ASTM procedures related to cementitious materials (e.g. ASTM C31, ASTM C192, ASTM

C511). Porosity test (ASTM C642 procedure), however, was started earlier since the samples do not need to be saturated. For carbonation depth determination, a specimen approximately 10-cm thick was cut off from the top side of a core corresponding to the exposed surface of the structure. This specimen was not immersed in limewater. Instead it was directly used for carbonation depth determination (see the following section). For the pore solution test, a slice (about 10 mm in thickness) was obtained from Core #5 as shown in Figure 3, and then saturated with a 0.3 M NaOH solution together with the samples used for migration test. The sample was crushed prior to pore water extraction, as described in the following section.

Table 2 – Nominal dimension of test specimens

Test	Diameter, mm (in.)	Length, mm (in.)
Porosity (ASTM C642)	145 (5.7)	50 (2)
Pore solution	Crushed samples	
Migration	100 (4)	50 (2)
Isotherms (4 R.H.)	100 (4)	10 (0.4)
Drying	103 (4.1)	10 (0.4); 50 (2); 103 (4.1)
Chloride ponding	145 (5.7)	80 (3)
Carbonation depth	145 (5.7)	100 (4)

Figure 1 – Field concrete cores received by SIMCO Technologies Inc.
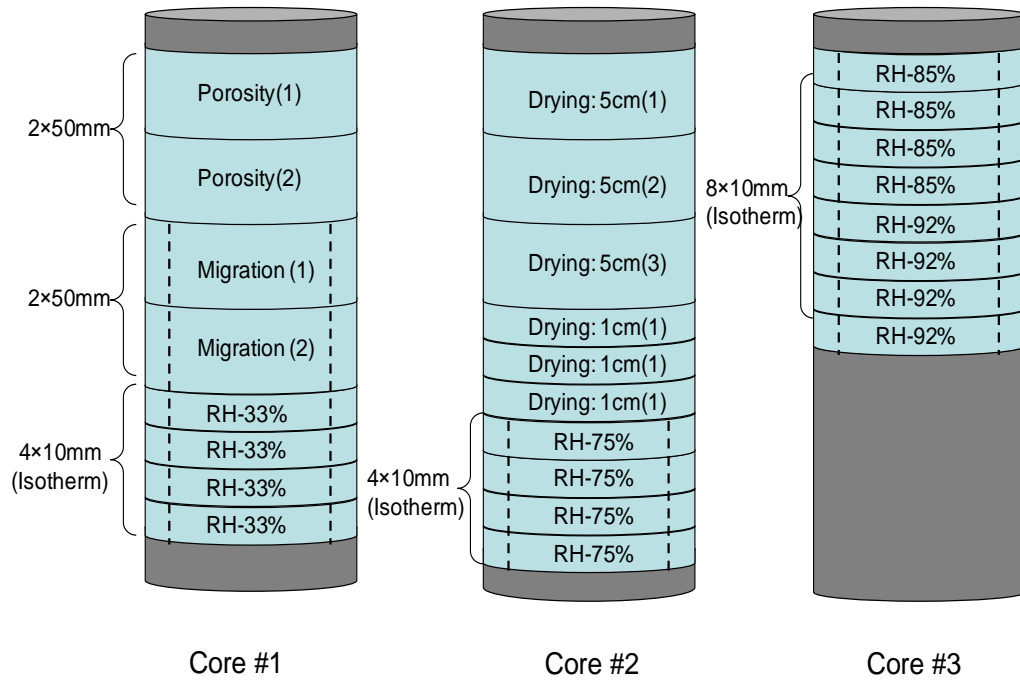
Figure 2 – Preparation of test specimens from field concrete cores
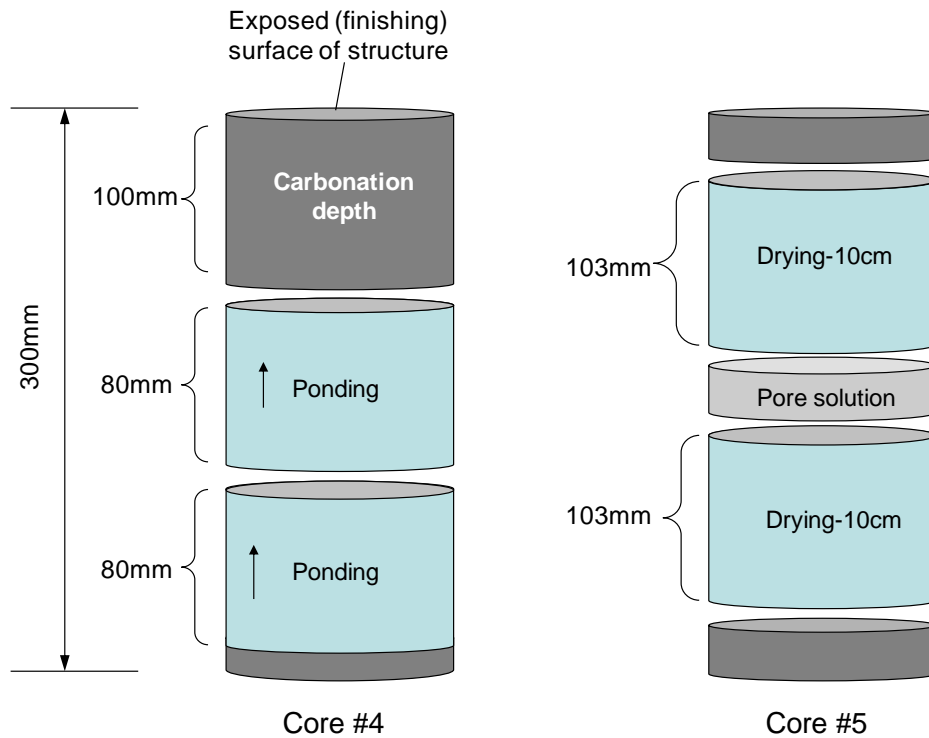
Figure 3 – Specimen preparation for drying test (10cm), chloride ponding, and carbonation depth determination

3. Experimental program and results

The experimental program included the following laboratory tests in order to determine the parameters required by SRNL for the E-Area Vault Concrete:

- Drying test to determine the intrinsic permeability and saturated hydraulic conductivity
- Isotherms test to determine the moisture sorption/retention curve (4 different relative humidity levels)
- Migration test to determine the diffusion coefficients and tortuosity
- Porosity (ASTM C642) test to determine the porosity
- Chloride ponding test to determine the chloride penetration profile
- Phenolphthalein spray test to determine the depth of carbonation
- Pore solution test to determine the major pore solution cations and anions

Depending on conditioning sequence and capacity of chambers, the various tests were started on different days as shown in Table 3. The transport properties results are summarized in Table 4. The details of the experiments are presented in the following subsections.

Table 3 – Schedule for the laboratory tests

Test	Starting date	End date[1]
Porosity (ASTM C642)	27/04/2010	May 2010
Pore solution	14/05/2010	May 2010
Migration	05/05/2010	May 2010
Isotherms (23°C, 4 R.H.)	06/05/2010	February 2011
Drying (23°C, 50%RH)	11/05/2010	November 2010
Chloride ponding (0.5M NaCl)	21/04/2010	August 2010
Carbonation depth	20/04/2010	April 2010

---

[1] Laboratory test finishing date; transport property analyses were performed after the tests were done.

Table 4 – Summary of test results

Test	Result
Porosity (ASTM C642)	15.78%
Dry bulk density (ASTM C642) (g/cm^3)	2.54
Pore solution (mmol/l):	
OH	126.1
SO_4^{2}-	3.3
Na^+	104.4
K^+	30.7
Ca^{2+}	0.1
Cl^-	2.7
Effective diffusion coefficient[2]	
D_e (E-11 m^2/s)	0.32 (Ca^{+2}) to 2.12 (OH^-)
	(See Table 8)
Tortuosity (-)	0.0040
Carbonation depth (mm)	16
(average)	
Chloride ponding (Cl profile)	10 mm penetration in 106 days
	(See Figure 10)
Isotherms	
SIMCO Model – β	-50.6
SIMCO Model – δ	0.09
Van Genuchten – a (MPa)	35.1
Van Genuchten – m	0.27
Permeability (E-22 m^2)	0.84
Sat. Hydraulic Conductivity	8.2
(E-14 cm/s)	

Carbonation depth

The carbonation depth was determined using phenolphthalein indicator according to the procedure recommended by RILEM CPC-18. Initially concrete pore fluid is typically at a pH greater than 12 and carbonation causes the pore fluid pH to decrease to around 8. Phenolphthalein is colorless at pHs less than about 9 and pink at pHs greater than 9; therefore the zone of carbonation within a concrete specimen treated with

---

[2] Defined as D_e = tortuosity $\times$ molecular diffusion coefficient of the species in open water

phenolphthalein is indicated by the lack of the pink color and areas not impacted by carbonation are indicated by a pink color.

The specimen used for determination of carbonation depth was cut off from the top of a concrete core to include the exposed surface of the structure as shown in Figure 3. The specimen was then split into two halves by compression along its axis (Figure 4).

Then, phenolphthalein solution was sprayed on the freshly split surfaces of the specimen. The carbonation depth was then determined from the coloration patterns following the phenolphthalein procedure as recommended by RILEM CPC-18 (Figure 5). The determined average carbonation depth is about 16 mm.
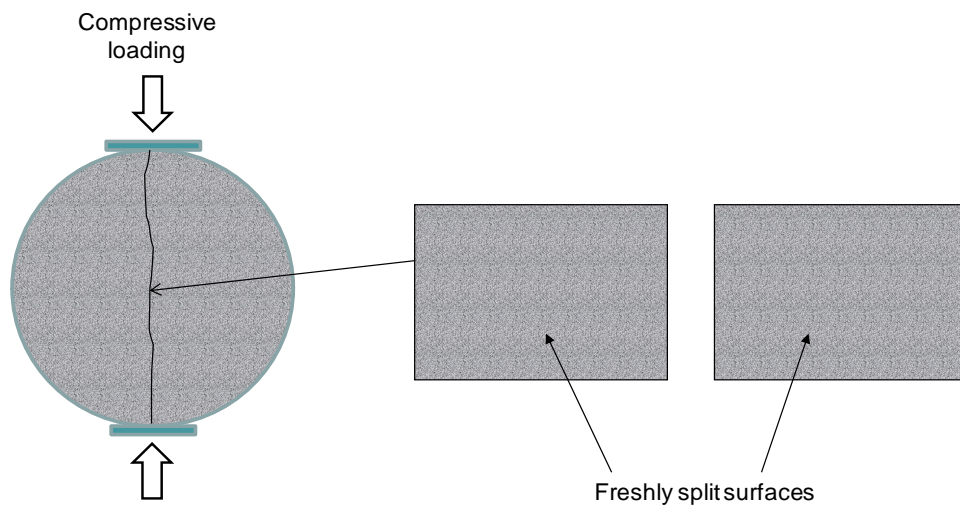
Figure 4 – Cylindrical specimen split into two halves for carbonation depth testing
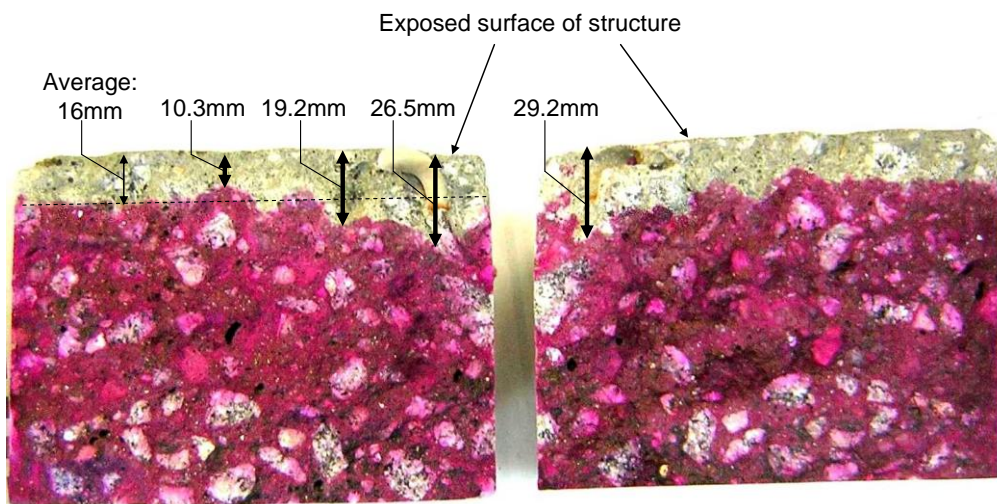
Figure 5 – Carbonation depth determination on field concrete core

Porosity

The volume percentage of absorption and voids in the field concrete material were evaluated by the ASTM standard procedure of C642. Two specimens cut from the same core were tested. Modification was made for the procedure. In the standard procedure, constant weight is estimated by mass variation of no more than 0.5% of the total mass of the specimen. However, in our previous research work it was found that this controlling threshold (0.5%) is usually too rough to count on all the pore space of high quality concretes, which may underestimate the total porosity by up to 1%. In order to obtain a more precise porosity estimation, the threshold was reduced to 0.1%. The test results are summarized in Table 5.

Table 5 – Porosity test results (ASTM C642)

	Parameters	Specimen 1	Specimen 2
A	Mass of oven dried sample (g)	1845.58	1752.71
B	Mass of surface dry sample in air (g)	1955.19	1858.05
C	Mass of surface-dry sample in air after immersion and boiling (g)	1959.62	1861.67
D	Apparent mass of sample in water after immersion and boiling (g)	1201.75	1201.75
g_1	Bulk density, dry (g/cm^3)	2.43	2.65
g_2	Apparent density (g/cm^3)	2.86	3.17
	Bulk density after immersion (g/cm^3)	2.57	2.81
	Bulk density after immersion and boiling (g/cm^3)	2.58	2.82
	Absorption after immersion (%)	5.94	6.01
	Absorption after immersion and boiling (%)	6.18	6.22
	Volume of permeable voids (%) (C-A)/(C-D)×100	15.05	16.51
	Average volume of permeable voids (porosity, %)	15.78	
	Average absorption after immersion and boiling (%)	6.20	

Pore solution chemistry

Pore solution composition is needed in order to analyze migration test results. Accordingly, field concrete samples were conditioned similar to the procedure used for migration test samples before extraction. Extraction directly from field concrete, without conditioning, was not attempted. The quality of the material, combined with its saturation state, would have prevented solution to flow out.

Pore solution was extracted from crushed samples taken from the field concrete core #5 (Figure 3). A disc sample was first sawn off from a concrete core, and vacuum saturated with 0.3M NaOH solution, similar to the procedure used for migration tests. Following this, the saturated sample was crushed in smaller pieces where large aggregates were removed. The pore solution was extracted by squeezing the crushed samples under compressive loading using the device shown in Figure 6. About 3 ml pore solution was extracted from about 300g crushed samples when the applied compressive loading reached 270,000 lbs.

The chemistry (i.e. the ionic concentrations) of the pore solution was analyzed by different techniques including potentiometric titration (for OH^- and Cl^- ions), ICP-OES (for Na^+, K^+, Ca^{2+} ions), and chromatography (for SO_4^{2-} ion). The analyzed pore solution chemistry is shown in Table 6.

Table 6 – Pore solution chemistry for field concrete vacuum saturated in 0.3M NaOH

Ion	OH^-	SO_4^{2-}	K^+	Na^+	Ca^{2+}	Cl^-
Concentration (mmol/l)	126.1	3.3	30.7	104.4	0.1	2.7

1 - Base
2 - Pore solution collector
3 - Cell (sample chamber: Ø57×76mm)
4 - Cylinder (piston: Ø56.7×76mm)
5 - Steel pad (thickness: 20 mm)
6 - Teflon pad

Pore solution collector
Pore solution canal
Collecting hole
Pore solution outlet
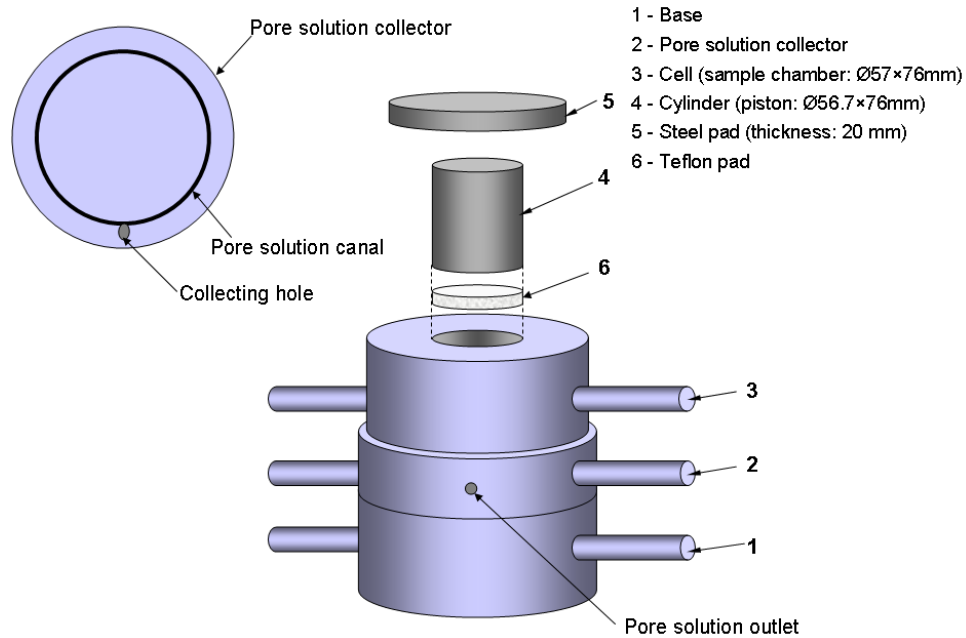
Figure 6 – Experimental setup for the pore solution extraction

Migration test

The objective of the migration test is to estimate the tortuosity and effective diffusion coefficients of the material. The test is a modified version of the ASTM C1202 procedure: *Standard Test Method for Electrical Indication of Concrete's Ability to Resist Chloride Ion Penetration*. The transient method developed by SIMCO Technologies consists in accelerating the ions under an external potential and measure the electrical current across the sample over a 15-day period. The measured currents are analyzed to provide the effective diffusion coefficients following the method described in reference Samson et al. (2008) and Appendix A.

Two cylindrical specimens of 100 mm in diameter and 50 mm in thickness were cut from the same 4-in. core (Figure 2). As mentioned in section 2, the specimens, after being cut, were kept in limewater for at least 30 days before being tested. Since a basic solution of 0.3M NaOH was used in the test, prior to testing, the specimens were also saturated with 0.3M NaOH solution through a vacuum procedure. The use of 0.3M NaOH solution prevents alteration to the material during the test as a result of portlandite dissolution and C-S-H decalcification.

The saturated specimens were then mounted onto the migration cells (Figure 7). The joints between the specimen and the cells were sealed with silicon in order to avoid

leakage of the solution. The outer surface of the specimen was also sealed with silicon to maintain the saturated condition and enforce 1D ionic transport.
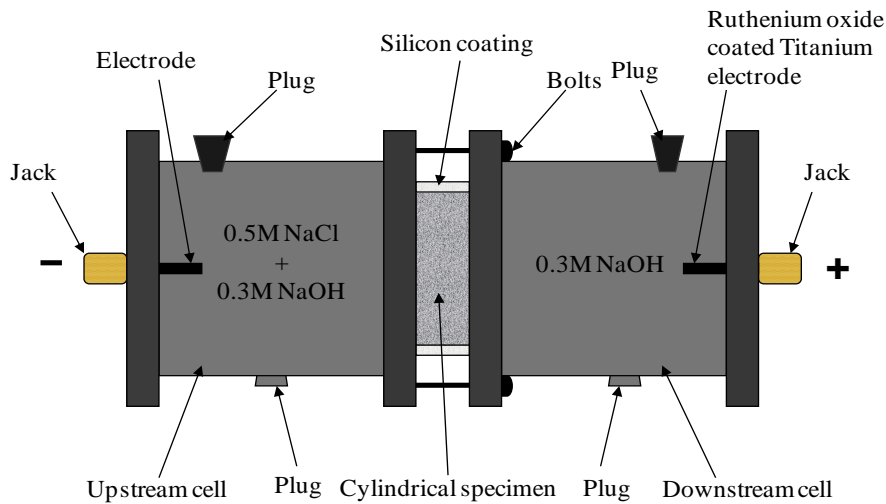
Figure 7 – Migration setup

The upstream cell was filled with solution of 0.5M NaCl dissolved into 0.3M NaOH solution, while the downstream cell was filled with 0.3M NaOH solution only (Figure 7).It should be mentioned that although the migration solutions were not renewed during testing, the ionic concentrations of the solutions changed little during the test period. This is because under the voltage used (16V), no significant electro-chemical reaction (e.g. chlorine gas) took place at the two electrodes, and therefore only very limited ions were consumed (e.g. the ions that penetrated into or through the specimens). More importantly, the volume of each cell is large enough (2700 ml) to keep the ionic concentration unchanged, which is much larger than that used in the standard test of ASTM C1202 (250ml). It has been verified that the chloride ion concentration and OH$^-$ concentration changed little (< 5% of the originals) after migration test. Therefore, constant concentration of the solutions can be assumed.

A constant DC potential of 16 volts was applied across each specimen during the test by a DC power supply. The test lasted 14 days, during which the current passing through each specimen was monitored periodically as shown in Table 7. Numerical analysis of ionic diffusivity was performed using STADIUM$^®$ IDC module. This specialized version of STADIUM$^®$ evaluates the tortuosity of the material by simulating the current through the samples (see reference Samson et al. (2008) and Appendix A). Other material parameters such as porosity and pore solution composition are used during the analysis. The simulation was performed based on the current measurements from the two specimens. From Table 7 it can be seen that the test results for the two parallel tests are quite close to each other (variation of averaged current = 0.4%), and therefore the simulation result can

be considered to be representative. The simulation result compared to the experimental measurements is shown in Figure 8, and the estimated ionic diffusion coefficients are given in Table 8. The estimated tortuosity is 0.0040.

Table 7 – Migration result

Time	Specimen #1			Specimen #2		
	I	Vs	Ve	I	Vs	Ve
(hrs)	(mA)	(V)	(V)	(mA)	(V)	(V)
0.00	2.15	16.58	17.88	2.52	16.88	17.89
3.50	2.24	16.44	18.01	2.62	16.54	18.02
22.92	2.40	16.33	17.93	2.70	16.29	17.93
48.17	2.50	16.22	17.82	2.76	16.17	17.82
93.58	2.84	16.16	17.82	2.82	16.15	17.82
121.50	3.11	16.06	17.76	2.94	16.07	17.76
146.00	3.28	16.10	17.80	3.13	16.09	17.79
170.58	3.12	16.22	17.81	3.21	16.22	17.82
194.83	2.89	15.98	17.68	3.28	16.04	17.53
215.08	2.93	16.03	17.72	3.32	16.04	17.73
288.00	3.39	15.74	17.58	3.68	16.04	17.67
313.33	3.58	16.16	17.78	3.85	16.18	17.79

Vs – Potential difference applied across the specimen

Ve – Potential difference applied on the two electrodes on the cells

Table 8 – Effective diffusion coefficients (E-11 m^2/s)

OH$^-$	Na$^+$	K$^+$	Ca^{2+}	SO$_4^{2-}$	Cl$^-$
2.12	0.54	0.79	0.32	0.43	0.82
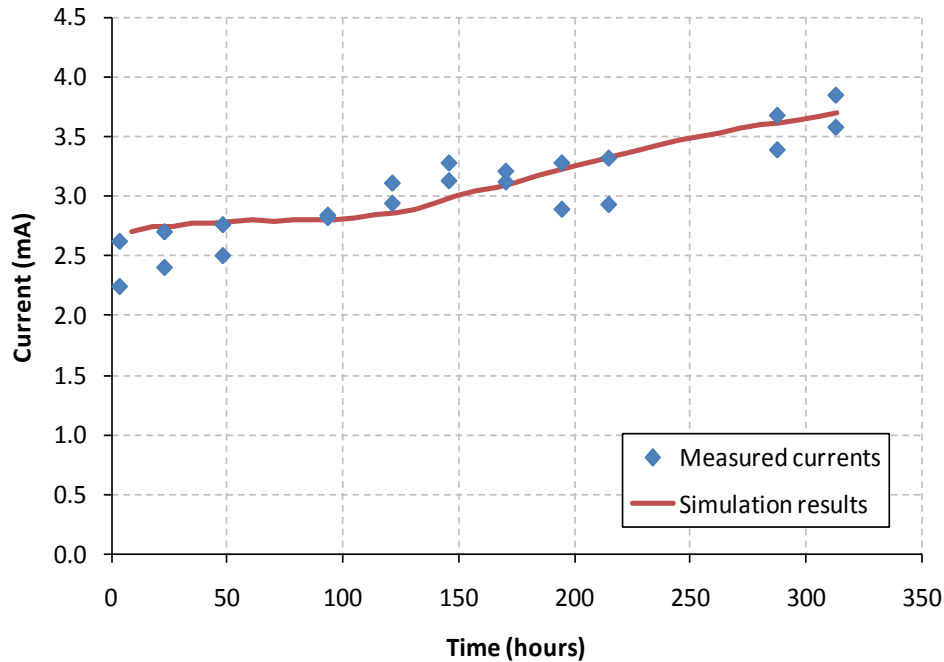
Figure 8 – Simulation results for field concrete

Chloride ponding test

This test is a modified version of ASTM C1543 (Standard Test Method for Determining the Penetration of Chloride Ion into Concrete by Ponding). Instead of using limited quantity of ponding solution held by dike above the specimens' surface, the specimen is immersed in large quantity of chloride solution, which contributes to maintain constant exposure conditions.

Two 80-mm thick cylindrical specimens were cut off from the central part of a 6-in. field concrete core (Figure 3) and then immersed in limewater for 20 days until testing. Each of the specimens was then coated with epoxy leaving only one cut surface uncoated as the exposed surface (Figure 9).

The specimens were then exposed to 3% (0.5M) NaCl aqueous solution. The exposure condition was kept constant during the immersion period by renewing the immersion solution. When the pH value of the chloride solution reached 10.5, the solution was renewed. Chloride concentration of the solution was also monitored, and the analysis results showed less than 5% change in chloride concentration between any two solution renewals.

The specimens were removed from the solution after being exposed to the solution for 106 days. Powder samples were then obtained from different depths in the specimens by grinding the specimens layer by layer from the exposure surface along the axis. The total chloride ion content in each powder sample was then analyzed in accordance with ASTM Test Method C1152C/C1152M. Finally, the chloride penetration profiles were obtained. The profiles analysis results are summarized in Tables 9A and 9B, and the chloride penetration profiles are shown in Figure 10.
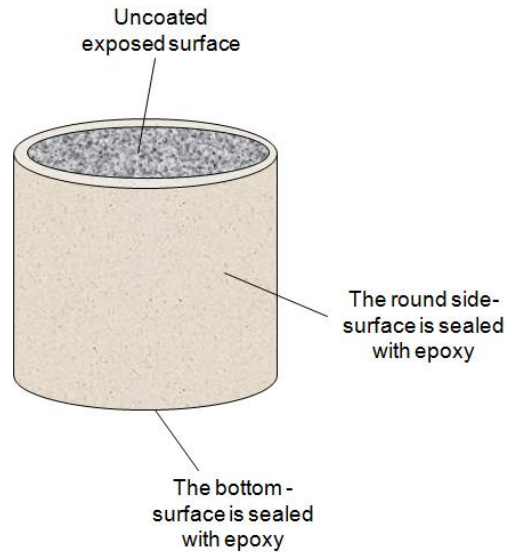
Figure 9 – Specimens for chloride ponding test

Table 9A – Chloride penetration profile analysis result for sample #1

Layer	Grinding depth Average (mm)	Mean depth (mm)	Sample mass (g)	Reading ($AgNO_3$ ml)	Cl^- (%)
1	2.55	1.2750	5.0020	9.1650	0.2210
2	5.12	3.8350	5.0020	4.4260	0.0524
3	7.68	6.4000	5.0010	3.4480	0.0176
4	10.11	8.8950	4.9990	3.0710	0.0042
5	12.76	11.4350	5.0020	2.9680	0.0005
6	15.07	13.9125	5.0000	3.0060	0.0019
7	17.78	16.4200	4.9980	2.9820	0.0010
8	20.04	18.9050	4.9990	2.9620	0.0003
9	22.53	21.2800	4.9980	2.9840	0.0011
10	25.18	23.8525	4.9980	2.9720	0.0006
11	27.63	26.4050	5.0020	2.9830	0.0010
12	30.94	29.2825	4.9990	2.9950	0.0015
13	32.92	31.9250	4.9980	2.9980	0.0016
14	35.12	34.0150	5.0010	2.9820	0.0010

Table 9B – Chloride penetration profile analysis result for sample #2

Layer	Grinding depth Average (mm)	Mean depth (mm)	Sample mass (g)	Reading (AgNO$_3$ ml)	Cl$^-$ (%)
1	2.66	1.3275	4.9990	9.5180	0.2339
2	5.04	3.8450	5.0050	4.1490	0.0427
3	7.64	6.3375	4.9970	3.4230	0.0169
4	10.14	8.8875	5.0040	3.1130	0.0059
5	12.67	11.4000	5.0030	2.9950	0.0017
6	15.19	13.9250	5.0000	2.9980	0.0018
7	17.59	16.3850	5.0030	3.0130	0.0023
8	20.12	18.8525	4.9950	2.9570	0.0003
9	22.64	21.3800	4.9980	2.9340	-0.0005
10	25.42	24.0300	4.9940	2.9420	-0.0002
11	27.64	26.5275	4.9950	2.9210	-0.0010
12	30.12	28.8775	4.9990	2.9170	-0.0011
13	32.75	31.4350	5.0020	2.9550	0.0002
14	35.42	34.0850	5.0030	2.9870	0.0014
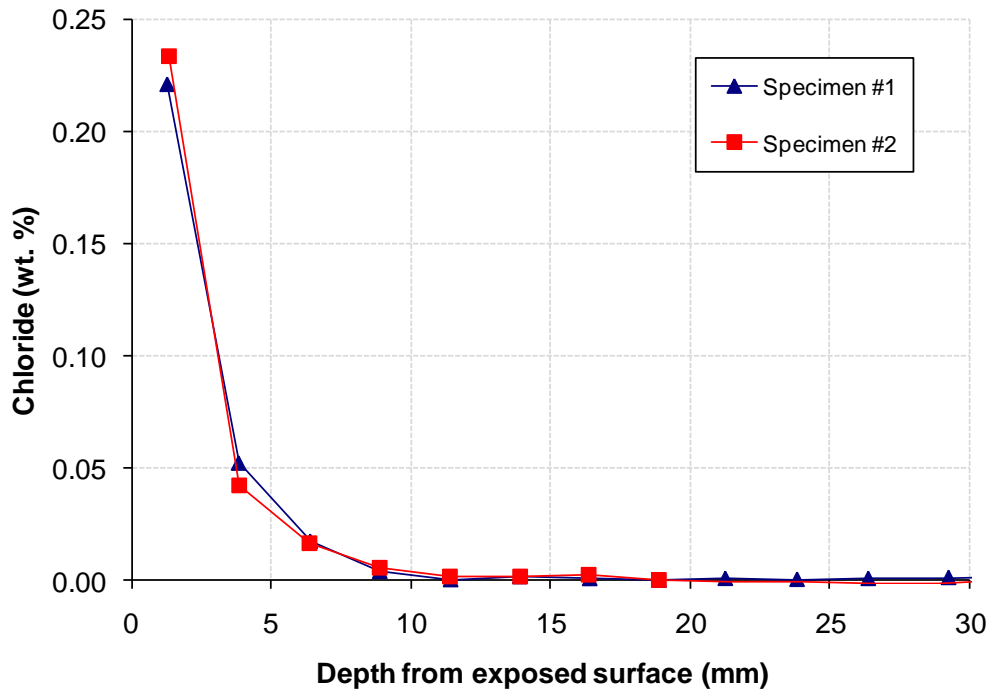
Figure 10 – Chloride penetration profiles in field concrete cores after 106-days exposure to 0.5M NaCl solution

Desorption isotherm

The desorption isotherm was estimated by measuring the equilibrium water content of the material at four different relative humidity (RH) values. Thin slices of concrete (100 mm diameter × 10 mm thickness) were cut from cores, as shown on Figure 2. For each relative humidity value, four slices were prepared. After cutting, the samples were conditioned in limewater until a constant saturated mass was reached. The saturated surface dry mass was recorded. Samples were then placed in four climate boxes (Figure 11), where four different relative humidities (33%, 75%, 85% and 92%) were maintained by saturated salt solutions (i.e. $MgCl_2.6H_2O$ for 33% RH, NaCl for 75% RH, KCL for 85% RH, and KNO_3 for 92% RH). An additional data point is at 50% RH is provided by drying test results. The salts were selected to cover a wide RH range. Also, desorption isotherms for good quality concrete are almost linear and do not exhibit a rapid drop in water content at high RH values. It was thus decided to test at 92% only in the high-RH range.

The boxes were prepared according to the principles recommended in ASTM E 104-85 Standard Practice for Maintaining Constant Relative Humidity by Means of Aqueous Solutions. The specimens were weighed periodically until constant masses were observed at each relative humidity.

An additional water content value at 50% RH was obtained with the drying test. In this case, the thin samples were kept in a humidity-controlled chamber (Figure 15) instead of climate boxes.

Figure 11– Humidity boxes for isotherm test

Upon reaching equilibrium, the equilibrium water content at 50% RH (w_{50}) was calculated according to:

$$w_{50}(\%) = \phi - \frac{M}{V} \times 100$$

where ϕ is the porosity (percentage), V is the volume of the specimen (cm^3), and M is the cumulative mass loss (g). The equilibrium mass values and corresponding water content are given in Table 10. The saturation, calculated as $S=w/\phi$, where ϕ is the porosity (percentage), is also provided in the table. The isotherm is then obtained by plotting the equilibrium water contents against the corresponding RH values, as shown on Figure 12.
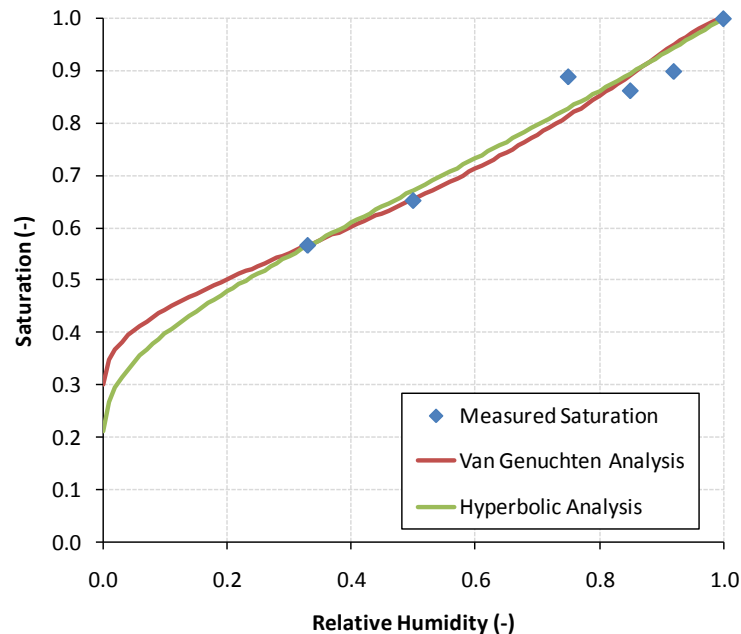
Figure 12 – Desorption isotherm of field concrete at 23°C

The moisture storage data were analyzed to obtain relevant moisture storage parameters. In STADIUM® moisture transport model developed by SIMCO Technologies (see Appendix B), the isotherm is expressed according to the relationship:

Table 10 – Experimental data for isotherm tests

Measurements	33%RH	50%RH (Drying)	75%RH	85%RH	92%RH	100%RH (ASTM C642)
Initial sat. mass (g)						
#1	190.15	379.57	197.38	182.52	176.75	
#2	199.88	366.87	199.87	186.86	200.12	
#3	196.73	420.37	207.03	200.13	175.42	
#4	190.89	-	191.37	195.86	185.70	
Equilibrium mass (g)						
#1	184.44	370.70	195.93	180.85	175.63	
#2	193.92	358.30	198.34	182.59	198.73	
#3	190.75	411.03	205.47	198.15	174.18	
#4	185.77	-	189.94	194.21	184.26	
Total mass loss (g)						Absorption
#1	5.71	8.87	1.45	1.67	1.12	114.0
#2	5.96	8.57	1.53	<u>4.27</u>	1.39	109.0
#3	5.98	9.34	1.56	1.98	1.24	-
#4	5.70	-	1.43	1.65	1.44	-
Volume (cm^3)						
#1	81.3	159.0	83.4	77.46	75.11	757.9
#2	85.0	154.3	85.0	78.29	85.62	659.9
#3	84.0	176.5	87.8	84.43	74.98	-
#4	82.0	-	81.3	83.86	79.10	-
Water content (%)						Porosity
#1	8.75	10.20	14.04	13.62	14.29	15.05
#2	8.77	10.22	13.98	<u>10.33</u>	14.16	16.51
#3	8.66	10.49	14.00	13.43	14.13	-
#4	8.83	-	14.02	13.81	13.96	-
Average	**8.75**	**10.30**	**14.01**	**13.62**	**14.13**	**15.78**
Saturation						
#1	0.55	0.65	0.89	0.86	0.91	0.95
#2	0.56	0.65	0.89	<u>0.65</u>	0.90	1.05
#3	0.55	0.66	0.89	0.85	0.90	-
#4	056	-	0.89	0.87	0.88	-
Average	0.55	0.65	0.89	0.86	0.90	1.00

Note: the underlined data from specimen #2 in 85% RH tests showed strong deviation from average and therefore were not used.

$$w = \frac{\phi}{\beta\phi(H^\delta - 1) + 1}$$

where ϕ is the porosity, H is the relative humidity, and β and δ are the fitting parameters. The fitting on Figure 12 was obtained with β=-50.6 and δ=0.09[3]. The isotherm was also analyzed[4] on the basis of Van Genuchten relationship:

$$S = \left[\left(\frac{p_c}{a}\right)^{\frac{1}{1-m}} + 1\right]^{-m}$$

where p_c is the capillary pressure (MPa) and a (MPa) and m are the fitting parameters[5]. The capillary pressure was calculated from relative humidity following Kelvin's relationship:

$$p_c = -\frac{\rho_l RT}{M_w}\ln(H)$$

where M_w is the molar mass of water (0.018 kg/mol), ρ_l is the density of liquid water, taken as 1000.0 kg/m³, R is ideal gas constant (8.3143 J/mol/°K), and T is the temperature (296 °C). Values of a=35.1 MPa and m=0.27 were estimated. Using these values, the capillary pressure is plotted against saturation on Figure 13.
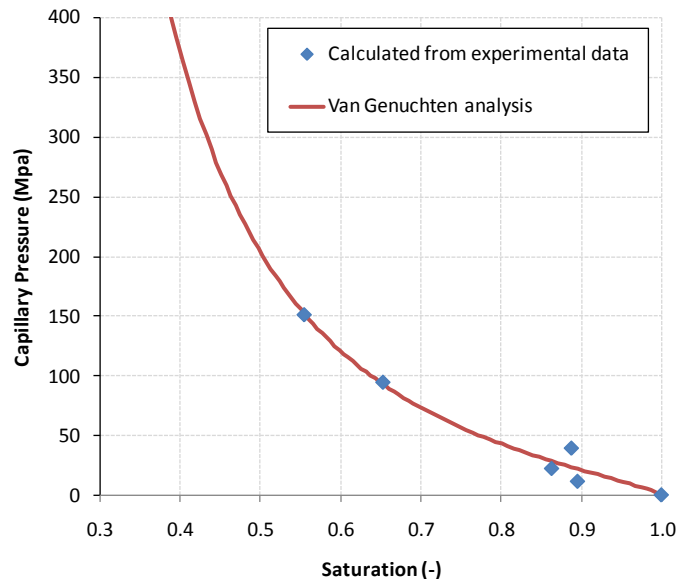
Figure 13 – Capillary pressure plot vs. saturation

---

[3] The fitting was performed with the Solver module in Microsoft Excel.
[4] Again using the Solver in Microsoft Excel.
[5] See Appendix C for a discussion on Van Genuchten parameters.

Drying test

The objective of the drying test is to estimate the intrinsic permeability of concrete samples. The test consists in exposing two series of initially saturated samples to a constant 50% RH: 10-mm and 50-mm thickness. The 10-mm series test is used to determine the equilibrium water content at the tested relative humidity, while the 50-mm series test is directly used to estimate the intrinsic permeability. The mass of the samples is monitored for the duration of the test. When equilibrium is reached for the 10-mm series, the test is terminated. The mass loss of the 50-mm series is then analyzed with the moisture transport model developed by SIMCO Technologies to yield the intrinsic permeability. Details on the test method are provided in reference (Samson 2008b) and Appendix D.

The test specimens were cut off from the field concrete cores (Figure 2). They were then saturated 40 days in limewater before being tested. The round side surface of each specimen was sealed with epoxy, while the two flat surfaces remained uncoated (Figure 14). This enforces one-dimensional mass transport in the samples.
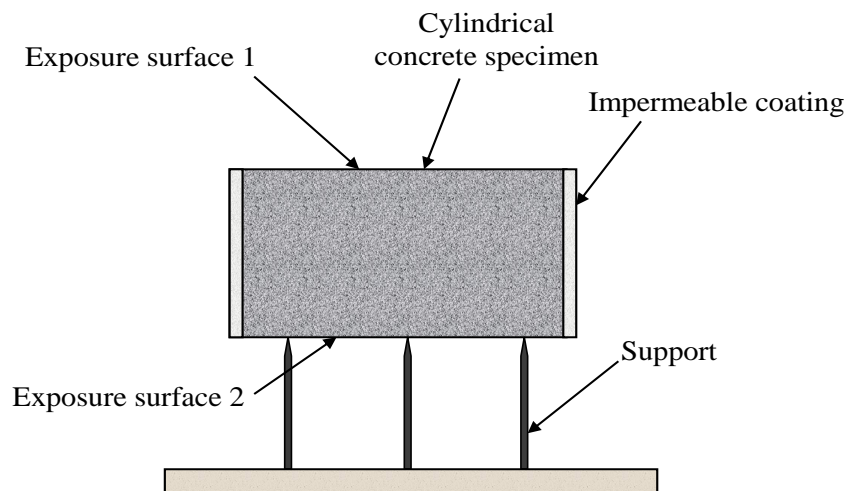
Figure 14 – Drying test setup

The test was performed in a climate chamber, where constant relative humidity of 50% and temperature of 23°C were maintained (Figure 15). The specimens were weighed periodically during testing. The cumulative mass loss was determined and plotted against test duration as shown in Figure 16. The complete data set can be found in Table 11 (Appendix E).

Figure 15 – Humidity-controlled chamber
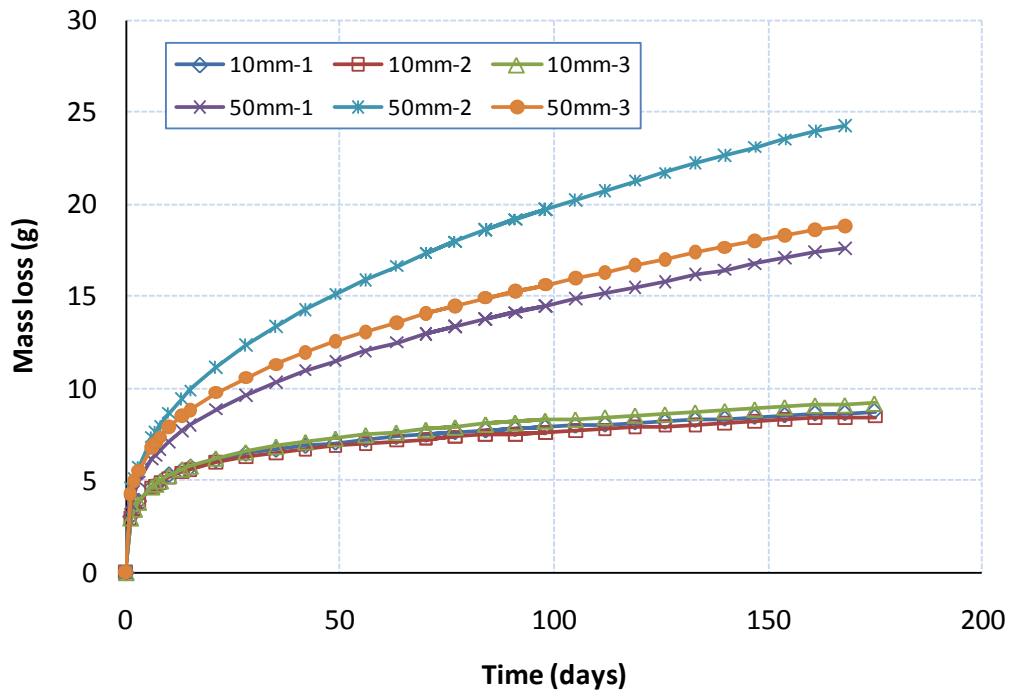
Figure 16 – Mass loss in drying test (10mm, 50mm series)

According to the drying test method, equilibrium of 10-mm thick specimens is considered to be reached when four successive mass changes determined at intervals of seven days exhibit less than 0.5% of the cumulative mass loss. Drying test for moderate quality concrete specimens usually take less than three months to finish. The field concrete specimens tested, however, showed very slow drying rate, which explains the long duration of the test. The equilibrium for the 10-mm thick specimens was finally reached after 170 days of testing. The equilibrium value is listed in Table 10 for the 50% relative humidity. Permeability was then analyzed through simulations based on the recorded mass loss in the 50-mm thick specimens, equilibrium water content and other material parameters such as tortuosity, porosity and isotherms. The simulation results in comparison to experimental records are shown in Figures 17 and were obtained with a permeability of 0.84E-22 m^2 (Table 4). This corresponds to a hydraulic conductivity of 8.2e-14 cm/s[6].
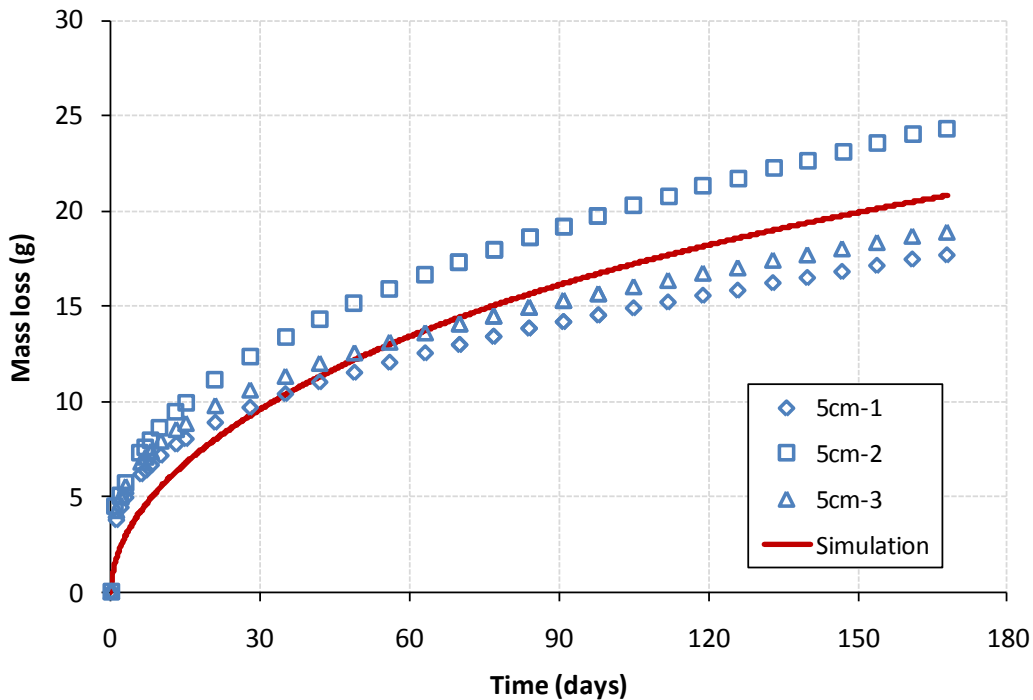
Figure 17 – Drying test permeability analysis (50-mm series)

A test series using thicker specimens was also performed in order to examine the possible impact of thickness of specimen on analyzed permeability. In order to use the same precision balance (0.01g) as for the other drying test, the thickness was cut at 103 mm (4.0 in, nominal thickness: 100 mm, see Figure 3). The mass change determinations for

---

[6] Calculation based on K=kρg/μ, with ρ=1000 kg/m^3, g=9.81 m^2/s, and μ=1.002 cP at 20°C (Robinson 2002).

this series test are given in Table 12 (Appendix E) and plotted against test duration as shown in Figure 18. Permeability analysis performed on this series is showed in Figure 18. The analysis gave a permeability of $0.83E\text{-}22$ m^2, which is very close to the value obtained on thinner samples ($0.84E\text{-}22$ m^2).
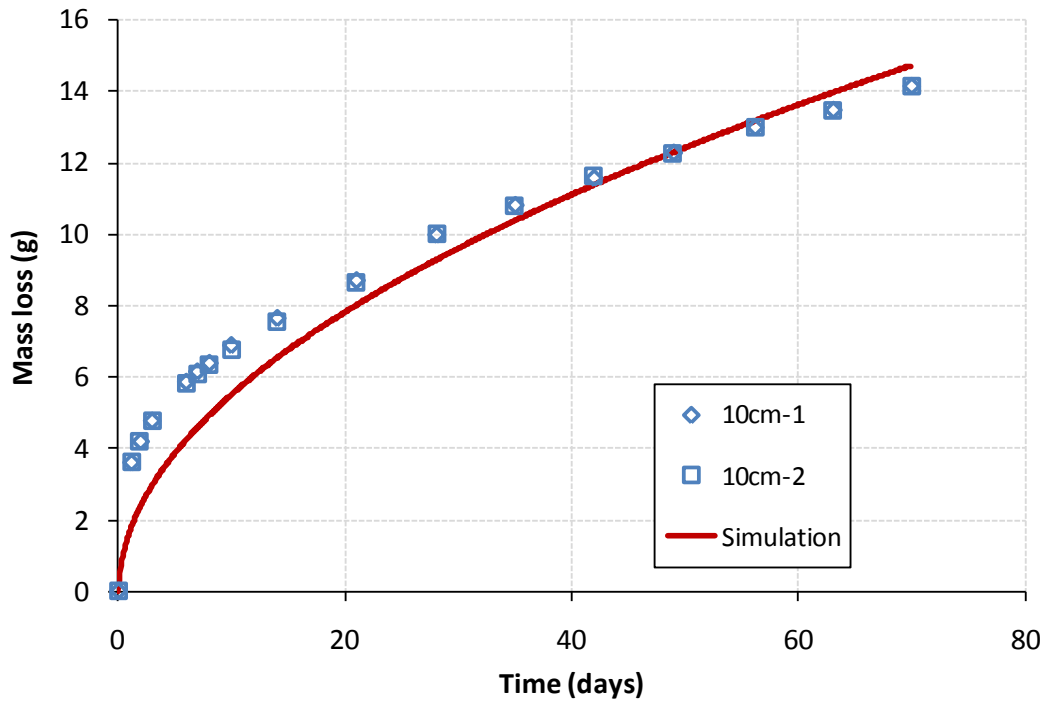
Figure 18 – Permeability analysis result for specimens of 100-mm thick

4. Conclusions

The concrete specimens supplied by SRNL were very high quality, low permeable material. The samples were more or less in equilibrium to ambient atmospheric conditions. No visible cracks were observed in the cores when they were received.

Test methods applied to characterizing the E-Area concrete cores are standard methods with the exception of the migration test, drying test and desorption isotherm test respectively used to evaluate tortuosity, permeability and water retention function of cementitious materials. The tests were developed by SIMCO Technologies since there are no equivalent standard methods.

The porosity measured on this material is high at 15.78% for a 0.45 water-to-binder ratio. However, other properties such as tortuosity and intrinsic permeability determined for the SRS material are comparable to other high quality quaternary concretes evaluated by SIMCO Technologies Inc. The high porosity maybe a consequence of the high cement content of the mixture.

5. References

Bolton D. (1980) The computation of equivalent potential temperature, *Monthly Weather Review* 108, 1046-1053.

Brouwers H.J.H., van Eijk R.J. (2003) Alkali concentrations of pore solution in hydrating OPC , Cement and Concrete Research 33, 191-196.

Fetter C.W. (1999) Contaminant Hydrogeology, Prentice-Hall, 2nd ed., New-Jersey (USA).

Galbraith G.H., McLean R.C., Kelly D. (1997) Moisture permeability measurements under varying barometric pressure, Building Research and Information 25, 348-353.

Glasser F.P., Marchand J., Samson E. (2008) Durability of concrete – Degradation phenomena involving detrimental chemical reactions, Cement and Concrete Research 38, 226-246.

Jones M.L., Dawson C.E. (1973) Salinity-temperature profiles in the Panama canal locks, Marine Biology 21, 86-90.

Marchand J., Samson E. (2009) Predicting the service-life of concrete structures – Limitations of simplified models, Cement and Concrete Composites 31, 515-521.

Millington R.J., Quirk J.P. (1961) Permeability of porous solids, *Transactions of the Faraday Society* 57, 1200-1207.

Robinson R.A., Stokes R.H. (2002) Electrolyte solutions, 2nd ed., Dover Publications (New-York, USA).

Samson E., Marchand J. (2007a) Modeling the transport of ions in unsaturated cement-based materials, Computers and Structures 85, 1740-1756.

Samson E., Marchand J. (2007b) Modeling the effect of temperature on ionic transport in cementitious materials, Cement and Concrete Research 37, 455-468.

Samson E., Henocq P., Marchand J., Beauséjour P., "Recent advances in the determination of ionic diffusion coefficients using migration test results", RILEM Proccedings 58-CONMOD 2008, E. Schlangen and G. de Schutter eds. (Delft, The Netherlands) (2008) pp. 65-78.

Samson E., Maleki K., Marchand J. and Zhang T, "Determination of the Water Diffusivity of Concrete using Drying/Absorption Test Results", Journal of ASTM International, Vol. 5, No. 7 (2008b) (Available onling at www.astm.org)

Sercombe J., Vidal R., Gallé C., Adenot F. (2007) Experimental study of gas diffusion in cement paste, *Cement and Concrete Research* 37, 579-588.

ASTM C31/C31M-09 "Standard Practice for Making and Curing Concrete Test Specimens in the Field".

ASTM C33/C33M-08 "Standard Specification for Concrete Aggregates".

ASTM C150-07 "Standard Specification for Portland Cement".

ASTM C192/C192M-07 "Standard Practice for Making and Curing Concrete Test Specimens in the Laboratory".

ASTM C511-09 "Standard Specification for Mixing Rooms, Moist Cabinets, Moist Rooms, and Water Storage Tanks Used in the Testing of Hydraulic Cements and Concretes".

ASTM C618-08a "Standard Specification for Coal Fly Ash and Raw or Calcined Natural Pozzolan for Use in Concrete".

ASTM C642-06 "Standard Test Method for Density, Absorption, and Voids in Hardened Concrete".

ASTM C989-09 "Standard Specification for Slag Cement for Use in Concrete and Mortars".

A. Migration test procedure

Theoretical background

The STADIUM® IDC laboratory module is used to analyze migration test results and estimate the diffusion coefficients of cementitious materials. It is based on the same mass transport model that powers the full version of STADIUM®.

The mathematical model has been described in several publications (see for instance reference (2008)). This appendix summarizes the model and its application to migration test analysis.

The model is based on a Sequential Non Iterative Algorithm (SNIA) that separately solves the transport equations and the chemical equilibrium relationships. The transport equations are discretized using the finite element (FE) method and solved simultaneously using a coupled algorithm. The calculation core begins a time step by solving the transport conservation equations without considering chemical reactions. When this step has converged, the chemical function analyzes each node of the FE mesh and makes sure that the pore solution concentrations and the mineral phases are in equilibrium. When this is completed, another time step starts.

There are four main components to the transport conservation equations: ionic transport, electrodiffusion potential, moisture transport and temperature (energy) conservation. Since migration tests are performed in constant temperature and saturated conditions, terms associated moisture transport and temperature gradients are neglected from the test analysis. The species mass conservation equation is written as:

$$\rho \frac{\partial c_i^b}{\partial t} + \frac{\partial (\phi c_i)}{\partial t} - \text{div}\left(D_i \phi \text{grad}(c_i) + \frac{D_i z_i F \phi}{RT} c_i \text{grad}(\psi) + D_i \phi c_i \text{grad}(\ln \gamma_i) \right) = 0$$

where c_i is the concentration of species i [mmol/L], c_i^b is the amount bound as a result of physical interaction [mol/kg], ϕ is the porosity [m³/m³], ρ is the density of the material [kg/m³], D_i is the diffusion coefficient [m²/s], z_i is the valence number of the ionic species i, F is the Faraday constant [96488.46 C/mol], ψ is the electrodiffusion potential [V], R is the ideal gas constant [8.3145 J/mol/°K], T is the temperature [°K], and γ_i is the activity coefficient. One such equation must be solved for each ionic species considered. The activity coefficients in the model are evaluated on the basis of the Harvie, Moller and Weare (HMW) implementation of Pitzer's ion interaction model.

As mentioned previously, chemical reaction terms are absent from the transport equations because they are solved separately by the chemical module. However, terms are included in the previous equation to take into account the physical interaction between the paste and chloride due to double layer effects. The physical binding term was estimated from binding experiments performed on hydrated C₃S pastes exposed to different chloride

28

concentrations. This term is zero for all ionic species except chloride, for which c_i^b is given by:

$$c_{Cl}^b = \xi p c_{Cl}^u$$

where ξ is a conversion factor involving the amount of C-S-H in the material that converts the isotherm estimated in units of [mol$_{Cl}$/kg$_{dry\ C3S}$] into [mol/kg$_{material}$], and p and u are fitting parameters. The binding experiments were performed at two different pH conditions: $[OH^-]$ = 40 mmol/L and 435 mmol/L. A linear interpolation between these two hydroxide concentrations allows estimating the physical binding at any pH. To balance the charges, a similar term but opposite in sign is applied to OH^-.

The electrodiffusion term in the species conservation equation is primarily responsible for maintaining the electroneutrality in the pore solution. Its role is to balance individual ionic mobility so that there is no net accumulation of charge at any location in the pore solution. This term also accounts for the driving force induced by the external potential applied during the migration test. To solve the diffusion potential, the ionic transport equations are coupled to Poisson's equation, which relates the potential in the material to the ionic profile distributions:

$$\text{div}\left(\tau_s \text{grad}(\psi)\right) + \frac{F}{\varepsilon}\left(\sum_{i=1}^{N} z_i c_i\right) = 0$$

where ε [6.9×10^{-10} C/V/m] is the permittivity of water, τ_s is the intrinsic tortuosity of the material and N is the number of ionic species in the pore solution.

Chemical equilibrium calculations follow transport calculations to enforce the equilibrium between the pore solution and the solid matrix at each node of the FE mesh. This is achieved mainly by precipitating and/or dissolving minerals. It is assumed that the chemical reaction rates are faster than the transport rate, even under an externally applied potential. The validity of this assumption was emphasized in (Samson 2008). The equilibrium of each phase is modeled according to:

$$K_m = \prod_{i=1}^{N} c_i^{\nu_{mi}} \gamma_i^{\nu_{mi}} \qquad \text{with} \quad m = 1, ..., M$$

where M is the number of solid phases, N is the number of ions, K_m is the equilibrium constant (or solubility constant) of the solid m, c_i is the concentration of the ionic species i [mmol/L], γ_i is its chemical activity coefficient, and ν_{mi} is the stoichiometric coefficient of the ith ionic species in the mth mineral. Similar to the transport equations, the chemical activity coefficients are calculated using Pitzer's interaction model. If the solution is not in equilibrium with the paste, solid phases are either dissolved or precipitated to restore equilibrium. The pore solution is thus adjusted to enforce the equilibrium relationships of

the mineral phases. After the pore solution concentrations are modified, the solid phases are also corrected according to:

$$S_m^t = S_m^{t-1} - \frac{\phi X_m \Gamma_m}{\rho}$$

where S_m is the amount of a given solid phase [g/kg of material], t indicates the time step, Γ_m is the molar mass of the solid m [g/mol], and X_m represent the amount of a given solid phase that has to dissolve to reach equilibrium [mol/m^3].

The penetration of chlorides in concrete structures leads to the formation of a chloride-AFm solid compound called the Friedel's salt [11], $3CaO.Al_2O_3.CaCl_2.10H_2O$. During migration tests, chloride interacts with the paste even though the externally applied potential significantly increases the ionic velocity in the pore solution. In STADIUM®, Friedel's salt is not considered a pure phase but rather forms solid solutions with AFm phases: monosulfate and iron-based C_4FH_{13}. The equilibrium relationship for the solid solution is given by:

$$K_{ss} = \frac{(Cl)^2}{(C_{ss})^{2/|z|}} \frac{\chi_{ss}}{\chi_{Friedel}} f_{ss}$$

where K_{ss} is the equilibrium constant of the solid solution, (Cl) is the activity of chloride in the pore solution [mmol/L], (C_{ss}) is the activity of the exchanging species in the AFm end-member [mmol/L], z is the valence number of this species, χ represents the mole fraction of the solids [mol/kg of material], and f_{ss} is a correction factor that accounts for the nonideality of the solid solution.

The diffusion coefficients in the mass conservation equation are expressed as:

$$D_i = \tau_s D_i^o$$

where τ_s is the intrinsic tortuosity of the material and D_i^o is the self-diffusion coefficient of species i [m^2/s]. The self-diffusion coefficients are found in many textbooks and are constant. STADIUM® IDC performs iterations until it finds the tortuosity that allows reproducing the measured currents. The current I [A] are calculated in the model as the sum of the ionic fluxes:

$$I = SF \sum_{i=1}^{N} z_i j_i$$

where j_i [mol/m^2/s] is the ionic flux of species i, and S [m^2] is the surface of the sample. The expression for the flux is:

$$j_i = -D_i \phi \text{grad}(c_i) - \frac{D_i z_i F \phi}{RT} c_i \text{grad}(\psi) - D_i \phi c_i \text{grad}(\ln \gamma_i)$$

The next figures show examples of IDC simulations:

30
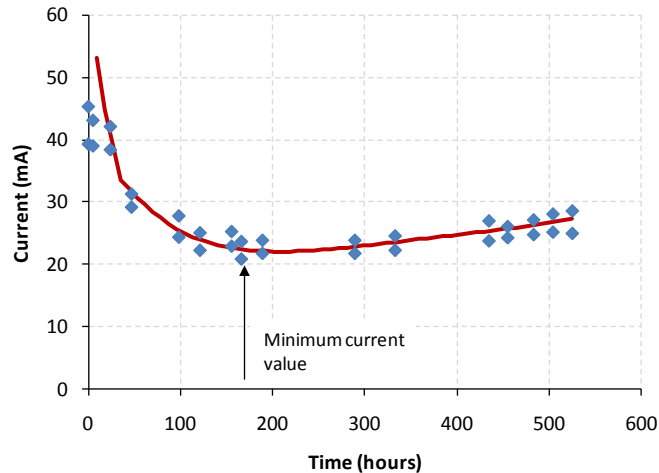
Figure 1 - Simulation of migration test measurements 0.45 w/c OPC mixture, ASTM Type I/II cement

Detailed experimental procedure

1.1 Scope

This test evaluates the diffusion coefficient of ion species in cementitious materials. It is a modified version of the AASHTO T259 and ASTM C1202 Standard Test procedures.

1.2 Summary of Test Method

The test method consists in monitoring the intensity of electrical current passed through a cylindrical test specimen over a 10 to 15-day testing period. An appropriate DC potential is maintained constant across the specimen by an electrical power supply. The upstream cell is filled with a chloride-containing electrolytic solution and connected to the negative electrode, while the downstream cell is filled with a base solution and connected to the positive electrode. If desired, chloride ion penetration through the specimen can be monitored by periodically analyzing the chloride content in the downstream cell.

1.3 Significance and use

▪ The ion diffusion coefficients are the main transport parameters. These coefficients must be evaluated and input into STADIUM® in order to perform a numerical simulation to estimate the service life of a concrete structure.

▪ The output data are the recorded current intensities during testing. This information is required to evaluate the ion diffusion coefficients.

1.4 Apparatus and test cells

- Migration cell assembly [See Section 1.10]

- Constant voltage power supply – output: 0-30V DC; capacity: 0–2 A

- Digital voltmeter: measures DC potential in the 12–24 V range and current intensity to 0.1 mA accuracy in the 0–200 mA range and to 0.01 A accuracy in the 0.2–1 A range.

- Electrically conductive wires to connect the power supply output to the electrodes through jacks attached to the test cells. The electrical resistance of each wire should be less than 0.01 ohm.

- Measuring probes inserted through small holes in the cells to measure potential difference across the specimen. One end of the probe connects to the jack on the voltmeter.

- Vacuum saturation apparatus (vacuum pump, container, pressure gauge, etc.)

- Specimen sizing apparatus (rulers)

- Balance (repeatability: 0.01g)

- Funnel and containers (made of chemical-resistant material).

1.5 Reagents and materials

- Aqueous solution of 0.5M sodium chloride (NaCl) mixed with 0.3M sodium hydroxide (NaOH) [See Section 1.10]

- Aqueous solution of 0.3 M sodium hydroxide (NaOH) [See Section 1.10]

- Sealant: waterproof silicon sealant is recommended.

- Distilled or deionized water for solution preparation.

1.6 Test specimens

Cylindrical specimens are required for the test. It is recommended to test at least two samples per concrete mixture. Specimens should be 96–102 mm (i.e., approximately 4 in.) in diameter. Concrete specimens should be 50 ± 2 mm (2 in.) thick. Mortar specimens should be 35–50 mm thick. Sample preparation and selection depend on the purpose of the test. Test specimens may be obtained from laboratory-cast cylinders or cores extracted from existing structures. All specimens should be properly identified prior to testing. A companion sample is needed for porosity measurement according to ASTM C642 Standard Test Method. This supplementary test provides data for migration test analysis. For relevant results, these additional samples should have identical histories (curing, exposure conditions, and storage conditions) to the testing samples.

1.7 Specimen Conditioning

Test specimens should be vacuum saturated with 0.3M NaOH for approximately 18 hours following the procedure described in ASTM C1202. The saturation procedure is summarized as follows: immerse the specimens in the 0.3M NaOH solution contained in the vacuum container. Turn on the vacuum pump. When the pressure gauge shows maximum vacuum pressure (less than 1 mm Hg, or 133 Pa), keep the pump running for about 2 hours. With all valves closed, turn off the pump and maintain vacuum conditions for 18 hours. Open the air valve to release the pressure.

1.8 Test Procedure

- Dry the surfaces of the vacuum-saturated specimens with a clean cotton cloth or soft tissue.

- Measure the dimensions of each specimen. Diameter and thickness should be measured to a precision of at least 0.1 mm or better. Each parameter is determined by the average of 2 measurements (minimum) at different positions. Weigh the surface-dried specimen to a precision of 0.1g.

- Seal and mount each specimen onto the two connecting rings (See Section 1.10) using silicon, and completely coat all side surfaces with silicon (about 2–3 mm thick, Figure 2).

- Place the specimens in a well ventilated area and cover the exposed surfaces with wet paper for about 2 hours until the silicon is almost dry and strong enough for handling.

- Remove any surplus silicon from the inner surface of the specimen along the ring edges to obtain maximum exposure surface. Make sure to minimize contamination of the exposed surfaces by silicon (Figure 2).

- Measure the diameter of the specimen's actual exposure area using two measurements at different positions across the radial section. This diameter should be approximately equal to the ring mouth diameter.

- Mount the specimen and the two rings onto the two cells (Figure 3). To avoid leakage, apply vacuum grease where the ring assembly comes into contact with the cells. Securely tighten the bolts holding the two cells together. Cells should be filled with water alternatively to verify that there is no leakage. After this control step, empty the water from the cells and remove surplus water with a soft tissue.

- Fill the downstream cell with 0.3M NaOH solution.

- Fill the upstream cell with 0.5M NaCl + 0.3M NaOH solution.

▪ Place the setups in their testing sites and connect all the electrodes on the upstream cells to the negative output of the electricity power supply. Connect all the electrodes on the downstream cells to the positive output of the power supply (Figure 3).

▪ Turn on the power supply. Adjust the potential output to obtain a potential difference of 16–20 V across all specimens. Potential difference across the specimen is measured with two bent probes. Connect the two probes into the voltmeter (plug in the jacks), set the proper range for the voltmeter (e.g., 0–20 V), insert the probes into the cells through the holes in the cells, and place each probe in contact with the surface of the immersed specimen. Wait for the reading to stabilize, then record the voltmeter reading (***Note:*** the potential difference across the specimen is 2–3 volts lower than the output as shown on the power supply or measured from the two electrodes of the cells).

▪ Measure the current passing through each specimen.

- If the current is in 5–100 mA range, the potential level has been properly set. Record the initial readings of the current intensity (to 0.1 mA accuracy) and the potential across the specimen (to 0.1 V accuracy). Record the date and time, the name of the technician performing the measurement and the digital voltmeter used.

- If the current passing through the specimen is below 5 mA, increase the output potential up to a maximum of 30 V to obtain a current in the proper range.

- If the current is above 100 mA, decrease the potential output to bring the current down to the proper level (i.e., lower than 70 mA).

- If the initial current under a low potential (e.g., 6 V) is higher than 100 mA, the test should be performed for 7-day period only.

- A single power supply can run a set of tests if they share the same potential output. The maximum number of tests depends on the supply output power and total current intensity. When tests share the same power supply, set the supply current control to maximum range to ensure a sufficient power output under the desired constant potential. During testing, both current intensity passing through the specimen and the potential difference across the specimen might vary within a certain range, even though the electrical output remains stable and constant.

▪ During the first day of testing, take measurements of the current intensity passing through each specimen and the potential difference across each specimen at 0, and 4 hours of duration respectively. Record the time of each measurement.

▪ After the first day, take measurements of the current passing through each specimen and the potential difference across each specimen at 24-hour time intervals for 14 days. Record the time of each of these measurements.
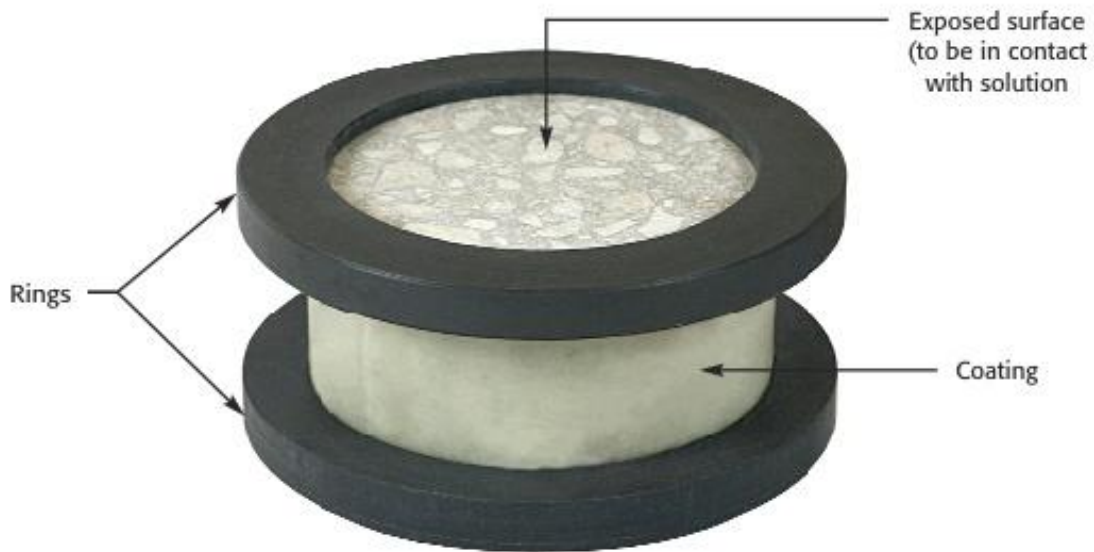
Figure 2 - Test specimen sealed and mounted onto the two rings and coated with silicon
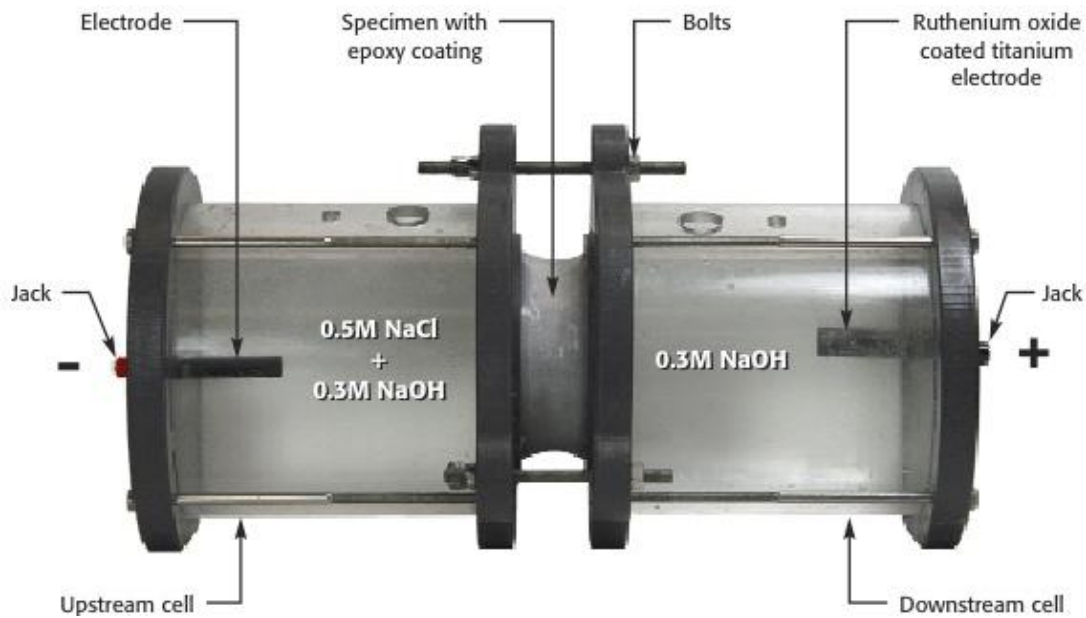
Figure 3 - Migration test setup

1.9 Report

Report the following, if known:

- Information on the specimens: origin (e.g., mixture ID and curing age of the concrete), dimensions, mass before and after vacuum saturation, and effective test exposure area (diameter) for both upstream and downstream sides.

- Porosity test results for companion samples.

- Experimental record sheet, including test specimen IDs, test conditions, date and time of each measurement, all potential readings across specimens, and currents passed through specimens for the entire testing period.

- Any abnormal phenomena observed during testing, such as changes in solution color, solution precipitation, excessive gas evolution from the electrodes, unusual odors, accidents or problems concerning the electricity supply, etc.

1.10 Additional information

<u>Migration Cell Assembly</u>

Cells

The migration test cells consist of two symmetrical chambers made of polymer materials (e.g., methyl methacrylate). Each cell is equipped with an electrode (see below) and an external connector (jack). The volume of each cell should be approximately 3 liters. The mouth of the cell should fit the connecting ring (Figure 4).

Connecting Rings

Two connecting rings are required for the test setup. The ring should be made of polymer materials and designed to hold the specimen from one side and connected to the cell from the other side. The exposure area should be as large as possible. A typical design for a 4-in. cylindrical specimen is shown in Figure 4.
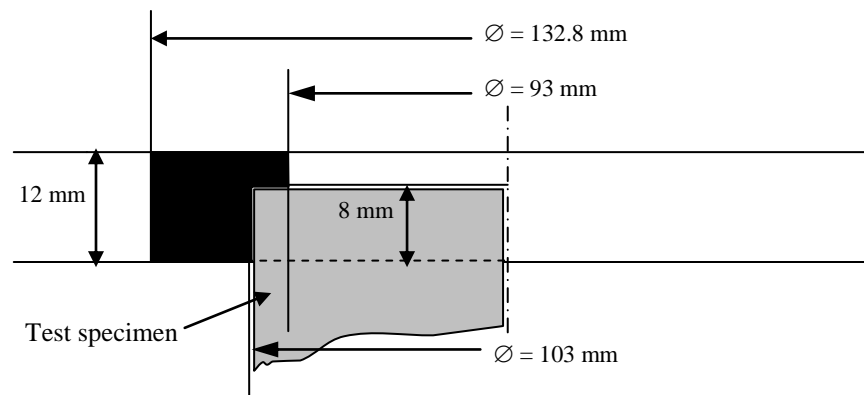
Figure 4 - Connecting ring for 4-in. specimen (96–103 mm)

Electrodes

A rod electrode is installed on each cell. Carbon electrodes should be avoided because they tend to decompose in the electrolytic solution under the application of a DC

potential. Electrodes made of titanium or ruthenium oxide with titanium coating are recommended. Each electrode should be securely connected to the external connector by the jack (Figure 3).

<u>Solution preparation</u>

The following procedure describes the preparation of the aqueous solutions:

- Accurately weigh the salt or base (e.g., NaCl or NaOH) of high purity (>99%) to at least 0.001 g accuracy (refer to Table 1).

- Completely dissolve the salt or base into a certain amount of distilled or deionized water.

- Dilute with more distilled or deionized water to a final volume of desired range.

- Thoroughly stir the solutions to obtain homogeneity.

Table 1 - Chemical composition of 1-liter (1000 ml) solutions

Salt /Base (purity: 99%)	Upstream solution (salt): 0.5M NaCl + 0.3M NaOH	Downstream solution (base): 0.3M NaOH
NaOH (g/liter)	12.121	12.121
NaCl (g/liter)	29.515	0

B. Desorption isotherm test procedure

1. Scope

This test method covers the measurement of the equilibrium water content of cementitious materials exposed to a specific relative humidity environment. This test method provides desorption isotherms.

2. Summary of Test Method

This test method consists of monitoring the mass of pre-saturated cementitious materials in a constant relative humidity environment at a constant temperature until materials reach moisture equilibrium. The different relative humidities are maintained in relatively small containers (boxes) using different supersaturated salt solutions.

3. Significance and Use

Isotherms give the equilibrium relationship between relative humidity and water content of the tested material at constant temperature.

The shape of the isotherms depends on many factors including: (a) concrete mixture proportions, (b) presence of chemical admixtures and supplementary cementitious materials, (c) composition and physical characteristics of the cementitious component and aggregates, (d) entrained air content, (e) type and duration of curing, (f) degree of hydration or age, (g) presence of microcracks, (h) presence of surface treatments such as sealers or form oil and (i) placement method including consolidation and finishing. Equilibrium water content is also function of temperature.

4. Apparatus

4.1 Humidity boxes – One or more relatively small containers (boxes) should be prepared where saturated salt solutions are placed on the bottom of the container. The dimension of the boxes and preparation of salt solution should respect the requirements stated in ASTM E104 "Standard Practice for Maintaining Constant Relative Humidity by Means of Aqueous Solutions". A support should be installed in each box that can properly hold the test specimens. The number of box depends on the number of relative humidities to be tested and the total amount of test specimens, which is on the user's choice.

4.2 Balance – The balance to be used to determine the mass of the specimens during the test should have a sufficient capacity and a precision of 0.01g. The balance should be installed in a place near the humidity boxes.

4.3 Hygrometers – Small size hygrometers are needed and should be properly installed in each humidity box in order to monitor the relative humidity and temperature inside the boxes during the test period.

4.4 Device for weighing specimens in water – A device should be prepared that allow to weigh the specimens in water (Figure 1).

4.5 Towel – absorbable tissues should be prepared to remove the surface water of pre-saturated specimens.

4.6 Container and limewater – a container with certain amount of lime water inside (saturated $Ca(OH)_2$ solution) are needed to saturate the specimens before test (To make saturated $Ca(OH)_2$ solution, dissolve 3g Ca(OH) into 1 litre water.)
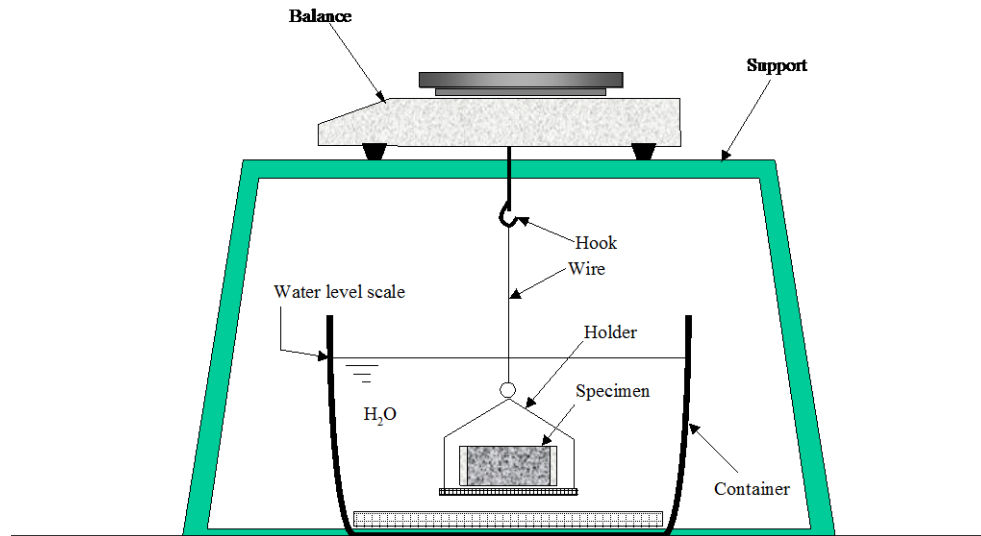
Figure 1 – Device for weighing specimen in water

5. Reagents and Materials

The salt needed depends on the relative humidity to be tested. Some salts that normally used to maintain constant relative humidities and recommended by ASTM E104 are as follows:

LiCl – for maintaining 11% R.H. at $23 \pm 2°C$.

$MgCl_2$ – for maintaining 33% R.H. at $23 \pm 2°C$.

$MgNO_3$ – for maintaining 53% R.H. at $23 \pm 2°C$.

NaCl – for maintaining 75% R.H. at $23 \pm 2°C$.

KCl – for maintaining 84% R.H. at $23 \pm 2°C$.

$BaCl_2$ – for maintaining 90% R.H. at $23 \pm 2°C$.

KNO_3 – for maintaining 94% R.H. at $23 \pm 2°C$.

K_2SO_4 – for maintaining 97% R.H. at $23 \pm 2°C$.

6. Test Specimens

6.1 Test specimens should be fully hydrated concrete (e.g., >3 months curing) to minimize possible microstructural changes during test.

6.2 Specimens should have sufficient exposed surface area and representative volume. This shall be obtained by sawing a number of thin slices from representative concrete specimens (e.g. cast concrete cylinders).

6.3 For normal weight concrete, a practical specimen should have a diameter of 100 ± 2 mm and a thickness of 10 ± 1 mm. Specimen of cement paste may be as thin as 3 to 5 mm with a section area ≥ 25 cm^2.

6.4 Minimum three (3) specimens are required for each relative humidity condition to be tested.

6.5 The test specimens should be kept constantly moist during specimen preparation.

6.6 The specimens should be fully saturated before being tested. To saturated the specimens, immerse the specimens in limewater (saturated $Ca(OH)_2$), monitor their weight (surface dry) change until constant weight is observed: weigh each specimen at time interval of 5-7 days until four successive mass determinations show mass variation <0.5% of its initial mass.

7. Procedure

7.1 All the humidity boxes to be used for the tests should be placed in a normal laboratory environment where constant temperature of $23 \pm 2°C$ is maintained.

7.1 Measure the dimension of each specimen to be tested : take three determinations of the thickness and two measurements of the diameter with precision of 0.01mm.

7.2 Weigh each specimen in pure water (W_1) using the device mentioned in section 4.4.

7.2 Carefully dry the surface of each specimen by absorbing the surface water using a moist tissue; then weigh it in air with precision of 0.01g, take down the initial mass of the surface dry-saturated specimen (W_0).

7.3 Properly place the specimens on the support inside the humidity box (vertically and slightly inclined position is recommended, see Figure 2) with space ≥ 2cm between the specimens, then, close the cover.

7.4 Weigh each of the specimen with precision of 0.01g at time interval of 5-7 days (normally one weighing per week) (Note 1). Determine the mass change between each two successive mass determinations.

Note 1: During each mass determination, the specimens should not be exposed to the environment outside the humidity box for more than one minute. If the balance is installed in a distance from the humidity box, seal the specimens in plastic bag during transportation.

7.5 Stop the test when four (4) successive mass determinations show mass change (absolute value) less than 0.5% of the cumulative mass loss during the test period.
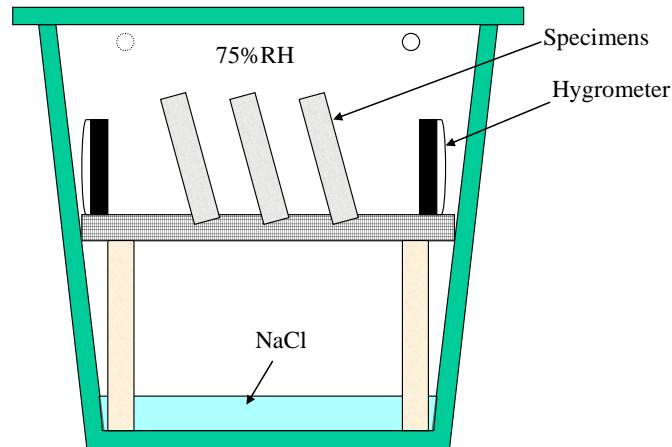
Figure 2 – Humidity box and tested specimens inside during isotherm test

8. Report

Report the following:

8.1 Information about the specimens - mixture ID and curing age of the concrete tested and porosity tested according to ASTM C642 standard procedure.

8.2 Experimental recording sheet that includes the ID of the test specimens, apparent mass in water (W_1), the initial mass of surface-dry specimens in air (W_0), date and time of each mass determination, and all the recordings of mass determination during the entire test period.

8.3 The equilibrium water content

The equilibrium water content at the relative humidity tested is calculated based on the following relationship:

$$\theta(RH)\% = \phi - 100 \times \frac{W}{V}$$

Where $\theta(RH)$ is the equilibrium water content (%) at the tested relative humidity(RH), Ø is the porosity (%) determined according ASTM C642 standard procedure , W is the cumulative mass loss (g) during the entire test period, V is the volume (cm^3) of the tested specimen ($V = W_0 - W_1$).

8.4 If more than two relative humidities have been tested, plot the equilibrium water contents obtained against the corresponding relative humidities. If more than four (4) water contents at different relative humidities have been obtained, analysis based on curve fitting may also be performed, which may provide approximation of the isotherm in larger range of relative humidity.

C. Van Genuchten expression

The Van Genuchten relationship commonly used in the field of cementitious material is given by:

$$S = \left[\left(\frac{p_c}{a} \right)^{\frac{1}{1-m}} + 1 \right]^{-m}$$

where p_c is the capillary pressure (MPa) and a (MPa) and m are the fitting parameters. The saturation S corresponds to w/w_s, where w is the water content and w_s is the water content at saturation, usually considered the same as porosity. This expression assumes that residual saturation S_r is zero, which is a common assumption in cementitious materials. Values of a=35.1 MPa and m=0.27 were estimated for this study.

In soil moisture transport, Van Genuchten relationship is usually expressed as:

$$S_e = \frac{S - S_r}{1 - S_r} = \frac{1}{\left[1 + (\alpha h)^n \right]^m}$$

The two expressions are equivalent. Based on Van Genuchten definitions (Fetter 1999):

$$n = \frac{1}{1 - m}$$

Comparing the expressions shows that:

$$\frac{p_c}{a} = \alpha h$$

Since by definition (Fetter 1999), the pressure potential h can be written as:

$$h = \frac{p_c}{\rho_w g}$$

It follows that:

$$\alpha = \frac{\rho_w g}{a}$$

Based on the values of a and m given previously, one would get n=1.37 and α=0.028 1/cm.

D. Drying test procedure

Theoretical background

The STADIUM® MTC laboratory module uses the moisture transport model in STADIUM® to analyze drying test results and evaluate the intrinsic permeability of the material as well as the moisture retention (desorption isotherm) function.

The moisture transport equation combines the mass conservation of liquid and vapor phases in a single expression based on the relative humidity state variable. Since the drying test is performed in isothermal conditions, terms associated with temperature variations are not considered. The mass conservation equation is given by:

$$\frac{\partial w}{\partial H}\frac{\partial H}{\partial t} - \text{div}\big(D_{mH}\text{grad}(H)\big) = 0$$

where H is the relative humidity [Pa/Pa], w is the water content [m^3/m^3] and the parameter D_{mH} [m^2/s] is the nonlinear transport coefficients. The nonlinear transport parameter D_{mH} considers the contribution of liquid and vapor phases:

$$D_{mH} = \frac{k_s k_r^l \rho_l R}{\mu M_w}\frac{T}{H} + \frac{D_v^o \tau_s \tau_r^g M_w p_v^s}{\rho_l R}\frac{(\phi - w)}{T}$$

where ϕ is the porosity [m^3/m^3], k_s is the intrinsic permeability [m^2], k_r^l is the relative liquid permeability [–], ρ_l is the liquid water density [kg/m^3], R is the ideal gas constant [J/mol/°K], μ is the dynamic viscosity of the liquid phase [Pa.s], M_w is the molar mass of water [kg/mol], D_v^o is the self-diffusion coefficient of water vapor [m^2/s], θ_g is the gas phase content [m^3/m^3], τ_s is the intrinsic tortuosity [–], τ_r^g is the relative tortuosity of the gas phase [–], and p_v^s is the saturation vapor pressure [Pa].

Most of the parameters in the previous expression can be found in the literature:

- T: corresponds to the testing temperature. The drying tests are usually performed at 23 °C.

- R: the ideal gas constant has a value of 8.3145 J/mol/°K.

- ρ_l: data on density of water between 0 °C and 100 °C found in reference (Robinson 2002) were fitted to a fourth-order polynomial and implemented in STADIUM®.

- μ: similar to density, data on viscosity of water between 0 °C and 100 °C (Robinson 2002) were fitted to a nonlinear function and implemented in STADIUM®.

- M_w: the molar mass of water is 0.018 kg/mol.

- D_v^o: the self-diffusion coefficient is given by an empirical function depending on temperature and ambient atmospheric pressure (Galbraith 1997).

- p_v^S: the calculation of saturation vapor pressure is based on a relationship found in Bolton (1980).

The calculation of D_{mH} also involves expressions for relative liquid permeability and relative gas tortuosity. The relationship for relative liquid permeability implemented in STADIUM® is based on a power function similar to the Millington and Quirk relationship (1961) used for ionic diffusivity. The relative gas tortuosity expression was derived on the basis of data found in the literature (Sercombe 2007).

Some parameters are obtained from other testing procedures. This is true of porosity and tortuosity. Porosity is measured from the ASTM C642 test procedure. Tortuosity is measured on the basis of a migration test. This testing procedure is part of the STADIUM® Lab package.

The final parameter needed for the analysis is the moisture isotherm function *w=f(H)*, which characterizes the moisture equilibrium of the material. In STADIUM®, this relationship is expressed as:

$$w = \frac{\phi}{\beta\phi(H^\delta - 1) + 1}$$

where β [–] and δ [–] are parameters that can be determined experimentally. Typical isotherm curves are shown in the next figure. In STADIUM® MTC, the parameter δ is estimated from the concrete mixture composition. The parameter β is calculated directly from the mass loss data measured from the 10-mm series during the drying test.
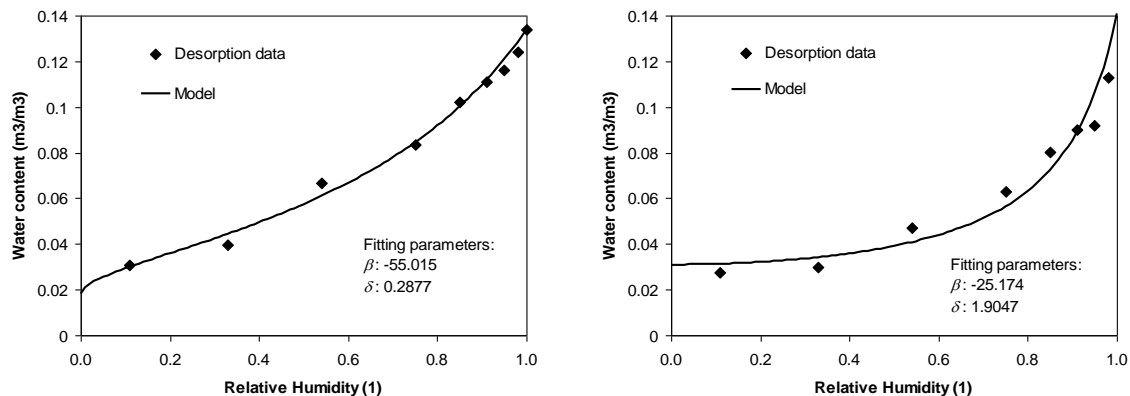
a) Ordinary concrete, 0.5 w/c   b) Ordinary concrete, 0.75 w/c

Figure 1 - Typical moisture isotherms

The only unknown parameter in the moisture transport model is the permeability. STADIUM® MTC finds the permeability iteratively by solving the moisture transport

equation until the model reproduces the measured mass loss of the 5-cm drying test series. The equation is discretized using the finite element method and an Euler implicit scheme for the transient term. The nonlinear system of equation resulting from the discretization is solved using Newton's method. The calculations begin assuming initial saturation of the material (H=1.0). The boundary conditions are expressed as an exchange term:

$$q = h_w(H - H_\infty)$$

where h_w is the exchange coefficient [m/s] and H_∞ is the relative humidity of the environment. The default value of h_w is 5.0e-9 m/s and the relative humidity is 0.5 (50%), according to the drying test laboratory procedure. The value of h_w corresponds to the exchange coefficient in a properly ventilated chamber.

The mass loss curves are calculated from the relative humidity profiles. At selected time steps, the model first calculates the water content from the relative humidity using the water desorption isotherm. The water content profile is then integrated to obtain the mass loss:

$$\Delta M|_t = \left[\int_0^L (\phi - w)dx \right] S$$

where $\Delta M|_t$ is the mass loss evaluated at time t [grams], L is the average thickness of the samples [cm], and S is the average exposed surface [cm^2]. The next figures show examples of STADIUM® MTC simulations.
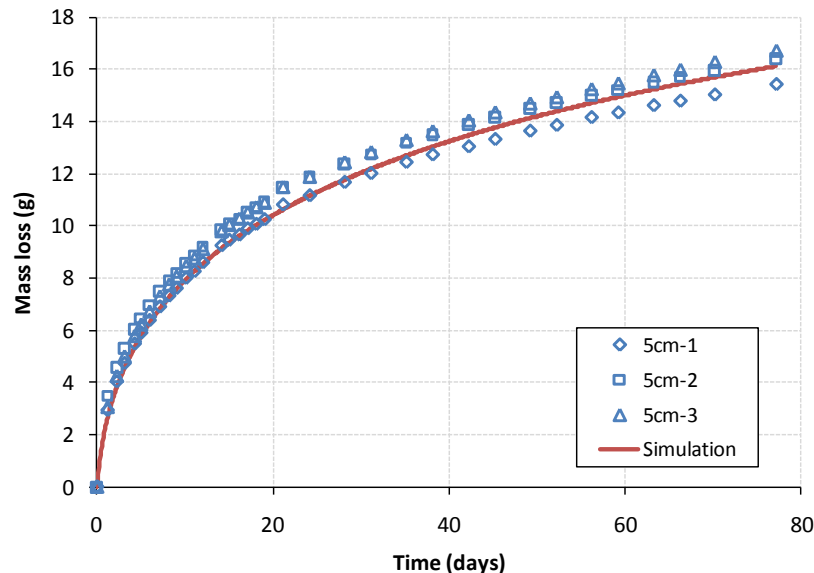
Figure 2 - STADIUM® MTC simulation of OPC mixture (Type V cement, 0.45 w/c)
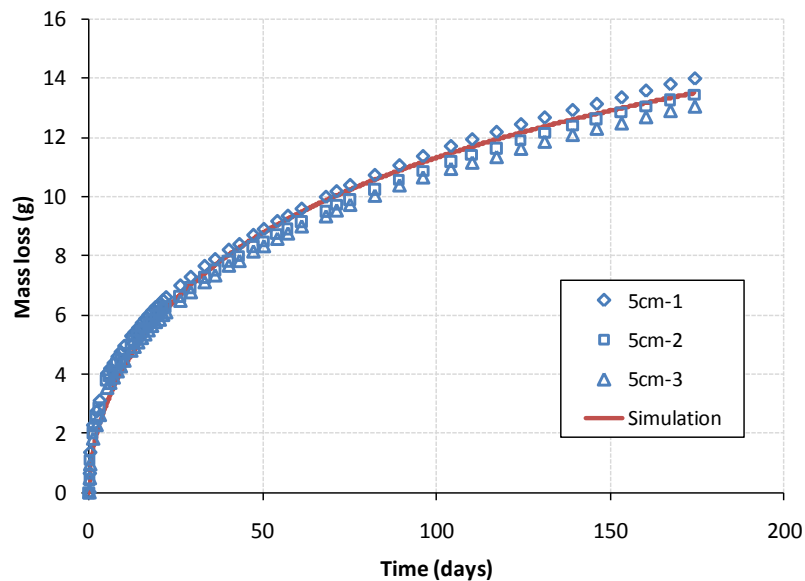
Figure 3 - STADIUM® MTC simulation of mixture with silica fume

Detailed experimental procedure

1.1 Scope

This test determines the drying rate of Portland cement concrete by measuring the mass loss due to evaporation and moisture transport in specimens exposed to constant temperature and relative humidity.

1.2 Significance and Use

Drying behavior reflects the mass transport properties of concrete (e.g., permeability) to a certain extent, and depends on a number of factors such as concrete mixture proportions, presence of chemical admixtures and supplementary cementitious materials, composition and physical characteristics of the aggregates and cementitious materials, curing conditions, degree of hydration, presence of microcracking, and surface treatments such as sealers and membranes. Drying behavior is also strongly affected by the moisture condition of the concrete as well as environmental conditions such as temperature, relative humidity, and air flow rate.

1.3 Apparatus

- Drying chamber: The test must be performed in a temperature and humidity controlled chamber with temperature maintained constant at 23±2°C and relative humidity at 50±4%. The chamber should have proper support (e.g., a shelf) inside to allow airflow around each specimen. The chamber should be sufficiently spacious to hold all the test specimens. The chamber should be well ventilated,

with airflow rate according to ASTM C157: 5.4 (Standard specifications for drying chamber).

- Hygrometer: During testing, 2–3 hygrometers should be placed near the specimens to monitor local relative humidity. Digital hygrometers are recommended.

- Absorbent tissues: at least two. Tissues should be at least 35cm × 35cm in size.

- Balance: The balance for weighing the specimens should have a capacity of ≥ 1500g and a repeatability of ≤ 0.01g. It should be mounted on a proper support (Figure 4) in the laboratory.

- Device for weighing specimens in water: The device should allow the operator to conveniently weigh the specimens in water using the same balance (Figure 4).

1.4 Sealing and Coating Materials

- Epoxy: Various brands of commercial epoxy may be used provided it has excellent coherence with concrete and is completely impermeable.
- In some cases, wax may also be used as sealing material.
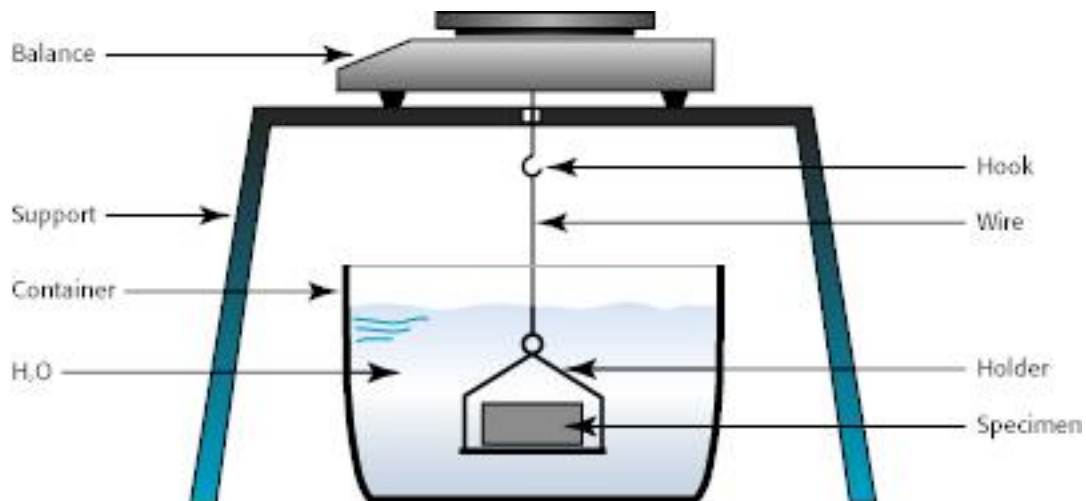
Figure 4 - Balance and device for weighing specimen in air and water

1.5 Test Specimens

- Three cylindrical specimens 10 ± 1 mm in length and three specimens 50 ± 2 mm in length should be prepared for each tested material. Test specimens may be cut from either laboratory-made cylinders or cores extracted from field structures.

- When testing laboratory-made concrete, the concrete should be cured in saturated conditions (e.g., in limewater or a 100% R.H. moist chamber) for at least 28 days, and the diameter of the cast cylindrical specimens should be at least 100 mm (4 inches). Prepare test specimens according to the following procedure:

  o One week prior to testing, cut test specimens as described in 1.5 from the middle portion of the cylinders (Figure 5).
  o Take the dimension of each test specimen to the nearest 0.1 mm (three length measurements and three diameter measurements).
  o Weigh each specimen in air (Note: when weighing a wet specimen, dry the surface with cloth or tissue before putting it on the balance) and in water, respectively using the balance and the device, as described in 1.4 and 1.5 and shown in Figure 4.
  o Coat and seal the side (round) surface of each specimen with impermeable material, as described in Section 1.4, leaving the two end-surfaces uncoated to act as exposed surfaces (Figure 6) (Note: before applying coating material, thoroughly dry the surface of the specimen by rapid blowing with compressed air).
  o Once the coating and sealing layer has dried and hardened, place the specimens in limewater until testing.

- When testing field concrete, cores with a diameter of at least 100 mm (4 inches) should be extracted from the structure. Once the cores are received at the laboratory, do the following:

  o Photograph the cores.
  o Cut test specimens from the cores, as described in 1.5 (Note: the test specimen may or may not contain the exposed surface of the structure, depending on the requirement).
  o Take the dimensions of each test specimen to the nearest 0.1 mm (two measurements of thickness and two measurements of diameter).
  o Immerse the specimens in limewater for one week, then weigh each specimen in air (see Note for 1.5) and in water
  o Coat and seal the side (round) surface of each specimen with impermeable material, as described in Section 4 (see Figure 6).
  o Once the coating and sealing layer has dried and hardened, weigh the specimens, then immerse them in limewater for 7 days and weigh them again. If the weight determined after immersion for the same specimen shows >0.5% variation from the previous mass of the specimen, re-immerse it in limewater for another 7 days and weigh it again. Once the weight determined after the additional 7 days' immersion shows <0.5% variation from the previous mass of the specimen, the specimen

is ready for testing. For the drying test, it is very important that the test be started when the samples are fully saturated. All mass should be taken in a SSD state.

▪ In both cases, the test specimens should be kept in limewater before beginning the drying test.

▪ Porosity and ion diffusion coefficient must be determined in order to analyze the drying test results.
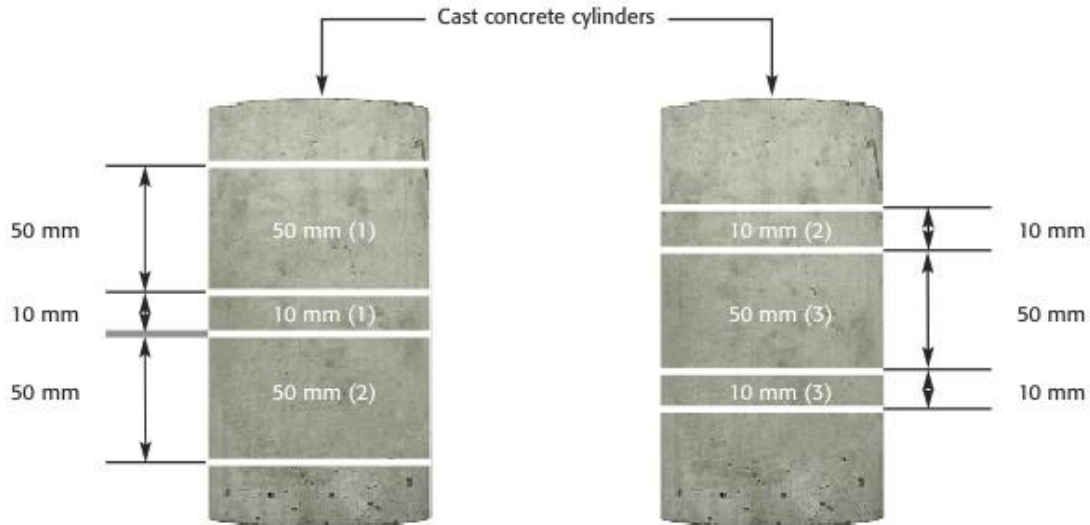
Figure 5 - Preparation of test specimens from the middle portion of laboratory cast concrete cylinders of 4 in (100mm) in diameter

1.6 Procedure

▪ Remove the surface water from the saturated test specimens (with sealed side surfaces) using moist tissue. Place the specimens near the balance. Protect the surfaces of specimens with moist tissue to prevent them from drying.

▪ Take the initial masses by weighing them on the balance one at a time (Figure 4). Each weighing should last no longer than 30 seconds. After each weighing, protect the specimen with the moist tissue to prevent it from drying.

▪ When the initial masses of all the specimens have been taken, transfer all the specimens at the same time to the drying chamber. Place them on the appropriate supports (Figure 6 or 7). Record the time and date on the work sheet, and the drying test begins.
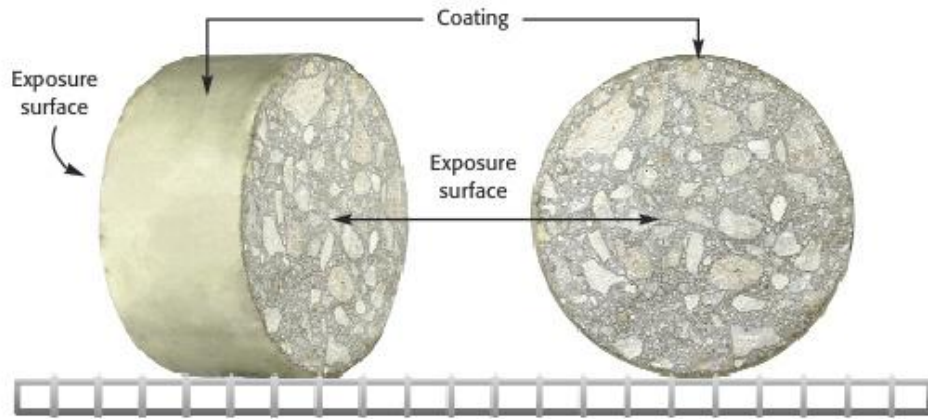
Figure 6 - Case 1: the specimen is placed on a shelf in the drying chamber
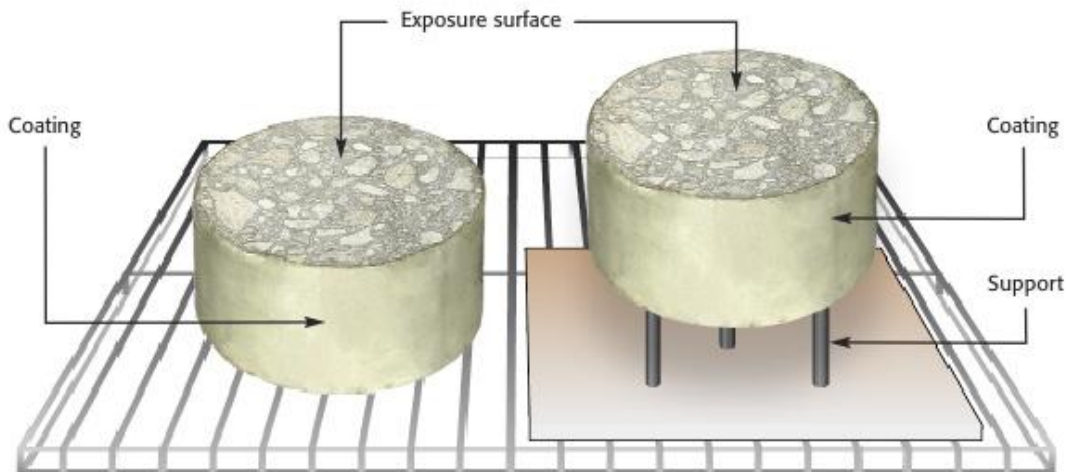
Figure 7 - Case 2: the specimen is placed on a support in the drying chamber

- Monitor the weight change of the specimens by periodically weighing them in the same place in the laboratory and using the same balance, according to the following schedule (Note: each weighing of all six specimens should be completed within five (5) minutes):

  o Week 1: one (1) measurement (including initial weighing) per day, with a time interval of 24 ± 2 hours

  o Week 2: three (3) measurements per week, with a time interval of 48 ± 2 hours.

  o After week 2: one (1) measurement per week, with a time interval of 7 ± 1 days.

- Stop the drying test when constant mass is observed for the 10-mm thick specimens. The constant mass is defined as four successive mass measurements that show less than ±0.5% variation from the previous measurement:

$$\left| \frac{100 \times (m_i - m_{i-1})}{m_i} \right| < 0.5$$

where m_i is the current measurement and m_{i-1} is the previous one.

1.7 Report

- Data on the specimens: (1) age of hydration; (2) date when the specimens were extracted; (3) dimensions of each specimen; (4) weights of each specimen before coating, taken in air and water
- Concrete mixture or material reference number and all other relevant information (cement type, cure duration, w/c ratio, etc.).
- Porosity tested according to ASTM C642 whenever possible.
- Ion Migration Coefficient (modified ASTM C1202).
- Completed experimental records: mass determinations over the entire test period.
- Cumulative mass losses plotted against testing time (Figure 8).
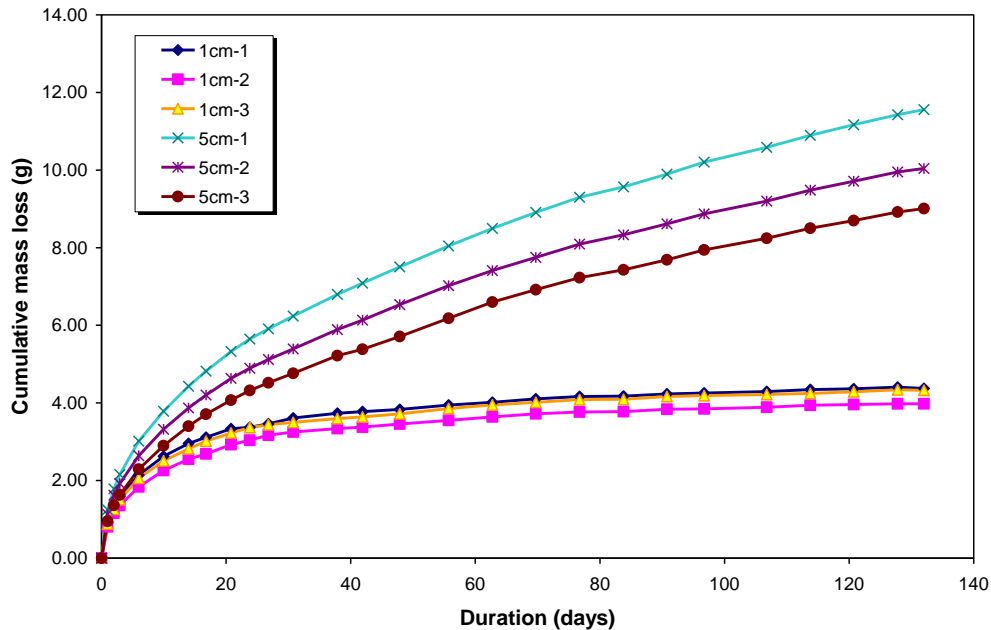
Figure 8 - Mass loss in specimens during drying test

E. Complete experimental data for drying test

Table 11 – Mass change determination in drying test

Duration	Cumulative mass loss (g)						Average	
Days	1cm-1	1cm-2	1cm-3	5cm-1	5cm-2	5cm-3	1cm	W_{50} (%)
0.00	0.00	0.00	0.00	0.00	0.00	0.00	0.00	15.78
1.02	3.04	2.98	2.97	3.75	4.54	4.26	3.00	13.94
1.93	3.50	3.44	3.45	4.41	5.09	4.98	3.46	13.66
2.88	3.87	3.80	3.83	4.93	5.73	5.52	3.83	13.43
5.99	4.64	4.62	4.66	6.15	7.34	6.80	4.64	12.94
6.92	4.77	4.73	4.81	6.35	7.61	7.06	4.77	12.86
8.01	4.94	4.89	4.99	6.63	7.97	7.36	4.94	12.75
9.96	5.30	5.14	5.28	7.13	8.65	7.90	5.24	12.57
13.06	5.55	5.43	5.63	7.72	9.45	8.51	5.54	12.39
15.01	5.72	5.58	5.79	8.00	9.89	8.83	5.70	12.29
20.91	6.09	5.97	6.23	8.86	11.11	9.76	6.10	12.05
27.91	6.44	6.25	6.56	9.65	12.35	10.58	6.42	11.85
35.01	6.66	6.52	6.86	10.36	13.40	11.30	6.68	11.69
41.90	6.87	6.72	7.11	10.98	14.31	11.98	6.90	11.55
48.90	7.04	6.87	7.30	11.48	15.12	12.53	7.07	11.45
55.97	7.20	7.02	7.49	12.01	15.92	13.09	7.24	11.35
63.11	7.35	7.14	7.63	12.50	16.65	13.58	7.37	11.26
70.03	7.48	7.24	7.77	12.94	17.35	14.05	7.50	11.19
76.88	7.62	7.35	7.91	13.37	17.97	14.46	7.63	11.11
70.03	7.48	7.24	7.77	12.94	17.35	14.05	7.50	11.19
76.88	7.62	7.35	7.91	13.37	17.97	14.46	7.63	11.11
84.01	7.71	7.46	8.07	13.80	18.63	14.92	7.75	11.03
90.93	7.79	7.53	8.16	14.14	19.19	15.28	7.83	10.99
97.94	7.87	7.62	8.26	14.49	19.74	15.63	7.92	10.93
84.01	7.71	7.46	8.07	13.80	18.63	14.92	7.75	11.03
90.93	7.79	7.53	8.16	14.14	19.19	15.28	7.83	10.99
97.93	7.87	7.62	8.26	14.49	19.74	15.63	7.92	10.93
105.01	7.96	7.68	8.34	14.86	20.27	16.00	7.99	10.88
111.94	8.02	7.76	8.46	15.17	20.77	16.33	8.08	10.83
118.96	8.14	7.89	8.56	15.52	21.29	16.71	8.20	10.76
125.95	8.17	7.94	8.62	15.79	21.72	16.99	8.24	10.73
133.03	8.27	8.03	8.73	16.18	22.26	17.39	8.34	10.67
139.94	8.34	8.10	8.80	16.45	22.65	17.67	8.41	10.63
146.93	8.44	8.18	8.89	16.77	23.11	17.99	8.50	10.57
153.94	8.52	8.29	9.01	17.09	23.54	18.32	8.61	10.51
161.06	8.62	8.37	9.11	17.42	23.99	18.65	8.70	10.45
168.01	8.64	8.37	9.12	17.64	24.31	18.86	8.71	10.44
174.93	8.74	8.46	9.21	5cm series stopped				
181.95	8.79	8.51	9.27				8.86	10.36
188.93	8.87	8.57	9.34				8.93	10.31

Table 12 – Mass change determinations for test series of 10cm

Duration	Cumulative mass loss (g)		Average (g)
Days	10cm-1	10cm-2	10mm
0.00	0.00	0.00	0.00
1.15	3.60	3.65	3.63
1.95	4.19	4.22	4.20
2.96	4.77	4.76	4.76
5.97	5.86	5.81	5.84
6.95	6.15	6.10	6.13
8.01	6.39	6.33	6.36
9.94	6.89	6.77	6.83
14.00	7.65	7.58	7.62
20.99	8.71	8.65	8.68
28.05	9.99	9.99	9.99
34.99	10.82	10.78	10.80
41.94	11.58	11.64	11.61
48.97	12.29	12.28	12.28
56.16	13.00	12.98	12.99
63.04	13.49	13.49	13.49
69.95	14.16	14.14	14.15
76.97	14.58	14.56	14.57
83.95	15.07	15.07	15.07
91.16	15.53	15.56	15.54

Page Intentionally Blank

Appendix B. 2012 SIMCO E-Area Concrete Long-Term Durability Simulation (SIMCO 2012)

Page Intentionally Blank

Washington Savannah River Company

Subcontract no. RA00097

E-Area Concrete Long-Term Durability Simulations
Final Report

January 25th 2012

Presented by:

SIMCO Technologies Inc.
203-1400 Boul. du Parc Technologique
Quebec QC   G1P 4R7
Canada
(418) 656-0266 tel | (418) 656-6083 fax

LIMITED LIABILITY STATEMENT: This report is for the exclusive use of SIMCO's Client and is provided on an "as is" basis with no warranties, implied or expressed, including, but not limited to, warranties of merchantability and fitness for a particular purpose, with respect to the services provided. SIMCO assumes no liability to any party for any loss, expense or damage occasioned by the use of this report. Only the Client is authorized to copy or distribute this report and then only in its entirety. The analysis, results and recommendations contained in this report reflect the condition of the samples tested exclusively, which were manufactured from materials provided to SIMCO by the Client or by third parties. The report's observations and test results are relevant only to the samples tested and are based on identical testing conditions. Furthermore, this report is intended for the use of individuals who are competent to evaluate the significance and limitations of its content and recommendations and who accept responsibility for the application of the material it contains.

The Stadium® model is a helpful tool to predict the future conditions of concrete materials. However, all durability-modeling parameters have a statistical range of acceptable results. The modeling used in this report uses mean laboratory- or field-determined single values as input parameters. This provides a single result, which provides a simple analysis evaluating contaminant penetration and/or material alteration. Previous conditions are assumed to carry forward in the prediction model; there are no assurances that the structure will be exposed to a similar environment as in the past.

1. OBJECTIVE

The objective of the project is to simulate the long-term durability of a concrete mixture exposed to different potential environments. The concrete used for the simulation corresponds to the E-Area mixture, which was cored and tested in the first portion of subcontract RA00097.

Using the transport properties evaluated previously, the material was exposed to different exposure scenarios, summarized in the following figures.
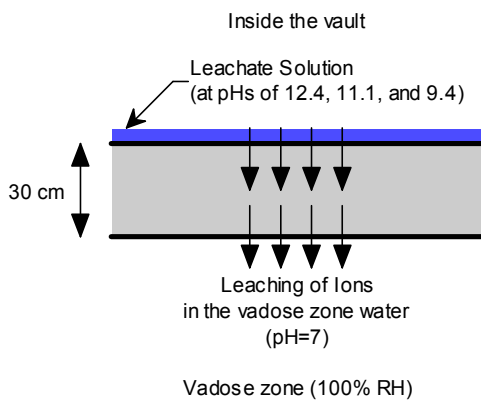
Figure 1 - Scenario 1: LAW Vault Floor with No Carbonation
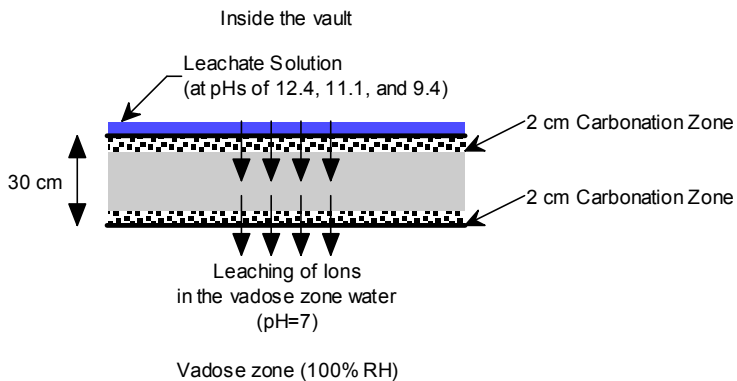
Figure 2 - Scenario 2: LAW Vault Floor with Carbonation (1994 to 2025)
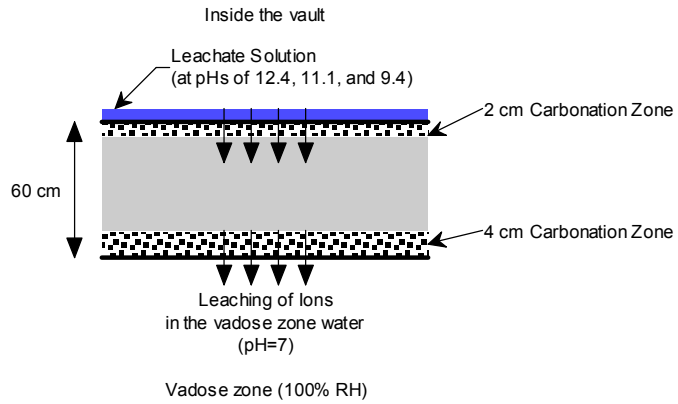
Figure 3 - Scenario 3: LAW Vault Wall with Carbonation (1994 to 2125)

All reactive transport simulations were performed with the model STADIUM®, developed by SIMCO Technologies. Details on the model and the different simulation parameters are provided in the next sections.

2. MODEL DESCRIPTION

STADIUM® is a model that simulates ionic transport in saturated/unsaturated, isothermal/non-isothermal cementitious materials. Stadium® simulates the ingress of the contaminants and leaching of the ionic species in the pore solution, and the modifications to the microstructure of the cementitious material, e.g. portlandite (calcium hydroxide) dissolution, calcium silicate hydrate (C-S-H) decalcification, ettringite and gypsum formation, etc. Details can be found in papers [Samson 2006, Samson 2007, Samson 2007b].

The present version of the model does not include any coupling with mechanical damages. It does not allow predicting the apparition of cracks resulting from the exposure to an aggressive environment (e.g. sulfate attacks) or internal chemical degradation such as alkali silica reaction (ASR).

The ionic transport is described by the extended Nernst-Planck equation applied to unsaturated and non-isotherm materials. This equation accounts for the electrical coupling as well as the chemical activity between ionic fluxes, transport due to water content gradient and temperature effects:

$$\frac{\partial(wc_i)}{\partial t} - div\left(D_i w \mathrm{grad}(c_i) + \frac{D_i z_i F}{RT} wc_i \mathrm{grad}(\psi) + D_i c_i \, \mathrm{grad}(\ln\gamma_i)\right.$$
$$\left.\frac{D_i c_i \ln(\gamma_i c_i)}{T} w \mathrm{grad}(T) + c_i D_w \mathrm{grad}(w)\right) = 0 \qquad (1)$$

where c_i is the concentration [mmol/L], w is the water content [m^3/m^3], t is time [s], D_i is the diffusion coefficient [m^2/s], z_i is the valence number of the ionic species i, F is the Faraday constant [96488.46 C/mol], ψ is the electrodiffusion potential [V], R is the ideal gas constant [8.3143 J/mol/°K], T is the temperature [°K], γ_i is the activity coefficient [$-$], and D_w is the water diffusivity [m^2/s], detailed later in this section. The following ionic species were considered for this project: OH^-, Na^+, K^+, SO_4^{2-}, Ca^{2+}, $Al(OH)_4^-$, $Fe(OH)_4^-$ and $H_2SiO_4^{2-}$. Also, HCO_3^- was considered for the simulations involving carbonation. The activity coefficients in the model are evaluated on the basis of the Harvie, Moller and

Weare (HMW) implementation of Pitzer's ion interaction model [Zhang 2005]. The term "grad" in equation (1) designates the gradient and "div" corresponds to the divergence operator.

The key material parameter that determines the rate of ingress of chloride and other contaminants in the structure is the diffusion coefficient D_i (see equation (1)). This parameter is influenced by multiple parameters[1]:

$$D_i = D_i^o \times \tau_s \times S(w) \times G(T) \times H(t) \times M(\phi) \tag{2}$$

where D_i^o is the self-diffusion coefficient of species i in open water [m^2/s] at a reference temperature T^{ref}, usually around 23°C. Values for D_i^o can be found in textbooks. The parameter τ_s is the intrinsic tortuosity of the material [–] and can take values between [0-1]. A value closer to zero corresponds to a lower diffusion coefficient and accordingly a better material. It is measured on material samples using the migration test procedure used to characterize the E-Area field samples. The various functions affecting the diffusion coefficient are given as:

$$
\begin{aligned}
S(w) &= \frac{w^{7/3}}{\phi_o^{7/3}} \\
G(T) &= e^{0.028(T-T^{\mathrm{ref}})} \\
H(t) &= \frac{a}{1+(a-1)e^{-\alpha(t-t^{\mathrm{ref}})}} \\
M(\phi) &= \frac{e^{4.3\phi/V_p}}{e^{4.3\phi_o/V_p}}
\end{aligned}
\tag{3}
$$

where ϕ_o is the porosity of the unaltered material, ϕ is the porosity at time t and V_p is the volumetric paste content of the cementitious material [m^3/m^3]. The function $S(w)$ models the influence of the water content on diffusion. It is based on the relationship derived by Millington and Quirk [1961]. The function $G(T)$ considers the effect of temperature [Zhang 2005b] on transport properties, compared to a reference value evaluated at the temperature T^{ref}. The function $H(t)$ takes into account the variation of transport properties

---

[1] The definition is different from the effective diffusion coefficient De, which is written as: De = ϕ D

as a result of the cement hydration process [Samson 2007]. The transport properties of cementitious materials are generally high at young age but tend to decrease with time, especially when supplementary materials such as fly ash are used in the production of concrete. The reduction rate is determined by the factor α while the ultimate value of $H(t \rightarrow \infty)$, when the hydration process is completed, is given by a.

Finally, the alteration to the material's microstructure caused by chemical reactions between the external environment and the cement paste can induce local porosity variations that affect the diffusion coefficients. The increase or decrease in the porosity of the microstructure is taken into account using the function $M(\phi)$, which was established on the basis of porosity and diffusion coefficient measurements performed over a wide range of cementitious materials [Samson 2007][2]. A similar approach has been widely used to predict the long-term effect of contaminant transport in soils (see for instance [Xu 2006]). The porosity variations are calculated by accounting at each node for changes in the solid phase distribution evaluated at the previous time step. The description of the chemical module is given later in the section.

The electrodiffusion term in equation (1), involving the potential ψ, is mainly responsible for maintaining the electroneutrality of the pore solution. Its role is to balance each individual ionic mobilities so that there is no net accumulation of charge at any location in the pore solution. It is usually neglected in models dealing with ionic transport in groundwater where the concentration levels can be low. However, in cementitious materials, where pore solution concentrations are high (pH around 13.2), this term can have a significant influence on the ingress rate of contaminants in structures. This was emphasized in [Samson 2007b]. To solve the diffusion potential ψ, the ionic transport equation is coupled to Poisson's equation, which relates the electrodiffusion potential in the material to the ionic profile distributions:

---

[2] At this time, the STADIUM® code does not predict fracturing (microstructure or macro fracturing) caused by exposure to external contaminants. In addition to exposure to external contaminants, fracture patterns are a function of element geometry, initial conditions (cracking incurred during construction and curing), and specific loading conditions. Methodology to address fracture damage and consequences of microfracturing caused by exposure to chemical contaminants is included in the SIMCO scope for the CBP CRADA.

$$\text{div}\big(\tau_s w \text{grad}(\psi)\big) + \frac{F}{\varepsilon} w \left(\sum_{i=1}^{N} z_i c_i\right) = 0 \qquad (4)$$

where ε [C/V/m] is the medium permittivity, τ_s is the tortuosity of the material [–] and N is the number of ions in the pore solution.

To account for water flow in the presence of water content gradients in unsaturated materials, the previous equations are coupled to equation:

$$\frac{\partial w}{\partial H}\frac{\partial H}{\partial t} + \frac{\partial w}{\partial T}\frac{\partial T}{\partial t} - \text{div}\big(D_{mH}\,\text{grad}(H) + D_{mT}\,\text{grad}(T)\big) = 0 \qquad (5)$$

where H is the relative humidity [–] and D_{mH} [m^2/s] and D_{mT} [m^2/s/°K] are the moisture transport coefficients, defined as:

$$D_{mH} = \frac{k_s k_r^l \rho_l R}{\mu M_w}\frac{T}{H} + \frac{(\phi - w)\tau_s \tau_r^g D_v^o M_w p_v^s}{\rho_l R T} \qquad (6)$$

$$D_{mT} = \frac{k_s k_r^l \rho_l R}{\mu M_w}\left(\ln(H) - \frac{T}{p_v^s}\right) + \frac{(\phi - w)\tau_s \tau_r^g D_v^o M_w H p_v^s}{\rho_l R T^2} \qquad (7)$$

where k_s is the intrinsic permeability [m^2], k_r^l is the relative permeability [–], ρ_l is the water density [kg/m^3], μ is the dynamic viscosity of the liquid phase [Pa.s], M_w is the molar mass of water [kg/mol], τ_r^g is relative gas tortuosity [–], D_v^o is the self-diffusion coefficient of water vapor [m^2/s], p_v^s is the saturation vapor pressure [Pa]. The diffusion-type equation (5) gives the distribution of relative humidity within the material. The moisture transport parameters are nonlinear functions of the relative humidity and temperature [Samson 2012]. The term D_w in equation (1) corresponds to the first term on the right-hand side of equation (6). It should be noted that in the present project, all simulations were performed in saturated conditions, for which H=1. Consequently, there are no water content gradients that affect the diffusion of species.

Finally, the temperature distribution in the material is calculated from the classical heat condition equation:

$$\rho C_p \frac{\partial T}{\partial t} - \text{div}\big(\kappa \, \text{grad}(T)\big) = 0 \tag{8}$$

where ρ is the density of the material [kg/m^3], C_p is the specific heat of the material [J/kg/°C], and k is the heat conductivity [W/m^2/°C].

For N ionic species considered in the model, there are N+3 variables in the system of equations: N×c_i, ψ, w and T, which are solved using N ionic conservation equations (1), coupled with equations (2)-(4). This system of nonlinear equations is solved using the Newton-Raphson method with all equations solved simultaneously. The spatial discretization of this coupled system is based on the finite element approach using the standard Galerkin procedure. An Euler implicit scheme is used to discretize the time-dependent part of the model. The numerical details are given in reference [Samson 2007b].

The second module in STADIUM$^{®}$ consists in a chemical equilibrium code. Following the transport step, the chemical equilibrium module verifies, at each node of the mesh, the equilibrium between the concentrations and the solid phases of the hydrated cement paste, e.g. Portlandite (calcium hydroxide), calcium silicate hydrates (C-S-H), ettringite, and mono-sulfates. The equilibrium of each phase is modeled according to:

$$K_m = \prod_{i=1}^{N} c_i^{\nu_{mi}} \gamma_j^{\nu_{mi}} \quad \text{with} \quad m = 1, \ldots, M \tag{9}$$

where M is the number of solid phases, N is the number of ions, K_m is the equilibrium constant (or solubility constant) of the solid m, c_i is the concentration of the ionic species i, γ_i is its chemical activity coefficient, and ν_{mi} is the stoechiometric coefficient of the ith ionic species in the mth mineral. If the solution is not in equilibrium with the paste, solid

phases are either dissolved or precipitated to restore equilibrium. Solid phases can also be formed when aggressive species penetrate into the porous network of the material, e.g. ettringite, gypsum, hydrated sodium sulfate, and halite. The list of mineral considered in this project is provided in Table 6.

It is also possible to model the formation of mineral phases from an ion-exchange mechanism. This was implemented in STADIUM$^{®}$ to specifically address the penetration of chloride in concrete structures, which leads to the formation of a chloride-AFm solid compound called Friedel's salt [Glasser 2008], $3CaO.Al_2O_3.CaCl_2.10H_2O$. The formation of Friedel's salt upon chloride penetration is modeled following an ion-exchange mechanism with monosulfates:

$$\text{monosulfate} + 2Cl^- \leftrightarrow \text{Friedel's salt} + SO_4^{2-} \tag{10}$$
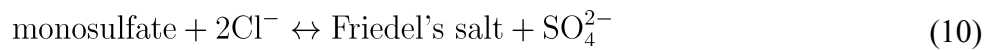
This reaction obeys the following equilibrium relationship [1]:

$$K_{Cl/SO_4} = \frac{\{Cl\}^2}{\{SO_4\}} \frac{[AFm_{SO4}]}{[AFm_{Cl}]} \tag{11}$$

where $[AFm_{SO4}]$ and $[AFm_{Cl}]$ are the solid content [mmol/g] in monosulfate and Friedel's salt respectively. The curly brackets {…} correspond to the chemical activity of the ionic species. In the present project, chloride was not considered in the simulations, due to its low concentration within the leachate solution and vadose zone water.

Papers describing laboratory validation of the model for different type of exposures can be found in [Samson 2006, Samson 2007b, Maltais 2004]. Field validation test cases were also performed [Marchand 2002, Maltais 2004b].

3. MIXTURE CHARACTERISTICS

The field concrete tested in this project was prepared with a ternary binder made of Type II cement, blast furnace slag and type F fly ash, and prepared at a water-to-binder ratio of 0.45. Table 1 shows the mixture proportions of the concrete. It should be mentioned that no information about the chemical compositions of the different binders was available for the analysis. Compositions of materials available in SIMCO Technologies' concrete mixture database were used to perform the simulations. They are presented in Table 2.

Table 1 – E-Area LLWF LAW Vault and IL Vault Concrete Formulation

Component	Quantity	
	lbs/cu yd	kg/m^3
Type II cement (ASTM C 150)	120	71
Grade 120 Blast furnace slag (ASTM C 989)	275	163
Type F Fly ash (ASTM C 618)	135	80
No 10. sand (ASTM C 33)	1,270	754
No. 67 aggregate (maximum ¾ in) (ASTM C 33)	1,750	1038
Water (maximum)	240	142
Maximum water to cementitious material ratio	0.45	0.45
Specified minimum dry density	147 lbs/cu ft	2356
Minimum compressive strength at 28 days	4000 psi	28 MPa

Table 2 – Chemical composition of binders

Oxides	Chemical composition (% mass)		
	ASTM Type I/II cement	Slag	Type F Fly Ash
CaO	63.70	40.10	4.08
SiO$_2$	20.40	36.80	47.90
Al$_2$O$_3$	4.82	8.67	24.30
SO$_3$	2.75	2.29	0.20
Fe$_2$O$_3$	3.48	0.74	15.10
Na$_2$O	0.11	0.38	0.89
K$_2$O	0.40	0.31	1.69
MgO	1.25	11.20	0.97

The initial mineral phases of the hydrated cement paste were estimated from the cement and admixtures chemical composition. The methodology developed at SIMCO Technologies Inc. to estimate the initial mineral phase content in hydrated cement pastes is based on the mass conservation of the calcium, silica, alumina, iron and sulfur that is available to form hydration products. The method was mostly inspired by the work of Taylor [1997].

The main hypotheses of the calculation are listed in the following paragraphs:

- It is assumed that SO_3 in cement and supplementary cementitious admixtures is highly soluble and is almost totally available to form hydration products. Accordingly, 90% of the total sulfur content will be found in monosulfate (AFm_{SO4}) and ettringite (AFt). The remaining 10% is not available, due to possible substitution in C-S-H.
- Depending on the amount of alumina (Al) and sulfur (S) available, different assemblages will be formed. If there is not enough Al to transform all available S into monosulfate, the amount of S and Al available will compete to form monosulfate and ettringite.
- The calculation of the C-S-H content is based on a C/S ratio of 1.65 according to the composition: C-S-H = CaH_2SiO_4 + 0.65 $Ca(OH)_2$
- The formation of Fe-hydrate C_4FH_{13} ($Ca_4Fe_2O_7.13H_2O$) is then calculated on the basis of the remaining calcium and available iron.
- Finally, portlandite (calcium hydroxide) is calculated using the remaining calcium.

The results are presented in Table 3. According to the calculations, there is not enough calcium available to form Fe hydrates and portlandite. This is mostly due to the presence of slag and fly ash, which favors the formation of C-S-H.

Finally, Table 3 also incorporates the transport properties that have been measured in the first part of the subcontract from field cores. It is important to note that although permeability is listed in the table, it is not used in any simulation since they were all performed in saturated conditions, i.e. without considering the impact of moisture gradients on species diffusion. Also, transport properties for concrete mixtures prepared with fly ash are known to decrease and improve over time. In the present case, the properties were measured after 20+ years. The initial drop in properties was thus neglected and it was assumed that the transport parameters provided in Table 3 were constant over time.

Table 3 – Concrete mixture properties

Properties	Values
Initial phase content	(g/kg)
Portlandite	0.0
C-S-H (CaH$_2$SiO$_4$)	53.6
Monosulfate	20.2
Ettringite	0.0
C$_4$FH$_{13}$	0.0
Transport properties	
Porosity (%)	15.8
Tortuosity (–)	0.0040
Permeability (e-22 m^2)	0.84

4. DESCRIPTION OF THE SIMULATIONS

Model: The service life simulations were performed for three different cases. The base scenario is illustrated on Figure 4. The 1-D simulations were performed on a 30-cm (12 in.) slab[3] for all cases. In the base case, the slab was exposed on one side ($x=0$) to a specified leachate solution and on the other side to vadose zone water, represented with typical groundwater ($x=L$). Three different leachate solutions were simulated. It was assumed that the groundwater composition corresponds to pure water at a pH of 7, because the Savannah River Site (SRS) groundwater has a low ionic composition. The simulations were performed over 10,000 years.

Inside the vault

Leachate Solution
(at pHs of 12.4, 11.1, and 9.4)

30 cm

Leaching of Ions
in the vadose zone water
(pH=7)

Vadose zone (100% RH)
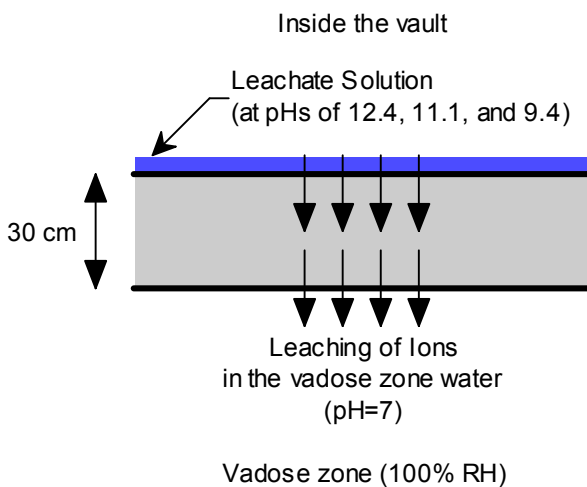
Figure 4 – Base scenario for simulations

The second scenario is illustrated on Figure 5. In this case, the slab is first exposed to a carbonate-laden environment for 31 years before being subjected for 10,000 years to the same conditions as scenario no.1. Conditions were set so that after 31 years, the carbonated layer was approximately 2-cm thick.

Finally, the third scenario involves a thicker 60-cm slab, exposed for 131 years to a carbonate-laden environment before being subjected for 10,000 years to the same

---

[3] The orientation of the slab is irrelevant for the calculations since gravity is a negligible factor for ionic and mass transport. The same results would be obtained with a vertical buried wall.

conditions as scenario no.1 (Figure 6). Conditions were set so that after 131 years, the top part of the slab was carbonated over 2 cm, whereas the bottom part was carbonated over 4 cm.

Inside the vault

Leachate Solution
(at pHs of 12.4, 11.1, and 9.4)

2 cm Carbonation Zone

2 cm Carbonation Zone

30 cm

Leaching of Ions
in the vadose zone water
(pH=7)

Vadose zone (100% RH)
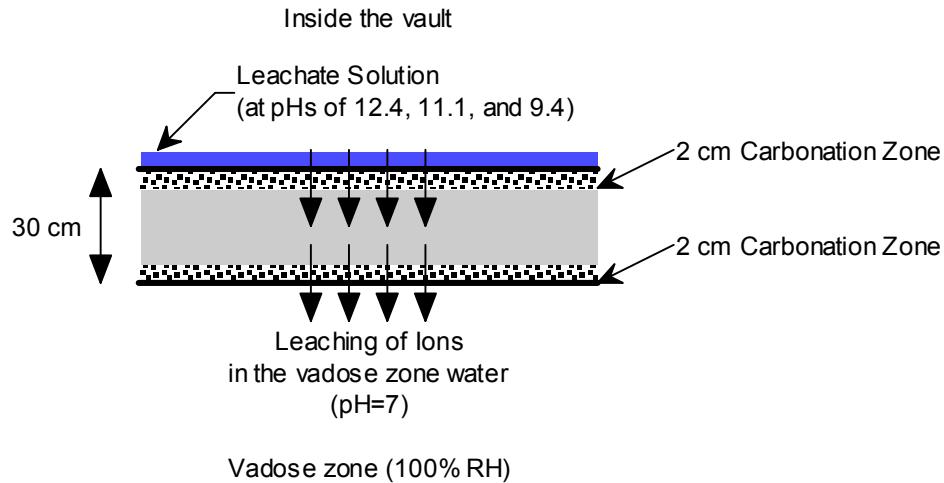
Figure 5 – Scenario no.2: 31 years exposed to carbonate before leachate contact

Inside the vault

Leachate Solution
(at pHs of 12.4, 11.1, and 9.4)

2 cm Carbonation Zone

4 cm Carbonation Zone

60 cm

Leaching of Ions
in the vadose zone water
(pH=7)

Vadose zone (100% RH)
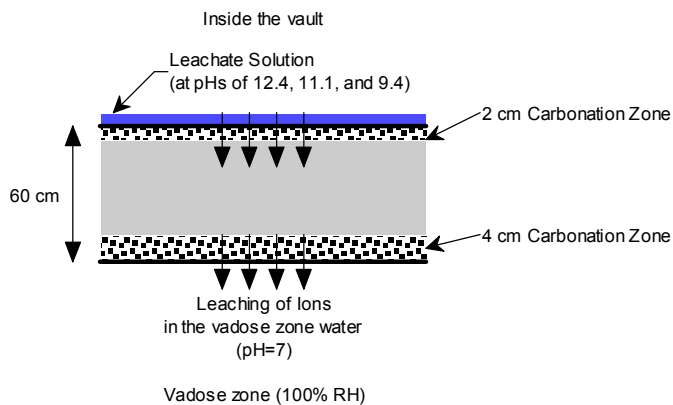
Figure 6 – Scenario no.3: 131 years exposed to carbonate before leachate contact

Composition of Leachate Solutions: Compositions of three hypothetical leachate compositions were provided by SRS. The compositions are given in Table 4. The main species of the leachates are OH^-, Na^+, Ca^{2+}, and $Al(OH)_4^-$. Hydroxide concentration was calculated by balancing electrical charges. The concentration in chloride, iron, magnesium, sulfate and carbonate are very weak. Consequently, and in order to keep calculation time over 10,000 years reasonable, those species were neglected as they are very unlikely to form detrimental phases. Consequently, only Na^+, $Ca2^+$ and $Al(OH)_4^-$

were taken from SRS solution compositions, with OH- calculated to balance the charge. The simplified solutions are also provided in the table. In all cases, the leachate is exposed at x=0.

At x=L cm, it was assumed that the material was in contact with pH-7 pure water. No alkalies, calcium or alumina was applied at this location.

Table 4 –Leachate composition used for the simulations

Ionic species	Concentrations (mol/L)		
	pH=9.4	pH=11.1	pH=12.4
$Al(OH)_4^-$	9.40E-04	9.40E-04	9.40E-04
Ca^{2+}	1.00E-03	3.19E-03	2.18E-02
Cl^-	4.80E-05	4.80E-05	4.80E-05
Fe^{3+}	3.60E-11	3.60E-11	3.60E-11
Mg^{2+}	2.03E-07	2.03E-07	2.03E-07
Na^+	1.33E-04	1.33E-04	1.33E-04
SO_4^{2-}	2.08E-06	2.08E-06	2.08E-06
HCO_3^-	6.55E-06	6.55E-06	6.55E-06
Charge balance (OH^-)	1.13E-03	5.51E-03	4.27E-02
Simplified leachate			
$Al(OH)_4^-$	9.40E-04	9.40E-04	9.40E-04
Ca^{2+}	1.00E-03	3.19E-03	2.18E-02
OH^-	1.19E-03	5.57E-03	4.28E-02
Na^+	1.33E-04	1.33E-04	1.33E-04

For scenarios no. 2 and 3, the material was first exposed to carbonate-laden environment. For scenario 2, the environment was selected to have a 2-cm carbonated layer after 31 years before the contact with leachate and soil (pH=7) was applied. In the case of scenario 3, the environment was selected to have a 2-cm carbonated layer on one side and 4-cm layer on the other side after 131 years. The exposure conditions were selected on the basis of the calcite equilibrium in an open environment with p_{co2}=$10^{-3.5}$ atm [Stumm 1996]. They are summarized in Table 5.

Table 5 – Exposure conditions for carbonation step (scenarios 2 and 3)

Element	Scenario no.2		Scenario no.3	
	$x=0$	$x=L$	$x=0$	$x=L$
pH	9.5	9.5	9.0	9.4
Concentrations (mol/L)				
OH^-	3.2E-05	3.2E-05	1.0E-5	2.2E-05
Na^+	1.743E-02	1.743E-02	5.0E-3	1.12E-2
HCO_3^-	1.74E-02	1.74E-02	5.0E-3	1.12E-2

Corrosion: Chloride present in the leachate was neglected. As discussed in reference [Glasser 2008], chloride does not have a major impact on the microstructure of the material but is a major concern for structure durability due to its role in the initiation of reinforcement corrosion. However, the amount of Cl^- in the leachate water (4.80e-5 mole/L) is too low to trigger the corrosion process [Alonso 2000].

The presence of CO_2 is also a concern for corrosion. This is especially the case for environmental carbonation, where CO_2 enter the material and reacts to form $CaCO_3$. The various steps leading to the formation of calcite consume hydroxide ions, which lowers the pH of the pore solution. When carbonation reaches the rebars, the steel is depassivated due to the drop of pH and will corrode if oxygen and water are available. In the present case, the risks for carbonation-induce corrosion are minimal, since the carbonate content in the leachate water is very low (6.55E-6 mole/L).

Equilibrium Mineral Assemblages: The minerals that were considered for the durability analysis are listed in Table 6. The portlandite, C-S-H, and monosulfates were present initially in the hydrated cement paste. Ettringite was also considered since it may form upon portlandite dissolution and C-S-H decalcification. To take into account the presence of carbonates in scenarios 2 and 3, calcite and monocarboaluminate were

included in the calculation. All the equilibrium constants in Table 6 are expressed on the basis of OH^-, SO_4^{2-}, Ca^{2+}, $Al(OH)_4^-$, $Fe(OH)_4^-$, $H_2SiO_4^{2-}$ and HCO_3^-.

The chemical equilibrium of C-S-H is modeled on the basis of Berner's approach [Berner 1988] that assigns separate C/S-dependent equilibrium relationships to the $Ca(OH)_2$ and CaH_2SiO_4 fractions of this hydration product. In this approach, a portion of C-S-H is associated to portlandite (26.4% mass) and added to real portlandite. The remainder of C-S-H (73.6% mass) is considered to be CaH_2SiO_4.

Table 6 – Mineral phases considered for the calculations

Minerals	Composition	$\log(K_{sp})$ @ 25°C
Portlandite[†]	$Ca(OH)_2$	-5.15 if C/S > 1.65 f(C/S) if 1≤ C/S ≤ 1.65
C-S-H [†]	CaH_2SiO_4	-8.16
Monosulfate	$3CaO.Al_2O_3.CaSO_4.12H_2O$	-29.4
Ettringite	$3CaO.Al_2O_3.3CaSO_4.26H_2O$	-44.0
Monocarboaluminate	$3CaO.Al_2O_3.CaCO_3.10H_2O$	-35.27
Calcite	$CaCO_3$	-12.28

[†] C-S-H $\rightarrow$ 0.65 $Ca(OH)_2$ + CaH_2SiO_4

Temperature and Moisture Boundary Conditions: The temperature was set at a constant temperature of 20°C. The simulations were all performed in saturated conditions. A relative humidity value of 1.0 was set at $x=0$ and $x=L$.

Finite Element Mesh and Time Steps: The simulations were performed with non-uniform meshed that had higher element density near the boundaries. For 30-cm slabs, 70 elements were used, whereas for scenario 3 (60-cm slab), 80 elements were used.

The initial time step was set at 10000 sec. It increased progressively when the norm of the transport calculations met predefined criteria up to a maximum value of 20 days.

5. SIMULATION RESULTS

Scenario no.1

All simulations showed the progressive decalcification of C-S-H as a result of exposure to low-pH environment, except for the leachate with a pH of 12.4, where the side of the slab exposed to high pH shows no sign of degradation. This is illustrated on Figure 7 to Figure 12.
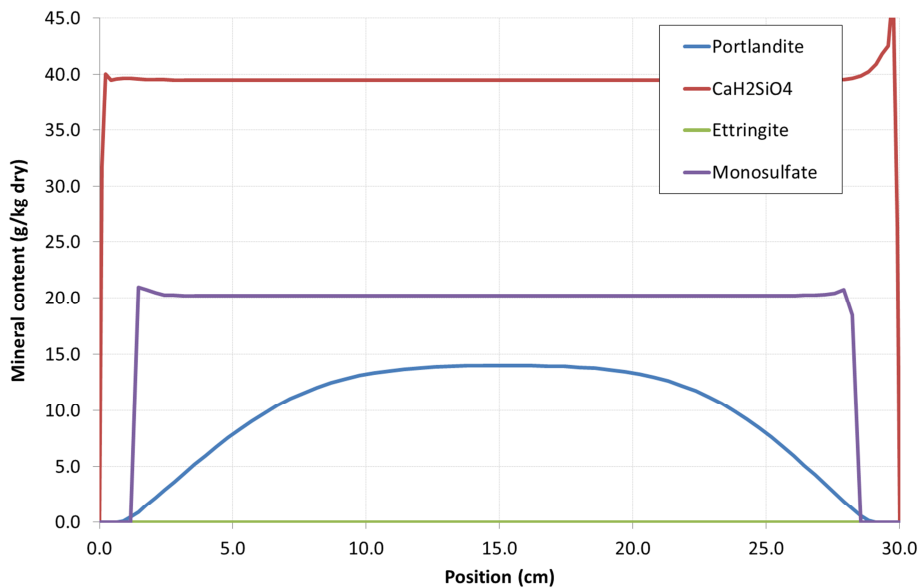
Figure 7 – Mineral distribution after 1,000 years for scenario 1 (leachate: pH 9.4)
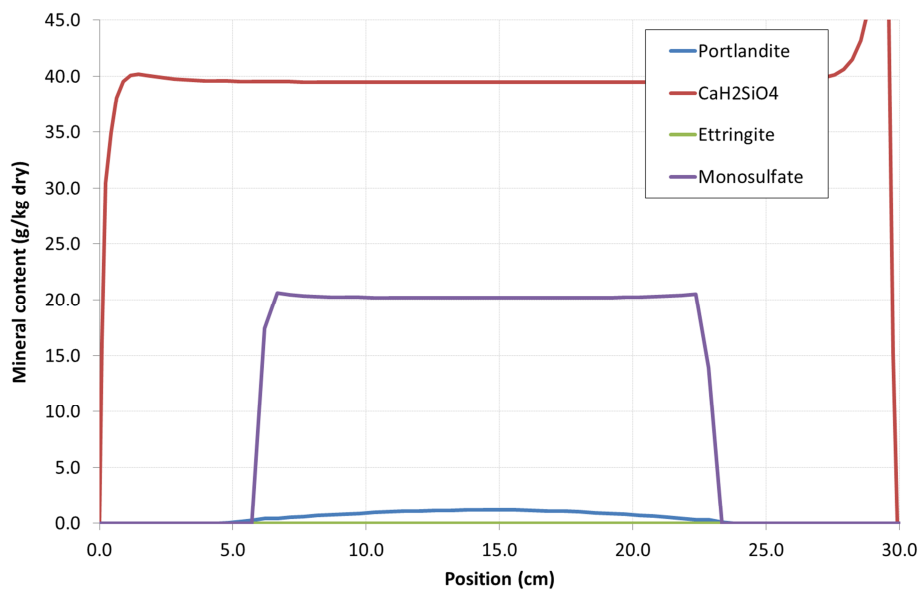
Figure 8 – Minerals distribution after 10,000 years for scenario 1 (leachate: pH 9.4)
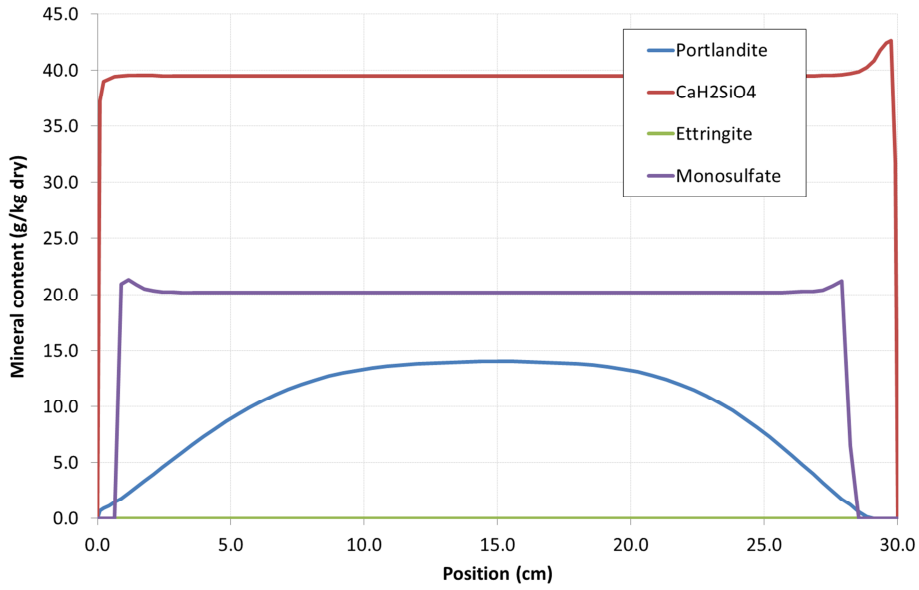
Figure 9 – Mineral distribution after 1,000 years for scenario 1 (leachate: pH 11.1)
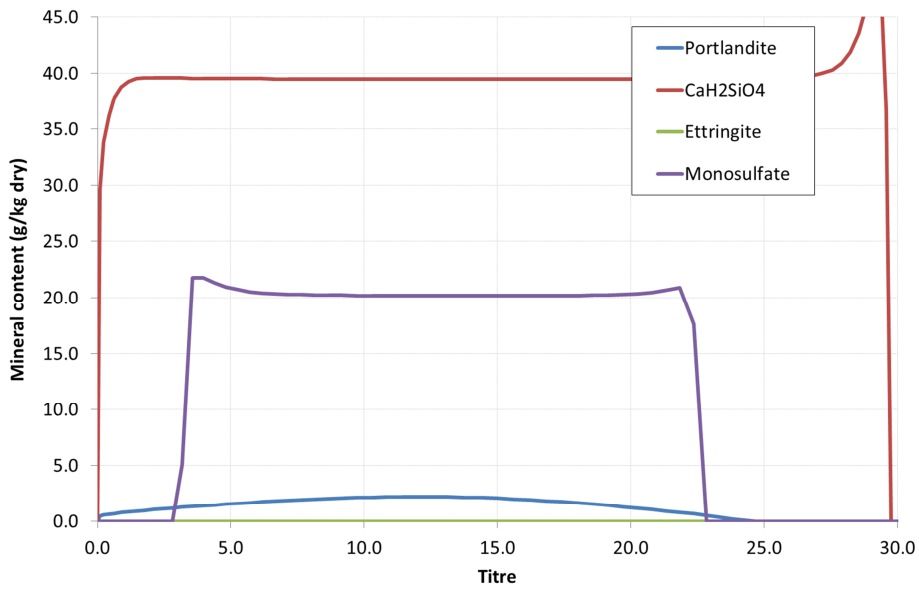
Figure 10 – Mineral distribution after 10,000 years for scenario 1 (leachate: pH 11.1)
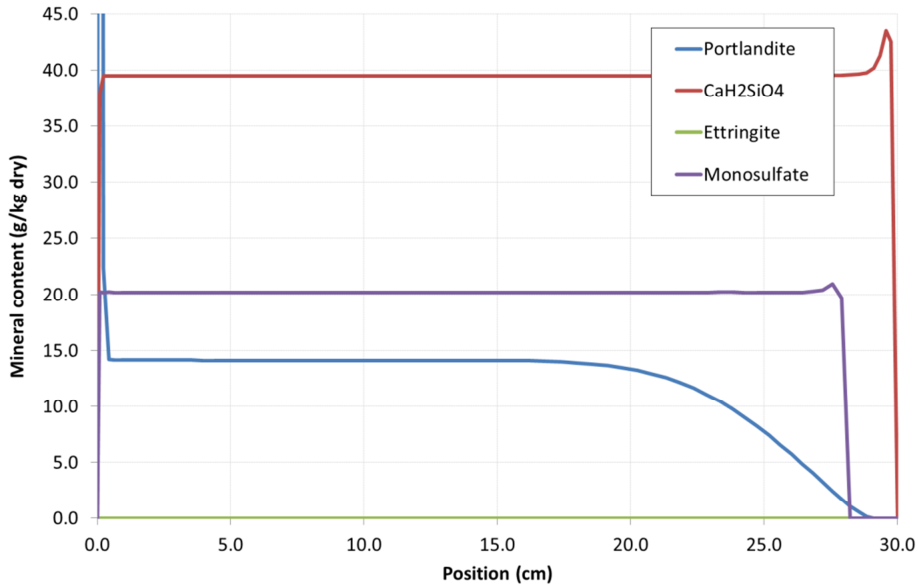
Figure 11 – Mineral distribution after 1,000 years for scenario 1 (leachate: pH 12.4)
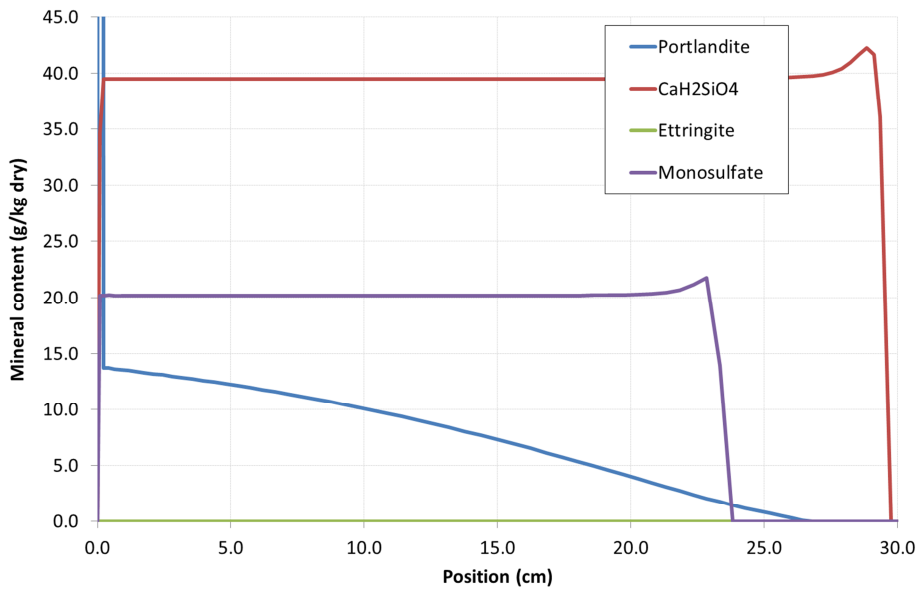
Figure 12 – Mineral distribution after 10,000 years for scenario 1 (leachate: pH 12.4)

The previous figures show that the dissolution of the hydrated cementitious paste not only induces the decalcification of C-S-H (illustrated by a loss of portlandite) but also progressive dissolution of monosulfate. Also, an increase in CaH_2SiO_4 can be observed

near boundaries where C-S-H decalcifies. This feature was also observed experimentally in pure C$_3$S pastes exposed to low pH solutions, as illustrated on Figure 13.
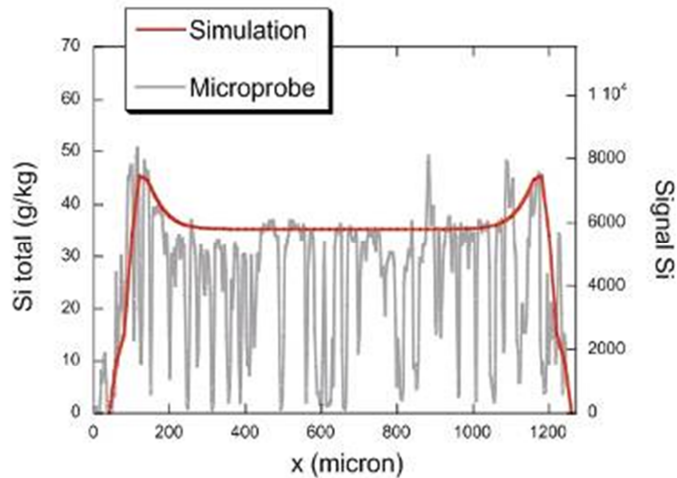
Figure 13 – Microprobe measurement of silica profile in C$_3$S paste exposed to low pH (Data: SIMCO Technologies)

The simulation can be summarized by plotting the decalcified thickness as a function of time. For this purpose, decalcification is defined as the location where 95% of portlandite is dissolved. The results for the face exposed to leachates are illustrated on Figure 14. The case with the pH at 12.4 is not plotted since no decalcification is predicted. According to the simulations, almost 9 cm of decalcification after 10,000 years can be expected if the leachate has a pH of 9.4, and less than 1 cm if the pH rises to 11.1.

In the case of the surface exposed to soil (Figure 15), similar degradation levels are reached for cases with leachates of pH 9.4 and 11.1 at x=0. The decalcified thicknesses are almost the same until 8,000 years, where the case with the 9.4-pH leachate shows slightly higher decalcification rate. However, having a 12.4-pH leachate on the other side of the slab reduces decalcification at the soil/concrete interface by maintaining a higher level of calcium and hydroxide in the material. But overall, decalcification reaches almost 10 cm in the worst case.

The decalcification depth in Figure 14 and Figure 15 were fitted to a rational function
, where d is the decalcified thickness (cm) and t is the time
(years). The fitting parameters are listed in Table 7.
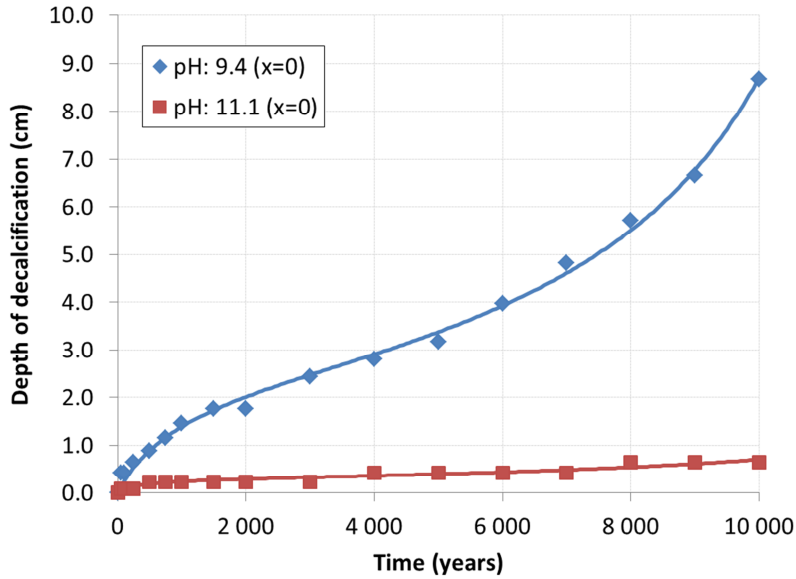
**Figure 14 – Decalcified thickness as a function of time for the surface
exposed to leachates (_x_=0)**
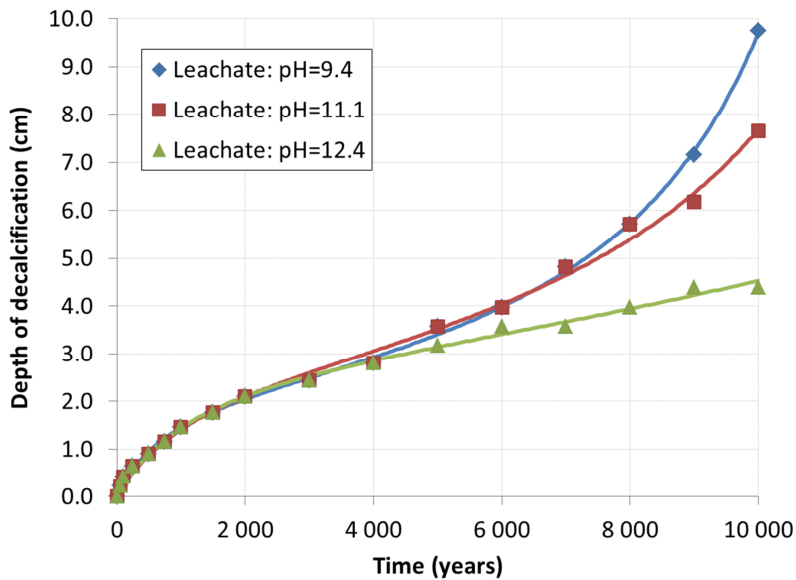
**Figure 15 – Decalcified thickness as a function of time for the surface
exposed to soil (pH=7, _x=L_)**

Table 7 – Fitting parameters for Scenario 1 degradation curves

Cases	Fitting parameters		
	a	b	c
pH: 9.4, leachate interface ($x=0$)	2.60E-03	9.39E-04	-7.41E-08
pH: 11.1, leachate interface ($x=0$)	9.48E-04	3.16E-03	-1.91E-07
pH: 12.4, soil interface ($x=L$)	2.45E-03	7.19E-04	-2.79E-08
pH: 11.1, soil interface ($x=L$)	2.38E-03	7.42E-04	-5.33E-08
pH: 9.4, soil interface ($x=L$)	2.96E-03	1.13E-03	-9.30E-08

Scenario 2 – Effect of carbonation

The solid phases after 31 years of exposure to a carbonate-laden environment are illustrated on Figure 16 for scenario 2. Typically, the model predicts the formation of a calcite layer at the surface of the material, as well as a small amount of monocarboaluminate in front of the calcite layer. Also, the simulation results illustrated on Figure 16 show that calcite also contribute to the decalcification of C-S-H. Calcite first forms using calcium coming from the dissolution of portlandite. Then, the source of calcium shifts to C-S-H. This leads to the complete disappearance of portlandite and CaH_2SiO_4 at the environment/concrete interface, as seen near $x=0$ on Figure 16.

After the initial exposure period, the slab was exposed to the same boundary conditions as in scenario 1. The solid phase distribution results are shown on Figure 17 to Figure 22. The main difference with scenario 1 is the presence of ettringite formed in the material, just in front of the monosulfate dissolution fronts. Those ettringite peaks were not present in scenario 1 simulation results. The sulfate needed to form ettringite directly comes from monosulfate dissolution. In scenario 1, the sulfate had the possibility of leaching out of the material, thus maintaining low sulfate levels in the pore solution. In scenario 2, the calcite peak near the surface reduces the porosity locally, thus contributing to maintain sulfate inside. Nevertheless, the amount of ettringite is limited and should not be a concern for cracking.

Thickness of decalcification as a function of time is plotted on Figure 23 and Figure 24. Similar to scenario 1, the decalcification thicknesses were fitted to a rational function , where d is the decalcified thickness (cm) and t is the time (years). Fitting parameters are given in

Table 8. It should be noted that after exposure to carbonate environment, the portlandite profile for the surface in contact with pH 11.1 and 12.4 leachates does not show evolution of the decalcified thickness, which remains at approximately 1 cm.

Table 8 – Fitting parameters for Scenario 2 degradation curves

Cases	Fitting parameters			
	a	b	c	d
pH: 9.4, leachate interface (x=0)	1.05E+00	6.37E-05	-1.08E-04	3.03E-09
pH: 11.1 and 12.4, leachate interface (x=0)	1.1128	0.0	0.0	0.0
pH: 12.4, soil interface (x=L)	7.88E-01	1.76E-04	-9.90E-05	7.04E-09
pH: 11.1, soil interface (x=L)	7.73E-01	2.23E-04	-6.82E-05	2.53E-09
pH: 9.4, soil interface (x=L)	7.58E-01	3.46E-04	1.80E-05	-6.62E-09
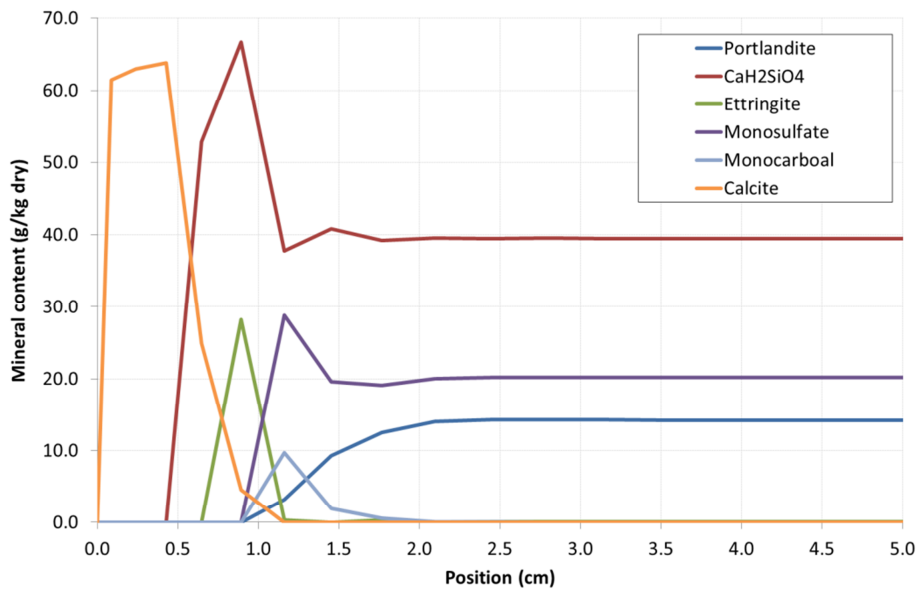
Figure 16 – Details of solid phases after 31 years of carbonation (scenario no.2)
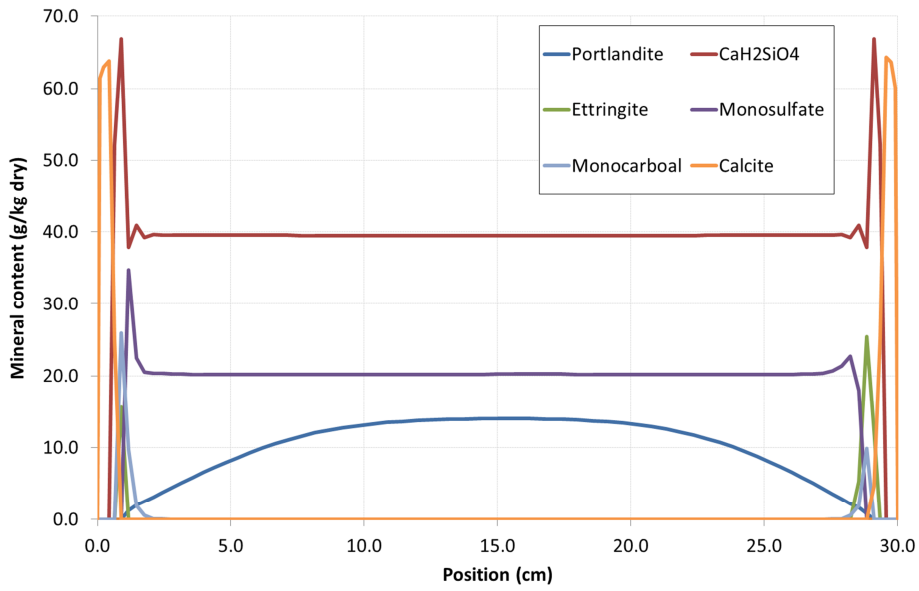
Figure 17 – Mineral distribution after 1,000 years for scenario 2 (leachate: pH 9.4)
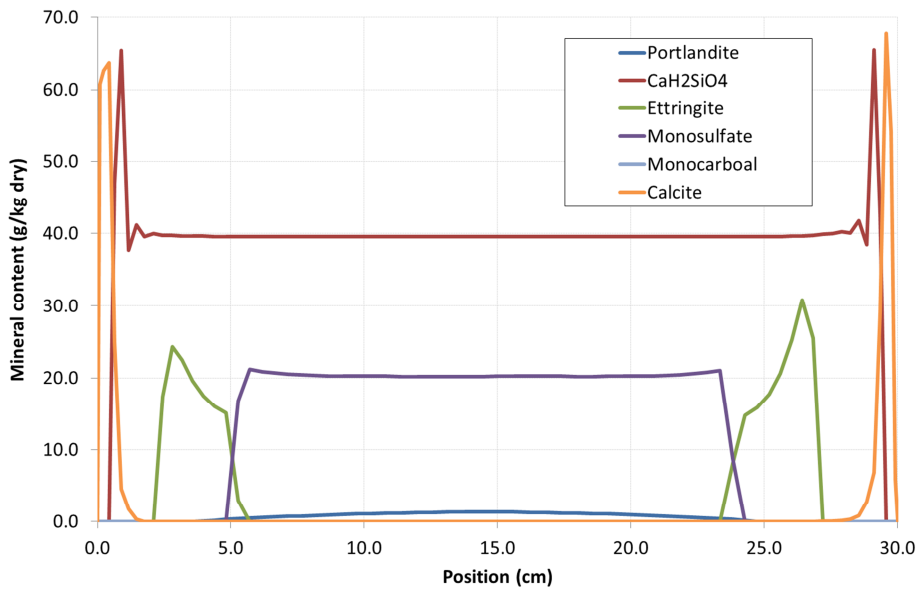
Figure 18 – Mineral distribution after 10,000 years for scenario 2 (leachate: pH 9.4)
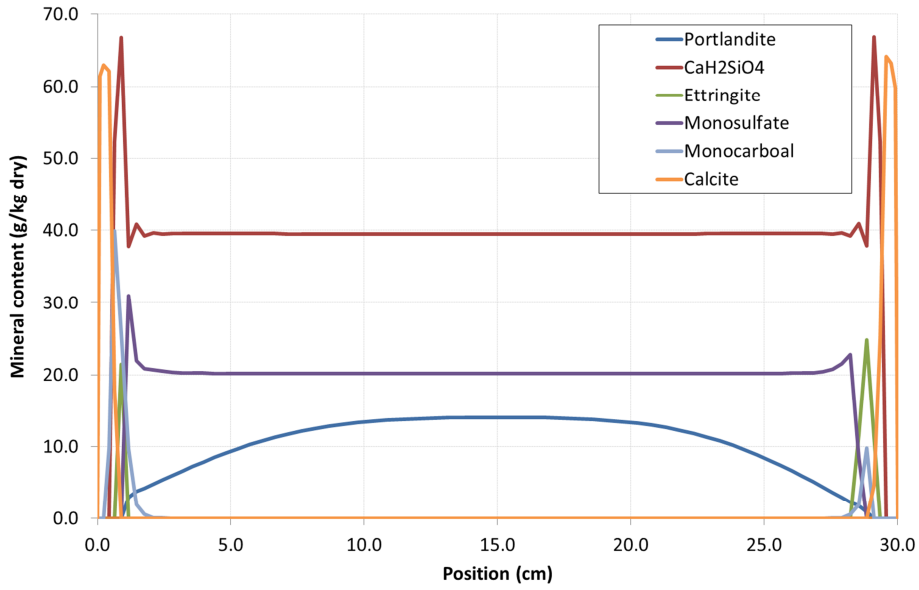
Figure 19 – Mineral distribution after 1,000 years for scenario 2 (leachate: pH 11.1)
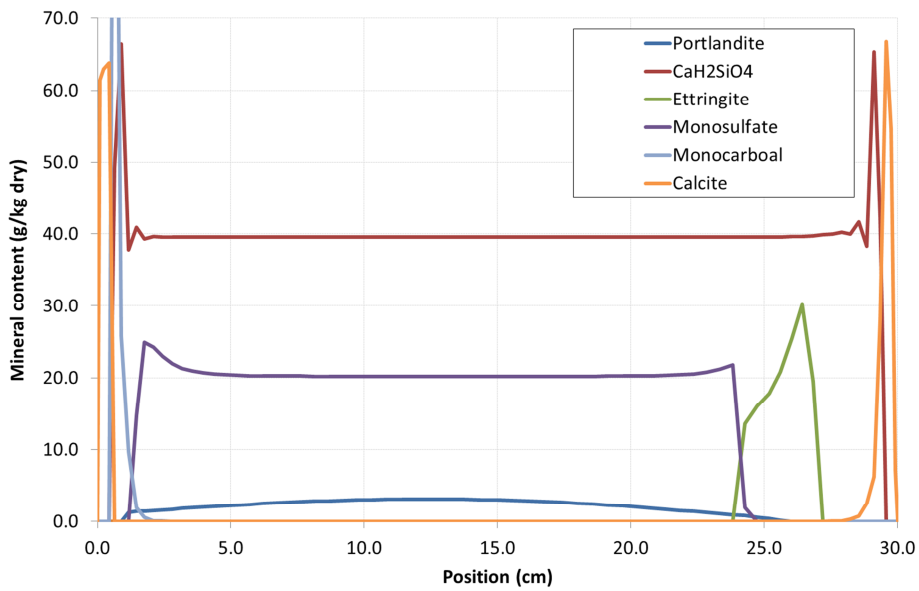
Figure 20 – Mineral distribution after 10,000 years for scenario 2 (leachate: pH 11.1)
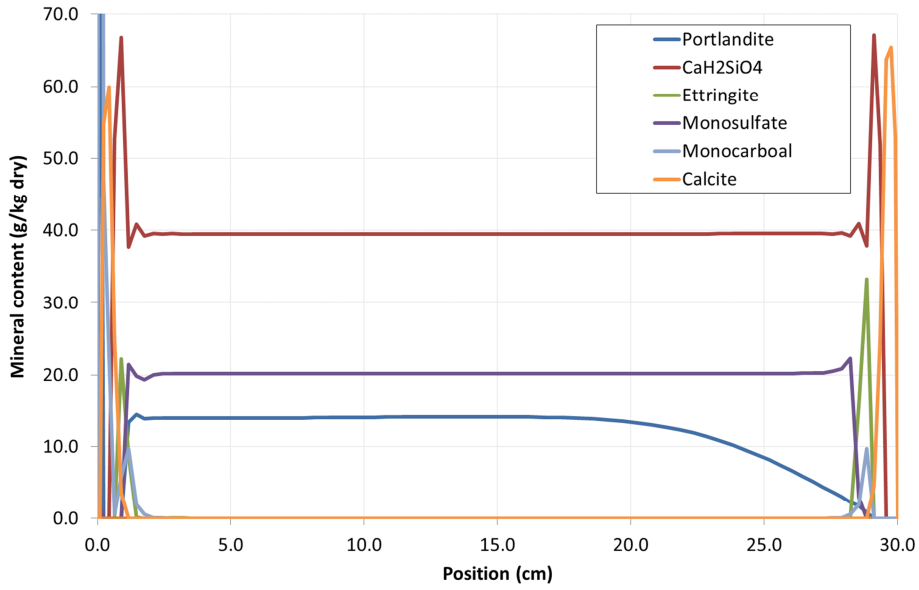
Figure 21 – Mineral distribution after 1,000 years for scenario 2 (leachate: pH 12.4)
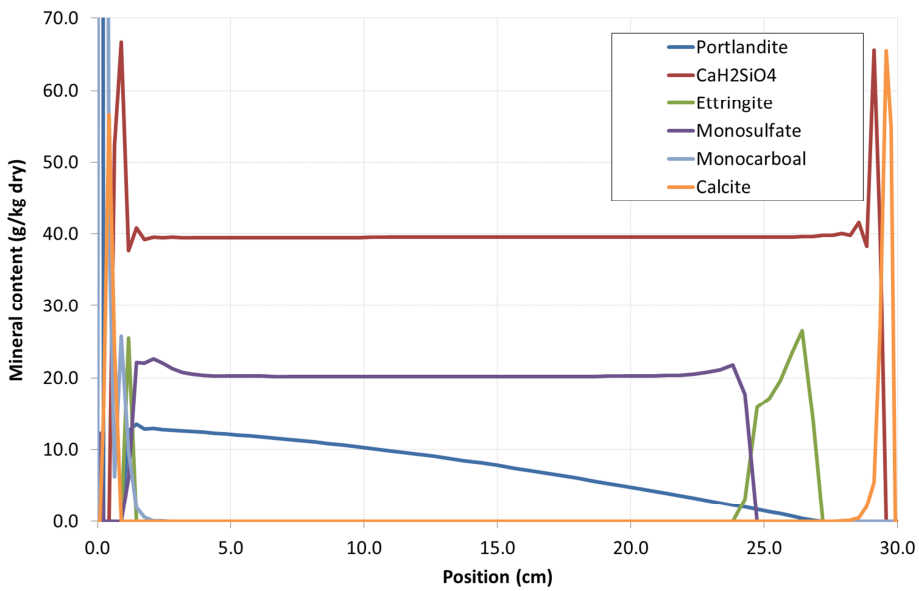
Figure 22 – Mineral distribution after 10,000 years for scenario 2 (leachate: pH 12.4)
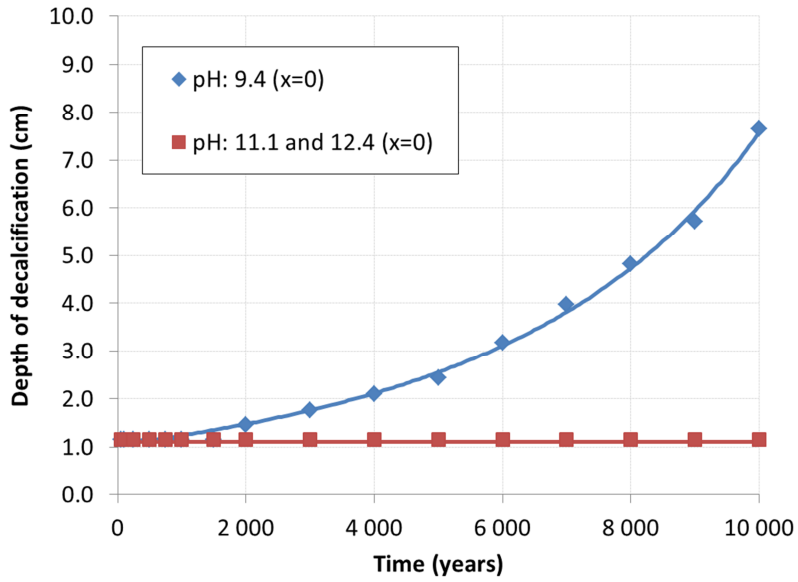
Figure 23 – Decalcified thickness as a function of time for the surface exposed to leachates (*x*=0)
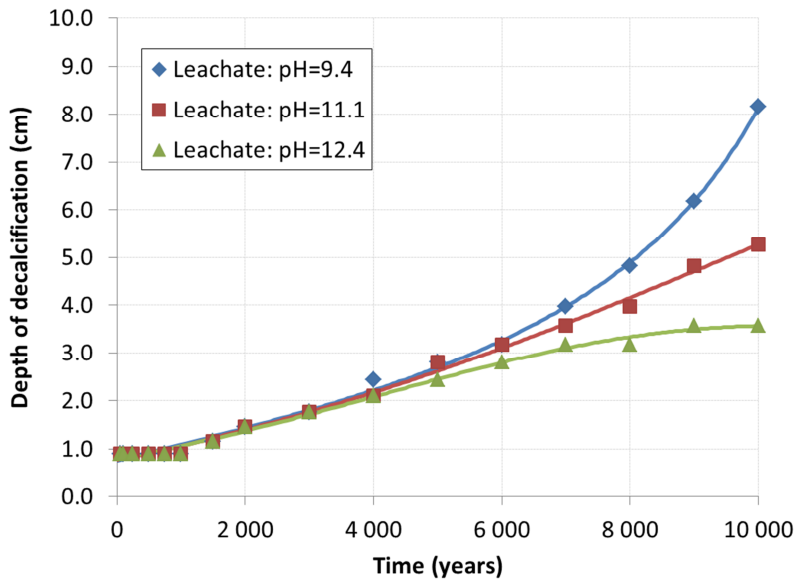
Figure 24 – Decalcified thickness as a function of time for the surface exposed to soil (x=*L*)

The carbonated layer has an impact on the long-term degradation of the concrete slab. Comparisons with decalcified thicknesses obtained in scenario 1 are shown in Figure 25 and Figure 26. Overall, considering a period of carbonation before exposure to leachates and soil reduces the predicted decalcified thickness, due to pore clogging by calcite near the concrete boundaries.
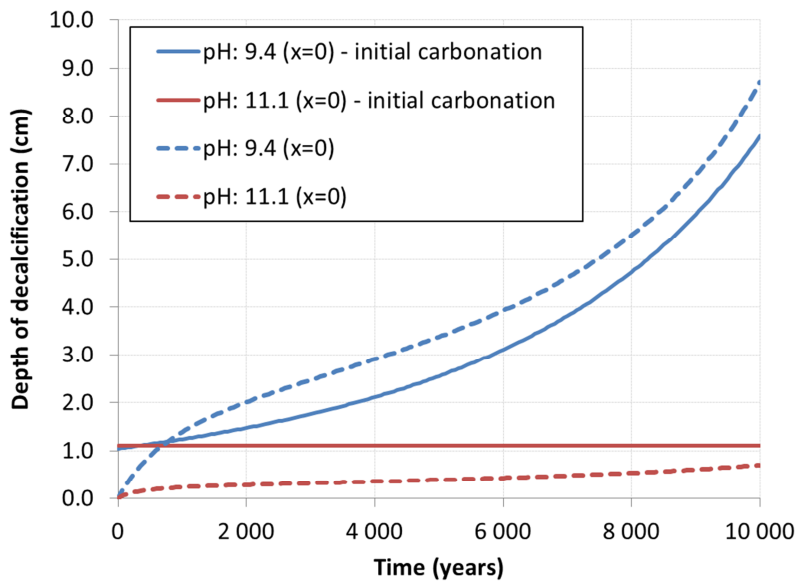
Figure 25 – Comparison of scenarios 1 and 2 decalcified thicknesses for the surface in contact with the leachate (*x*=0)
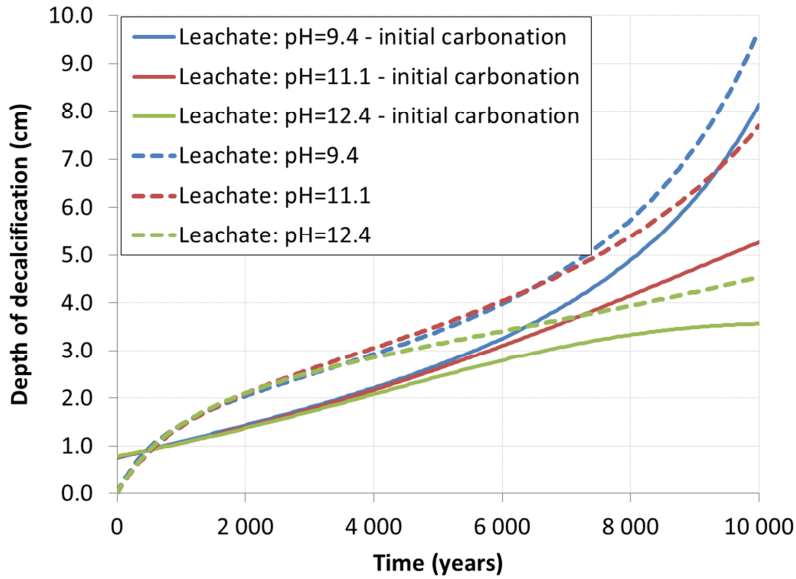
Figure 26 – Comparison of scenarios 1 and 2 decalcified thicknesses for the surface in contact with the soil (*x=L*)

Scenario 3 – Thicker slab carbonated for 131 years prior to exposure

The solid phases after 131 years of exposure to a carbonate-laden environment are illustrated on Figure 27 for scenario 3. Similar to the second scenario, the model predicts the formation of a calcite layer at the surface of the material, as well as a small amount of monocarboaluminate in front of the calcite layer. In accordance with the scenario requirements (Figure 6), the carbonated layer at the soil/concrete interface is thicker than on the top surface. Again, the simulation results show that calcite contributed to the decalcification of C-S-H.

After the initial exposure period, the slab was exposed to the same boundary conditions as in scenario 1. The solid phase distribution results are shown on Figure 28 to Figure 33. Overall, the comments made on scenario 2 phase distributions also apply to scenario 3, the phases dissolved and precipitated being identical.

However, a significant difference can be observed in the decalcification rate, as plotted on Figure 34 and Figure 35. Compared to Figure 23 and Figure 24, the numerical results

for scenario 3 show a much slower decalcification rate. Also, it can be observed on Figure 35 that the degradation rate for the concrete surface exposed to the soil is independent of the leachate pH on the other surface. All these observations can be attributed to the larger size of the slab. The increased size offers a larger supply of alkalis, calcium and hydroxide leaching toward both surfaces, which reduces the decalcification rate. The fitting parameters, based on the same rational function as in scenario 2, are listed in Table 9.

It should be noted that on Figure 34, only the decalcification rate of the low pH leachate is plotted, as the other cases did not yield decalcification other than the one caused by the initial carbonation.
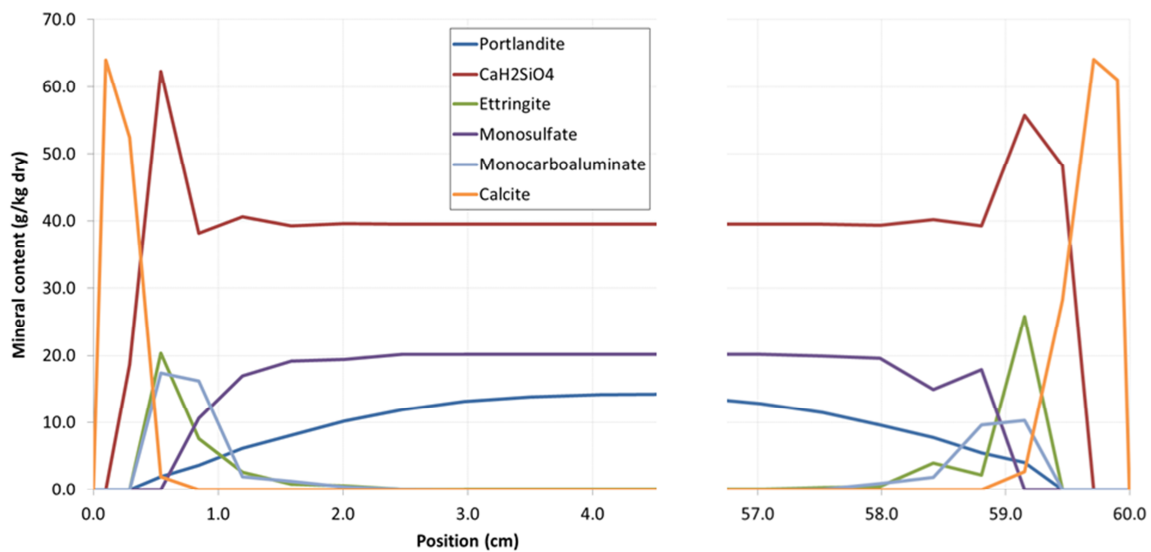
Figure 27 – Details of solid phases after 131 years of carbonation (scenario no.3)

Table 9 – Fitting parameters for Scenario 3 degradation curves

Cases	Fitting parameters			
	a	b	c	d
pH: 9.4, leachate interface (x=0)	4.54E-01	7.85E-04	1.53E-04	-4.24E-09
pH: 12.4, soil interface (x=L)	4.57E-01	4.77E-04	1.41E-05	3.49E-09
pH: 11.1, soil interface (x=L)	4.88E-01	2.05E-04	-1.02E-04	7.23E-09
pH: 9.4, soil interface (x=L)	4.63E-01	4.48E-04	-2.56E-05	6.37E-09
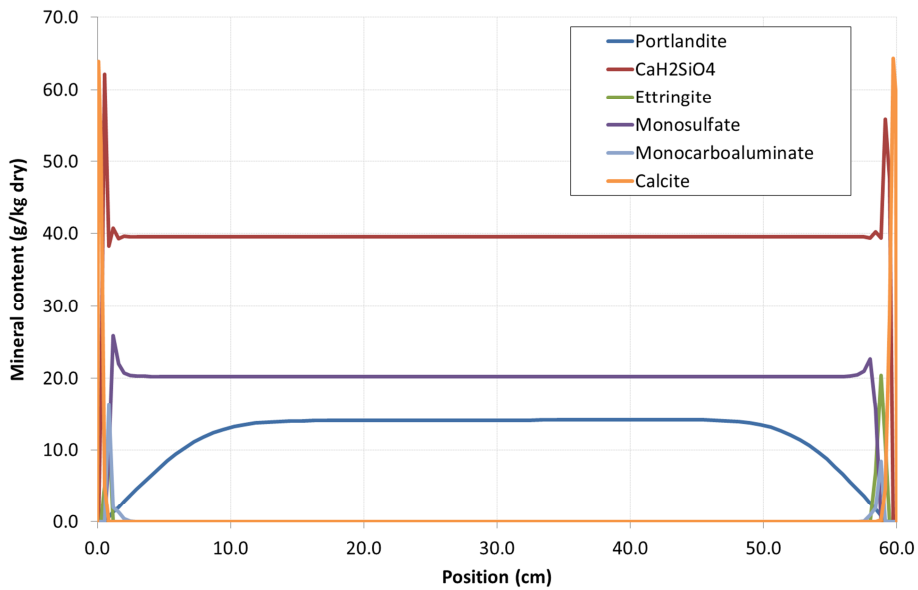
Figure 28 – Mineral distribution after 1,000 years for scenario 3 (leachate: pH 9.4)
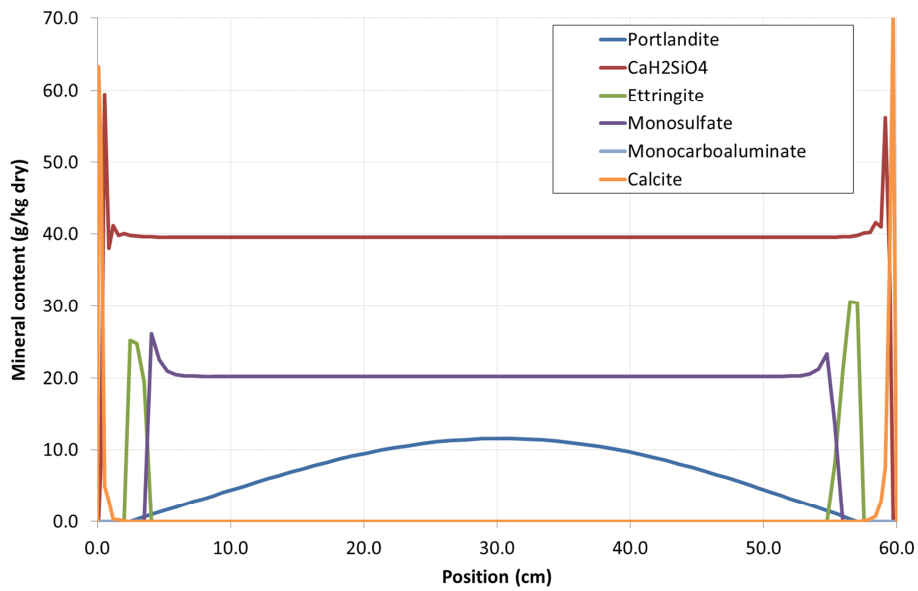
Figure 29 – Mineral distribution after 10,000 years for scenario 3 (leachate: pH 9.4)
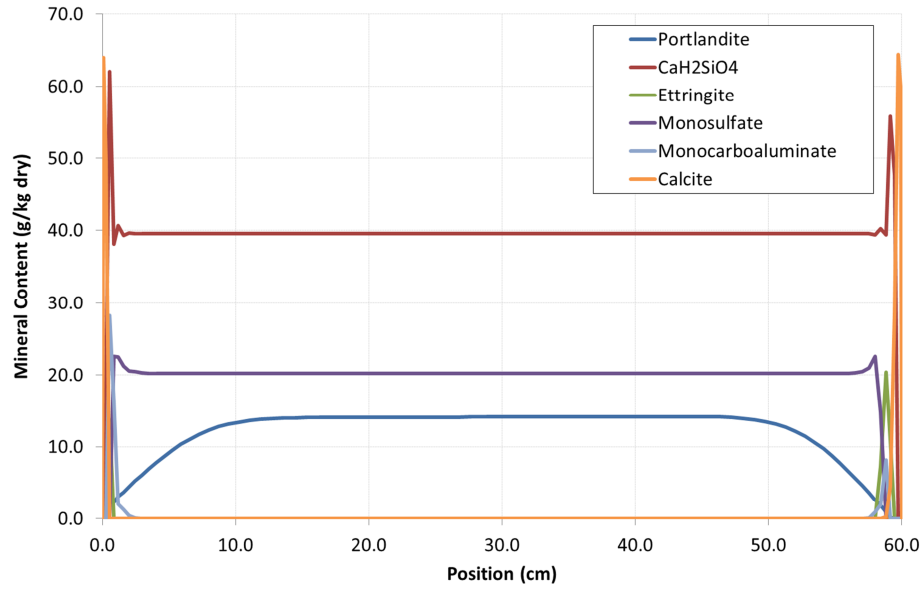
Figure 30 – Mineral distribution after 1,000 years for scenario 3 (leachate: pH 11.1)
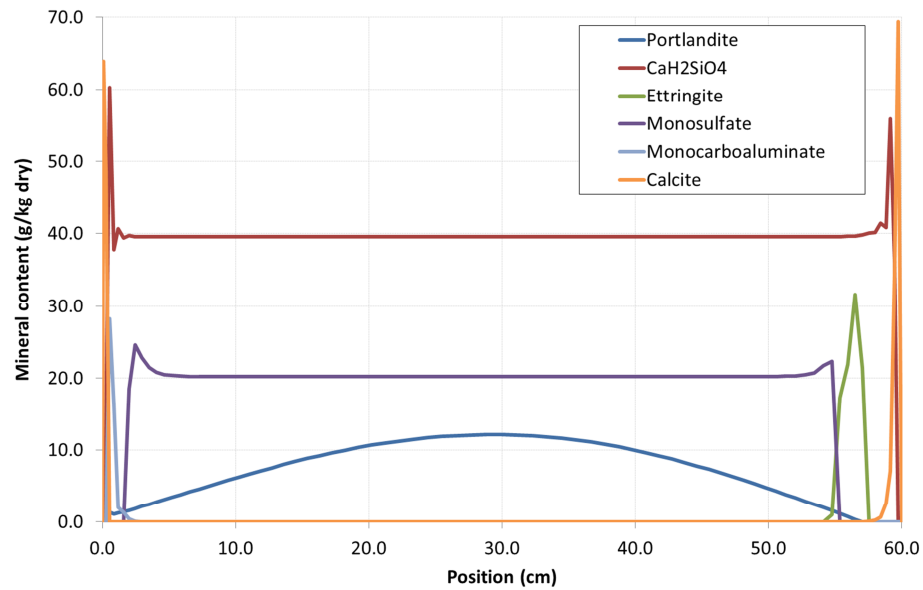
Figure 31 – Mineral distribution after 10,000 years for scenario 3 (leachate: pH 11.1)
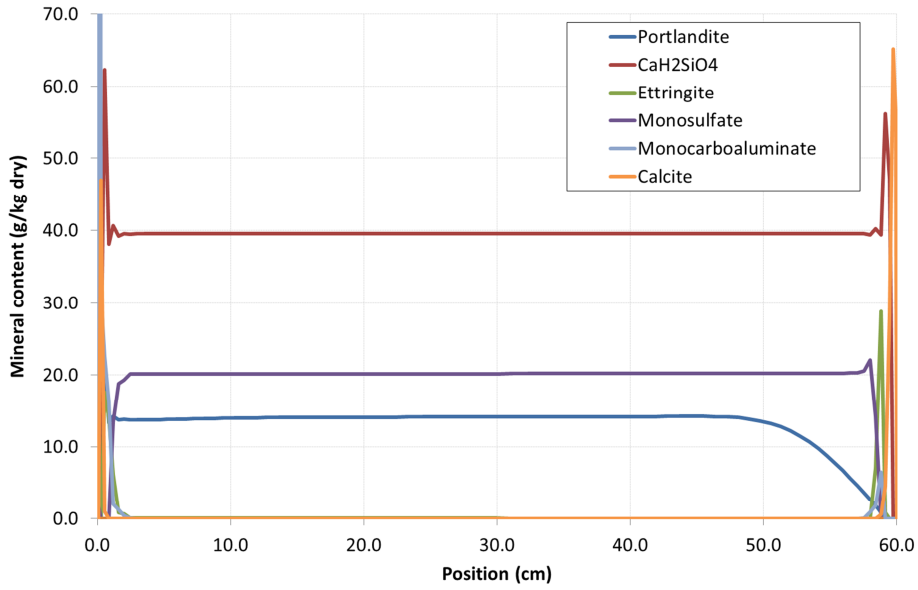
Figure 32 – Mineral distribution after 1,000 years for scenario 3 (leachate: pH 12.4)
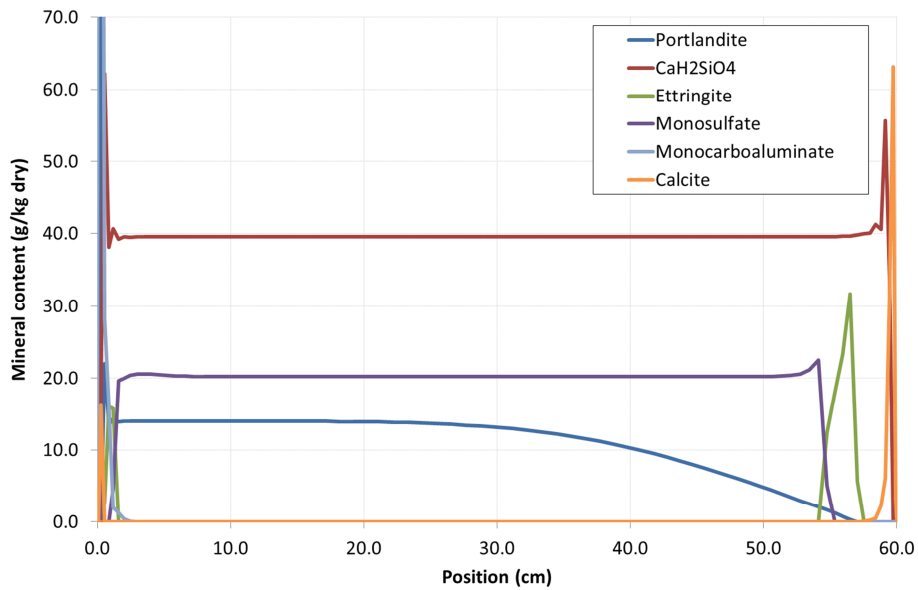
Figure 33 – Mineral distribution after 10,000 years for scenario 3 (leachate: pH 12.4)
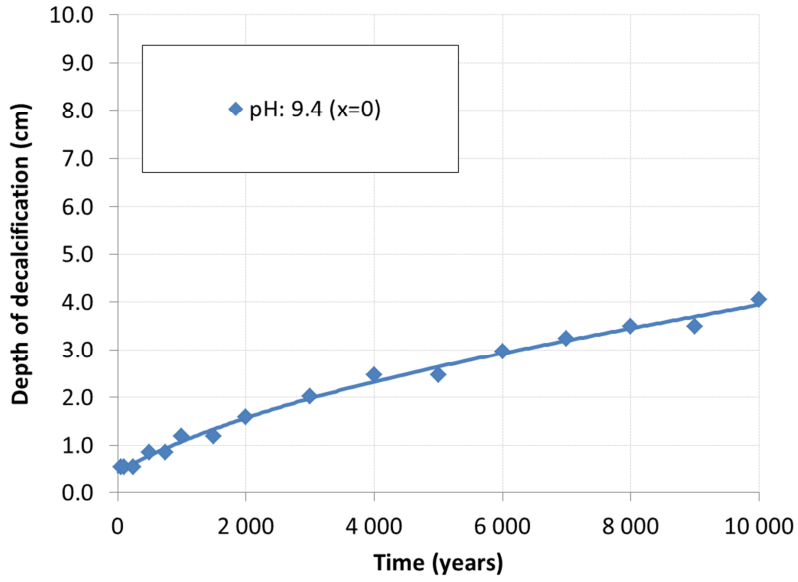
Figure 34 – Decalcified thickness as a function of time for the surface exposed to leachates (*x*=0)
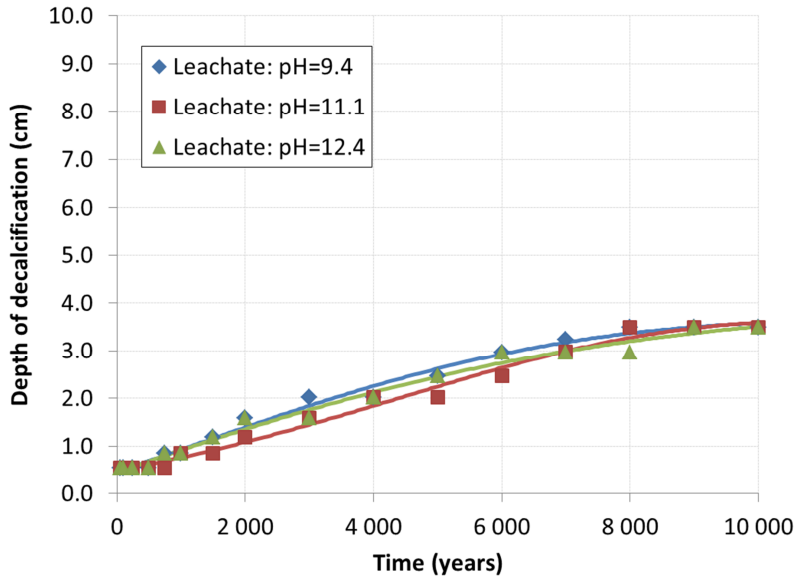
Figure 35 – Decalcified thickness as a function of time for the surface exposed to soil (*x*=L)

CONCLUSION

Simulations were performed using transport properties measured on cores from an E-Area concrete wall. The simulations consisted in exposing 30-cm and 60-cm concrete slabs to different leachate on one side, and a neutral soil on the other side. The long-term simulations showed that, assuming no initial carbonation, decalcification could reach almost 10 cm for the surface exposed to soil after 10,000 years of exposure to the low-pH leachate. Even though the material exhibits low transport properties[4], the very long exposure period results in severe degradation. Such a large decalcified thickness would most probably induce significant strength loss and could result in structural failure before 10,000 years are reached.

Other simulation series were performed to estimate the impact of considering initial carbonation of the slab prior to exposure to different leachates. In the case of a slab having the same thickness showing signs of carbonation after 31 years, there model predicts slightly less degradation, as the calcite layer formed initially clogs the pores and reduces the rate of calcium and hydroxide leaching. Still, the slab ends up being significantly degraded after 10,000 years of exposure.

A third scenario involving a thicker 60-cm slab with a thicker carbonated layer on one side showed less degradation. In this case, the decalcification was approximately cut by half, when compared to the 9.4-pH leachate case of the other scenarios. The increased size offers a larger supply of alkalis, calcium and hydroxide leaching toward both surfaces, which reduces the decalcification rate.

Finally, all simulations show a very limited concrete decalcification rate on the leachate side when the pH is at 11.1 or higher. Also, it is important to note that the model predicts a beneficial effect of having a high pH leachate on the decalcification rate at the soil interface if the slab is thin, due the calcium and hydroxide flux that limits portlandite dissolution.

---

[4] Comparison made with other concrete mixtures from SIMCO Technologies' material database.

6. REFERENCES

Alonso C., Andrade C., Castellote C., Castro P., "Chloride threshold values to depassivate reinforcing bars embedded in standardized OPC mortar", *Cement and Concrete Research*, V. 30, 2000, pp.1047-1055.

Berner U.R., "Modelling the incongruent dissolution of hydrated cement minerals", Radiochimica Acta, V. 44/45, 1988, pp. 387-393.

Glasser F.P., Marchand J., Samson E., "Durability of concrete – Degradation phenomena involving detrimental chemical reactions", *Cement and Concrete Research*, V. 38, 2008, pp. 226-246.

Maltais Y., Marchand J., Samson E., "Predicting the durability of Portland cement systems in aggressive environments – Laboratory validation", *Cement and Concrete Research*, V. 34, no. 9, 2004, pp. 1579-1589.

Maltais Y., Marchand J., Ouellet E., Samson E., Tourney P., "Service life prediction of high performance concrete mixture subjected to chloride penetration" *Proceedings of the Int. Conf. on Durability of HPC and Final Workshop of Conlife (Essen, Germany), M.J. Setzer & S. Palecki eds*., AEDIFICATIO Publishers (Freiburg, Germany), 2004b, pp. 19-36.

Marchand J., Samson E., Maltais Y., Lee R.J., Sahu S., "Predicting the performance on concrete structures exposed to chemically aggressive environment – field validation" *Materials and Structures*, V. 35, 2002, pp. 623-631.

Millington R.J., Quirk J.P., "Permeability of porous solids", *Transactions of the Faraday Society*, V. 57, 1961, pp. 1200-1207.

Samson E., Marchand J., Snyder K.A., "Calculation of ionic diffusion coefficient on the basis of migration test results", *Materials and Structures*, V. 36, 2003, pp. 156-165.

Samson E., Marchand J., "Multiionic approaches to model chloride binding in cementitious materials", in: *2nd Int. Symp. on Advances in Concrete through Science and Engineering*, J. Marchand et al. eds., RILEM Proceedings PRO 51, Quebec City (Canada), 2006.

Samson E., Marchand J., "Modeling the effect of temperature on ionic transport in cementitious materials", *Cement and Concrete Research*, V. 37, 2007, pp. 455-468.

Samson E., Marchand J., "Modeling the transport of ions in unsaturated cement-based materials", *Computers and Structures*, V. 85, 2007b, pp. 1740-1756.

Samson E., Maleki K., Marchand J., Zhang T., "Determination of the water diffusivity of concrete using drying/absorption test results", accepted for publication in *Journal of ASTM International*, 2008.

Samson E., Maleki K., Marchand J. (2012) A coupled hygro-thermal approach to model unsaturated moisture transport in cementitious materials, *in preparation*.

Stumm W., Morgan J.J., "Aquatic Chemistry – Chemical equilibria and rates in natural waters", Wiley Interscience, 3rd ed. (New-York, USA), 1996.

Taylor H.F.W., "Cement Chemistry", Thomas Telford, 2nd ed. (London, U.K.), 1997.

Xu T., Sonnenthal E., Spycher N., Pruess K., "TOUGHREACT – A simulation program for non-isothermal multiphase reactive geochemical transport in variably saturated geological media: applications to geothermal injectivity and CO_2 geological sequestration", *Computational Geosciences*, V., 32, 2006, pp. 145-165.

Zhang G., Zheng Z., Wan J., "Modeling reactive geochemical transport of concentrated aqueous solutions", *Water Resources Research* V. 41, 2005, doi: 10.1029/2004 WR003097.

Zhang T., Samson E., Marchand J., "Effect of temperature on ionic transport properties of concrete", in Proceedings of the ConMAT Conference, N. Banthia et al. eds., Vancouver (Canada), 2005b.

Page Intentionally Blank

Page Intentionally Blank

Distribution:

R. S. Aylward, 773-42A
B. T. Butcher, 773-43A
D. A. Crowley, 773-43A
G. P. Flach, 773-42A
F. L. Fox, 704-59E
J. C. Gilmour, 704-59E
J. C. Griffin, 773-A
L. L. Hamm, 703-41A
R. A. Hiergesell, 773-43A
E. N. Hoffman, 999-W
G. K. Humphries, 730-4B
D. I. Kaplan, 773-43A
T. F. Kmetz, 730-4B
M. G. Looper, 704-36E
S. L. Marra, 773-A
T. O. Oliver, 773-42A
M. A. Phifer, 773-42A
R. R. Seitz, 773-43A
D. F. Sink, 704-56E
F. G. Smith, III 703-41A
G. A. Taylor, 773-43A
K. L. Tempel, 704-56E
C. Wilson (1 file copy & 1 electronic copy),
773-43A – Rm. 213
Records Administration (EDWS)